

Spectroscopic investigations of delaminated and intercalated phyllosilicates

Zur Erlangung des akademischen Grades eines

DOKTORS DER NATURWISSENSCHAFTEN

von der Fakultät für

Bauingenieur-, Geo- und Umweltwissenschaften

der Universität Fridericiana zu Karlsruhe (TH)

genehmigte

DISSERTATION

von

Diplom-Mineraloge

Frank Friedrich

aus Mannheim

Tag der mündlichen

Prüfung: 15. September 2004

Hauptreferent: Prof. Dr. R. Nüesch

Korreferent: Prof. Dr. W. Smykatz-Kloss

Karlsruhe 2004

VORWORT

Die Herstellung von nanostrukturierten Materialien und die Untersuchung ihrer physikalischen Eigenschaften ist eine der derzeit materialwissenschaftlich interessantesten Fragestellungen. Ein besonderes Augenmerk gilt dabei der Modifizierung bereits großtechnisch eingesetzter schichtsilikatischer Rohstoffe.

Auf diesem Hintergrund entstand die vorliegende Arbeit unter der Betreuung von Prof. Dr. Rolf Nüesch in der Arbeitsgruppe Nanomineralogie am Institut für Technische Chemie im Forschungszentrum Karlsruhe (FZK). Ihm danke ich sehr für die Vergabe der Arbeit und für den mir gewährten Freiraum in der Umsetzung des Themas.

Bedanken möchte ich mich außerdem bei Herrn Prof. Dr. Werner Smykatz-Kloss (Institut für Mineralogie und Geochemie – IMG, Universität Karlsruhe) für die Übernahme des Korreferats und die freundschaftliche Unterstützung während der letzten Jahre.

Den Mitarbeitern der Abteilung Forschung, Projekte und Labors in der Firma Merck KgaA danke ich für die Bereitstellung des Probenmaterials.

Weiterhin gilt mein Dank den Freunden und Kollegen am Institut für Technische Chemie, Frau Dr. Katja Emmerich, Doreen Rapp, Felicitas Wolters, Kristina Kastner, Jens Glowacky, Matthias Schwotzer und meinem Zimmerkollegen Markus Hauser für das ausgezeichnete Arbeitsklima und die zahlreichen Diskussionen und Anregungen. Den Herren Richard Seile und Werner Metzger in der Werkstatt des Instituts für Technische Chemie danke ich für die Modifizierung der Autoklavenbehälter.

Zu ganz besonderem Dank bin ich aber Herrn Dr. Peter G. Weidler verpflichtet, dessen großartige Unterstützung vieles erst ermöglicht hat.

Herr Dr. Andreas Gehring (Institut für Geophysik, ETH-Hönggerberg, Zürich, Schweiz) war durch seine kritischen Anmerkungen und seine Diskussionsbereitschaft eine große Hilfe in der Interpretation vieler Ergebnisse.

Viele Untersuchungen im Rahmen meiner Arbeit wurden erst möglich durch die Kooperation und Unterstützung von Kollegen aus anderen Instituten:

Besonders danken möchte ich daher Herrn Stefan Heissler und Herrn Dr. Werner Faubel (Institut für Instrumentelle Analytik, FZK) für ihre großzügige Hilfe bei den spektroskopischen Messungen. Außerdem danke ich ihnen und der Firma Bruker Optics GmbH für die Durchführung einiger Messungen an dispersiven Raman Spektrometern. Frau Dr. Biliana Gasharova und Herrn Dr. Yves-Laurent Mathis (Institut für Synchrotron Strahlung, FZK) danke ich für die Unterweisung in die Fern-Infrarot-Messtechnik (FIR-Spektroskopie) an der Infrarot-Beamline (ANKA, FZK). Frau Dr. Dorothee Szabo (Institut für Materialforschung – IMF III, FZK) danke ich für die Einweisung in die Ultramikrotomie und Herrn Dr. Peter Uhlik (Department of Geology and Mineral Deposits, Comenius University Bratislava, Slovakia) danke ich herzlich für die Einführung in die Herstellung orientierter Proben zur hochauflösenden Transmissions-Elektronen-Mikroskopie (HRTEM). Herrn Send (Laboratorium für Elektronenmikroskopie, Universität Karlsruhe) danke ich für die HRTEM-Aufnahmen. Den Herren Prof. Dr. Helge Stanjek und Dr. Sven Sindern (Institut für Mineralogie und Lagerstättenlehre, RWTH Aachen) danke ich sehr für die Einweisung in die Röntgen-Fluoreszenz-Analytik.

Prof. Dr. Erich Labouvie (Rutgers University, New Jersey, USA) danke ich sehr für die kritische Durchsicht des Manuskript. Zudem möchte ich meinen Eltern und meinem Bruder für die während meines Studiums und besonders in den letzten Jahren gewährte großartige Unterstützung danken.

Mein ganz besonderer Dank gilt jedoch Annett Steudel. Alles wäre viel schwieriger gewesen ohne ihre geduldige Unterstützung in den letzten Monaten.

TABLE OF CONTENTS

Summary	i
Zusammenfassung	v
1. Introduction	1
1.1 Intercalation and delamination of muscovite	1
1.2 Spectroscopy of dickite and its intercalates	4
2. Material preparation	7
2.1 Chemical delamination of muscovite by nitrates of bi- and trivalent cations in autoclaves	7
2.1.1 Introduction	7
2.1.2 Intercalation/Delamination procedure in autoclaves	8
2.1.3 Intercalation/Delamination procedure in round bottom flasks	10
2.2 Preparation of dickite intercalation compounds	11
<i>References</i>	12
3. Vibrational spectroscopy	15
3.1 General remarks	15
3.2 Vibrational spectroscopy of layered silicates	18
3.3 Techniques	19
3.3.1 Mid infrared FTIR spectroscopy (MIR: 4000 – 400 cm ⁻¹)	19
3.3.2 Far infrared FTIR spectroscopy (FIR: 400 – 50 cm ⁻¹)	21
3.3.3 Near infrared FTIR spectroscopy (NIR: 8000 – 4000 cm ⁻¹)	23
3.3.4 FT-Raman spectroscopy	23
<i>References</i>	24

4. Analytical methods	25
4.1 X-ray diffractometry	25
4.2 Analytical chemistry	25
4.3 Microscopic techniques	26
4.3.1 Electron microscopy	26
4.3.2 Atomic force microscopy (AFM)	28
4.4 Specific surface area (BET-method)	29
<i>References</i>	29
5. Mineralogical characterization of the nitrate treated muscovites	31
5.1 Introduction	31
5.2 Materials and methods	31
5.3 Results and discussion	32
5.3.1 Grain size distribution and stack thickness	32
5.3.2 X-ray diffraction and HRTEM	37
5.4 Conclusions	46
<i>References</i>	47
6. Intercalation of Cu(II) and Zn(II) in muscovite observed by FTIR spectroscopic methods	49
6.1 Introduction	49
6.2 Materials and methods	49
6.3 Results	50
6.4 Discussion	58
6.5 Conclusions	62
<i>References</i>	63

7. Far infrared spectroscopy of interlayer vibrations of nitrate treated muscovite	67
7.1 Introduction	67
7.2 Materials and methods	67
7.3 Results	68
7.4 Discussion	71
7.5 Conclusions	76
<i>References</i>	77
8. Raman spectroscopy of phyllosilicates	79
8.1 Introduction	79
8.2 Materials and methods	79
8.3 Raman spectroscopy of muscovite	80
8.3.1 Results	80
8.3.2 Discussion	83
8.4 Raman spectroscopy of dickite and its intercalates	90
8.4.1 Measurement of usefull spectra	90
8.4.2 Structural analysis of the dickite Raman spectra	93
8.5 Conclusions	104
<i>References</i>	105
9. Near infrared and mid infrared spectroscopic study of dickite and its intercalates	107
9.1 Introduction	107
9.2 Materials and methods	107
9.3 Results	108
9.3.1 X-ray diffraction	108
9.3.2 Mid infrared spectroscopy (4000 – 400 cm ⁻¹)	109
9.3.3 Near infrared spectroscopy (8000 – 4000 cm ⁻¹)	115
9.4 Discussion and conclusions	119
<i>References</i>	130

10. Outlook	133
Appendix I Calculated NIR bands	135

SUMMARY

A characteristic feature of the phyllosilicate muscovite is its layered structure. Due to the resulting properties (e.g. anisotropic optical, electrical properties) this mineral is an important ingredient in paint industries, in polymer composites and it is used as electric insulator. Crucial for many of these properties is on one hand a high aspect ratio of the stacks, which will be enhanced by the delamination of the minerals. On the other hand for example an exchange of the interlayer cations changes the chemical properties of muscovite, its refraction behaviour and the surface properties. But due to the layered structure and the kinds of chemical bonds the interlayer cations of muscovite are difficult to access and are not exchangeable under normal conditions.

Therefore a method for the intercalation of bi- or trivalent metal cations (Cu^{2+} , Mg^{2+} , Zn^{2+} , Al^{3+}) in muscovite has been developed, which leads to the formation of swellable mica minerals and furthermore to the delamination of the minerals. This procedure, which has been patented successfully in Mai 2004, uses strongly supersaturated nitrate solutions for the delamination reactions. Autoclaves are used to extend the temperature and pressure range for the reactions.

The mineralogical investigations of the reaction products revealed the following results:

X-ray diffraction patterns of the products show strong changes in the region of the (001) peaks. These changes are interpreted as the formation of a rectorite-like mixed-layer phase. HRTEM investigations prove this statement. Bright field images show a remarkable decrease of particle size as well as domains with mixed-layered structures and superstructures.

Furthermore SEM investigations exhibit a decrease in grain size upon nitrate treatment. While the original muscovite has a medial grain size of about

120 μm , the treated samples revealed values below 70 μm (Mg: 60-70 μm , Cu: 40-50 μm , Zn: 30-40 μm).

Far infrared spectra of the nitrate treated samples for the first time definitely prove the incorporation of the foreign cations into the interlayer region. The changes of the characteristic K-O stretching vibration are only possible due to changes in the interlayer space of muscovite. Especially upon the treatment with Cu- and Zn-nitrate this band splits into bands at about 89 and 115 cm^{-1} , the characteristic vibrations of mica-smectite mixed-layer structures.

Additionally with mid infrared spectroscopic investigations it has been proven, that the intercalated cations not only are incorporated into the interlayers of the modified muscovite, but they migrate deeply into the ditrigonal hole of the tetrahedral layer. This is shown by the shift of the Si-O vibration from 529 to 535 cm^{-1} and by the intensity changes of the Si-O modes at 555 and 493 cm^{-1} . These spectral changes are attributed to distortions of the pseudo-hexagonal rings of the tetrahedral layer due to the motion of the cations.

A further proof for the migration of the cations even close to the octahedral layer are the changes of nearly all Al-O vibrations. Above all the increasing intensity of the band at 750 cm^{-1} and the shift of the mode at 789 cm^{-1} to higher wavenumbers (806 cm^{-1}) are linked to strong distortions of the $\text{Al}(\text{O}/\text{OH})_6$ -octahedra. For the Cu-nitrate treated samples these spectral changes even can be interpreted as the migration of the copper cations into the octahedral layer.

FT-Raman spectra of powdered muscovite samples are not interpretable, due to strong fluorescence and thermal background features. The investigations showed, that these features are strongly grain size dependent, because large single crystals revealed clear spectra. Furthermore, during the measurements strong interactions between Fe(III) in the sample material and the aluminium sample holders were detected. Thus the powders were sedimented on gold coated mirrors. This for the first time revealed relatively undisturbed FT-Raman spectra of fine grained muscovites.

In contrast to this the FT-Raman spectra of dickite and its intercalates do not show such features. The main reason for this can be attributed to the ten times

lower iron content of the dickite samples, compared to the muscovites. Besides, no grain size effects and no influence of the sample holder material are detected, hence measurements revealed clear and interpretable spectra.

The structural analysis of these Raman spectra and of further spectra in the mid and near infrared region provide a comprehensive view on the changes in the interlayers of dickite upon intercalation.

It can be shown that the intercalated molecules are bonded to the adjacent tetrahedral and octahedral layers via several kinds of H-bonds. The main bonds between DMSO and dickite are:

- (1) Every methyl group forms H-bonds to the oxygen atoms of the tetrahedral layer. Due to these bonds, they are locked into a relatively rigid interlayer structure.
- (2) The S=O units are hydrogen bonded to the inner surface OH groups of the octahedral layer. It is noteworthy that the inner hydroxyls obviously are not involved in H-bonds to the DMSO molecules.
- (3) Furthermore interactions between the CH₃ groups and the S=O units of neighbouring DMSO molecules lead to the formation of DMSO dimers and polymers within the interlayers.

The bonds between NMF and dickite can be assigned in a similar way. Here additional interactions between the N-H groups and the oxygens are involved in the bondings.

- (1) As well as the methyl groups the N-H units of the NMF molecules form hydrogen bonds to the O-atoms of the tetrahedral layer.
- (2) Additionally the C=O group forms H-bonds to the inner surface hydroxyls of the adjacent octahedral layers. Thus it is concluded that the NMF molecules are “standing” perpendicular to the TO-layers within the interlayer region.

ZUSAMMENFASSUNG

Ein charakteristisches Merkmal des Dreischichtsilicats Muskovit ist dessen lagiger Aufbau. Aufgrund der daraus resultierenden optischen Eigenschaften ist Muskovit ein wichtiger Rohstoff für die Farben- und Pigmentindustrie. Ausschlaggebend für diese optischen Eigenschaften ist zum einen ein hohes Aspektverhältnis (Durchmesser/Dicke) der Schichtpakete, das durch Delamination der Schichtstapel erhöht werden kann. Zum anderen würde ein Austausch der großen Zwischenschichtkationen die chemischen Eigenschaften der Muskovite und damit zum Beispiel ihr Lichtbrechungsverhalten verändern. Allerdings verhindern die Schichtstruktur und die Art der chemischen Bindungen zwischen den Schichtpaketen ein einfaches Trennen der Pakete, bzw. die chemische Modifizierung der Minerale.

Daher wurde eine Methode zur Interkalation von zwei- oder mehrwertigen Metallkationen (Cu^{2+} , Mg^{2+} , Zn^{2+} , Al^{3+}) in Muskovit entwickelt, die zur Herstellung quellfähiger Glimmerminerale und zu deren Delamination führt. Das im Mai 2004 erfolgreich patentierte Verfahren nutzt stark übersättigte Nitrat-Lösungen mehrwertiger Metallkationen zur Delamination. Zur Variation des Druck- und Temperaturbereichs werden Autoklavenbehälter verwendet.

Die mineralogischen Untersuchungen der Reaktionsprodukte ergaben folgende Ergebnisse:

Röntgendiffraktogramme der erhaltenen Produkte zeigen starke Veränderungen besonders im vorderen Winkelbereich der (00l)-Peaks. Diese Veränderungen werden als Bildung einer Rektorit-artigen mixed-layer Phase interpretiert. HRTEM-Untersuchungen bestätigen dies. Die Aufnahmen zeigen sowohl eine deutliche Abnahme der Partikelgrößen als auch Domänen mit Wechselagerungen und Überstrukturen.

Mittels rasterelektronenmikroskopischer Untersuchungen konnte zudem eine starke Abnahme der durchschnittlichen Partikel-Korngrößen durch die Nitrat-Behandlung ermittelt werden. Während der Ausgangsmuskovit eine mittlere Korngröße von 120 μm aufweist, ergaben sich für die Nitrat-behandelten Proben Werte unter 70 μm (Mg: 60-70 μm , Cu: 40-50 μm , Zn: 30-40 μm).

Fern-Infrarot Spektren der Nitrat-behandelten Muskovit-Proben belegen eindeutig das Eindringen der mehrwertigen Kationen in die Zwischenschichten des Minerals, da die Veränderung der charakteristischen K-O Schwingung bei 110 cm^{-1} nur zustande kommen kann durch Veränderungen im Zwischenschichttraum. Diese Bande zeigt besonders nach der Cu- und Zn-Behandlung ein Aufspalten in zwei Banden bei 89 und 115 cm^{-1} , charakteristische Schwingungen einer Mixed-Layer Struktur. Damit ist erstmals der Nachweis für die Interkalation von mehrwertigen Kationen in Muskovit gelungen.

Mittels spektroskopischer Messungen im mittleren Infrarot-Bereich konnte zudem nachgewiesen werden, dass die interkalierten Kationen nicht nur in die Zwischenschichten des modifizierten Muskovits eindringen, sondern tief in die ditrigonalen Lücken der Tetraederschicht migrieren. Dies wird unter anderem belegt durch den Shift der Si-O Schwingung von 529 zu 535 cm^{-1} , und Intensitätsänderungen der Si-O Schwingungen bei 555 und 493 cm^{-1} , was auf eine Verzerrung und Verdrehung der pseudohexagonalen Ringe der Tetraederschicht durch die Bewegung der Kationen hinweist.

Ein weiterer Beleg für die Migration der Kationen bis hin zur Oktaederschicht sind die Veränderungen beinahe aller Al-O Schwingungen. Vor allem die Intensitätsänderungen der Bande bei 750 cm^{-1} sowie die Verschiebung der Bande von 789 cm^{-1} nach 806 cm^{-1} , die sich auf starke Verzerrungen der $\text{Al}(\text{O}/\text{OH})_6$ Oktaeder zurückführen lassen. Im Falle des Cu-Nitrat-behandelten Muskovits können diese Veränderungen sogar als Eindringen der Cu-Kationen in die Oktaederschicht interpretiert werden.

FT-Raman Spektren pulverförmiger Muskovit-Proben sind aufgrund massiver Fluoreszenz-Erscheinungen und eines sehr hohen thermischen Untergrundes nicht auswertbar. Die Untersuchungen zeigen, dass diese

Erscheinungen stark Korngrößenabhängig sind, denn an großen Einkristallen konnten gute, auswertbare Spektren aufgenommen werden. Außerdem kam es während der Messungen zu Wechselwirkungen zwischen den Aluminium-Probenhaltern und im Muskovit enthaltenem Fe(III). Das Aufbringen der Pulver auf Goldspiegel ermöglicht hingegen erstmals Aufnahmen von FT-Raman Spektren von feinkörnigem Muskovit.

Im Gegensatz dazu zeigen die FT-Raman Spektren des Dickits und der Interkalate keinerlei Störeinflüsse bei einer Anregungswellenlänge im nahen Infrarot. Der hauptsächliche Grund dafür liegt im zehnfach geringeren Eisengehalt der Dickit-Proben gegenüber den Muskoviten. Da außerdem weder Korngrößeneffekte noch ein Einfluß des Probenhaltermaterials festgestellt wurden, ergaben die Messungen klare, sehr gut auswertbare Spektren.

Die Auswertung dieser Raman-Spektren sowie der Spektren im mittleren und nahen Infrarot ergeben ein umfassendes Bild der Zwischenschichtstruktur der interkalierten Dickite.

So zeigte sich, dass die Bindung des DMSO in der Zwischenschicht über die Bildung verschiedener Wasserstoffbrücken erfolgt:

- (1) Alle Methyl-Gruppen bilden H-Brücken zu den O-Atomen der Tetraeder-Schicht aus und sind sehr starr gebunden, dies zeigt sich durch das Aufspalten verschiedener Methylschwingungen.
- (2) Die S=O-Einheiten bilden H-Brücken zu den Oberflächen-OH-Gruppen der Oktaederschicht aus.
- (3) Zudem führen Wechselwirkungen zwischen Methyl-Gruppen und den S=O-Einheiten benachbarter DMSO-Moleküle zur Bildung von DMSO-Dimeren in den Zwischenschichten des Dickits.

Ähnliche Bindungsverhältnisse lassen sich für NMF ableiten. Hier kommt es zusätzlich zur Bildung von Bindungen über die N-H-Gruppen:

- (1) Sowohl die Methyl-Gruppe als auch die N-H-Einheiten des NMF-Moleküls bilden H-Brücken zu den O-Atomen der Tetraeder-Schicht aus.

- (2) Die C=O-Gruppe bildet H-Brücken zu den gegenüberliegenden OH-Gruppen der Oktaeder-Schicht aus. Daraus wird gefolgert, dass die NMF-Moleküle in den Zwischenschichten „stehen“.

CHAPTER 1

INTRODUCTION

1.1 INTERCALATION AND DELAMINATION OF MUSCOVITE

The characteristic features of phyllosilicates like muscovite or dickite are their layered structures of tetrahedral and octahedral layers. Due to the resulting properties (e.g. anisotropic optical, electrical properties) these minerals are important raw materials in paint industries, in polymer composites and they are used as electric insulators. Crucial for many of these properties is on one hand a high aspect ratio of the stacks, which will be enhanced by the delamination of the minerals. On the other hand for example an exchange of the interlayer cations changes the chemical properties of muscovite, its refraction behaviour and the surface properties. In contrast to clay minerals like smectites the interlayer cations of muscovite are difficult to access and are not exchangeable under normal conditions (Jasmund and Lagaly 1993, chapter 3; Osman *et al.* 1999a, 1999b). Thus the chemical modification and delamination of this mineral will be complicated. Therefore most of the methods proposed so far, use mechanical shear forces to delaminate dry powders or suspended micas in rotating barrels and cylinders (e.g. Kapygin, *et al.* 1968) or fired mica powders are quenched in cold water (Stavelly 1971). Other procedures developed, use molten salts for a chemical delamination (e.g. Bakes 1973). While these methods destroy the structure of the minerals extensively, procedures which modify the mica interlayers do not delaminate the layered structure (Reichenbach and Rich 1969; Jasmund and Lagaly 1993, chapters 2 and 3; Yates *et al.* 2000). Only the treatment with lithium nitrate as described by Caseri *et al.* (1992) and Meier *et al.* (1994) leads to a strong delamination of

muscovite. But this set-up however, does not allow the use of other salts for delamination and intercalation processes.

A better understanding of the intercalation and migration behaviour of ions and molecules within clay interlayers has been the motivation for a large number of spectroscopic studies and is also the goal of the present investigation. Especially the structural modification of the treated muscovites and the behaviour of the intercalated cations and their migration paths are of great interest. In contrast to muscovite, these mechanisms have been intensively investigated for clay minerals like smectites, due to their ability to adsorb and intercalate metal ions much easier than micas. But also in these smectites the exact position of the cations and the mechanisms of their diffusion into the interlayer region is still in discussion. The classic studies of Hofmann and Klemen (1950) and Greene-Kelly (1952) showed that a diffusion of small ions like lithium deep into the ditrigonal space of the tetrahedral layers is possible. They even proposed the movement into unoccupied octahedral cavities. In recent years a great deal of work has been done on the investigation of these mechanisms (e.g. Calvet and Prost 1971, Alvero *et al.* 1994). For example Trillo *et al.* (1993) proposed the migration of Li^+ into the tetrahedral sheets on the basis of MAS NMR measurements, but they could not confirm a further movement into the octahedral cavities. Contrarily Jaynes and Bigham (1987) postulated the movement of lithium into the octahedral sheet, as well as Mosser *et al.* (1990) interpreted Cu(II) EPR signals in a similar way and suggested a substitution of Cu for Al/Mg in the octahedral sheets of smectites.

In contrast to these clay minerals up to date no discussion of vibrational spectra of di- and trivalent cations intercalated into muscovite is available in literature. Therefore the possibility to intercalate cations like Al^{3+} , Cu^{2+} , Mg^{2+} and Zn^{2+} into the muscovite interlayers allows an extensive investigation of the interaction mechanisms between these new interlayer cations and the muscovite lattice and their migration paths into the muscovite structure. Therefore in addition to classical FTIR spectroscopy further methods like diffuse reflectance infrared (DRIFT) and far infrared spectroscopy (FIR) are used to investigate as well as the influence on the mica lattice, the vibrational behaviour

of the cations and the interlayer region. Additionally the use of various Raman techniques is investigated, to obtain additional spectroscopic informations on fine grained mica samples.

After the general introduction given in this chapter the delamination procedure for muscovite using oversaturated nitrate solutions in an autoclave system is explained in detail in chapter 2. Furthermore this method is compared to the results of the delamination method suggested by Caseri *et al.* (1992). In chapter 3 a detailed description of vibrational spectroscopy is given and the used spectroscopic methods and sample preparations are extensively described. Additional methods used for the characterization of the treated mica phases are explained in chapter 4.

In chapter 5 the resulting products are characterized in terms of their morphological and structural changes, using several microscopic and X-ray diffraction methods. Based on these results the formation of a partly delaminated mixed-layer phase is postulated. The achieved degree of delamination of these phases is estimated, based on measurements of the specific surface areas.

In the chapters 6, 7 and 8 the results of vibrational spectroscopic investigations are presented and discussed. In the first part the effects of the migrating cations on the muscovite structure are investigated by FTIR / DRIFT spectroscopy in the mid infrared range (chapter 6). The results of far infrared measurements are presented in chapter 7, they clearly prove that the new cations in fact are incorporated into the structure of the muscovite.

In chapter 8 unusual features obtained in Raman spectra of the muscovite samples are presented and their causes are discussed. To understand the conditions for obtaining usefull Raman spectra of fine grained phyllosilicates in the second part of the study Raman spectra of dickite and its intercalates dickite:DMSO and dickite:NMF are compared to the mica spectra.

1.2 SPECTROSCOPY OF DICKITE AND ITS INTERCALATES

In contrast to micas the minerals of the kaolinite group like dickite are 1:1 phyllosilicates with only one tetrahedral and one octahedral layer and without charge compensating interlayer cations. Thus the chemical modification mechanisms for these sheet silicates are different from those for mica minerals. While it is difficult to introduce single cations into the interlayers of kaolinite minerals, it is a widespread technique to intercalate various organic molecules. Especially intercalation compounds with dimethylsulfoxide (DMSO) are well investigated (see e.g. Anton and Rouxhet 1977, Vempati *et al.* 1996, Frost *et al.* 1998 and references therein). Thus this intercalate is an excellent reference material for the employment of infrared and Raman spectroscopy for the investigation of more uncommon intercalates like dickite:N-methylformamide (NMF).

Therefore in the second part of chapter 8 the conditions for FT-Raman measurements of dickite are compared to those of the mica measurements. Additionally the resulting Raman spectra are discussed. Furthermore in chapter 9 mid- and near-infrared spectral data of dickite and its intercalates are presented. Based on these extensive data a structural analysis of the possible arrangement of the incorporated molecules in the interlayer region is presented.

REFERENCES

- Alvero, R., Alba, M.D., Castro, M.A., and Trillo, J.M. (1994) Reversible migration of Lithium in montmorillonites. *Journal Physikal Chemistry*, **98**, 7848
- Anton, O. and Rouxhet, P.G. (1977) Note on the intercalation of kaolinite, dickite and halloysite by dimethyl-sulfoxide. *Clays and Clay Minerals*, **25**, 259 – 263.
- Bakes, St.E. (1973) Delamination of mica by molten salts. *US Patent* 3,770,651.
- Calvet, R. and R. Prost (1971) Cation migration into empty octahedral sites and surface properties of clays. *Clays and Clay Minerals*, **19**, 175 - 186.
- Caseri, W.R., Shelden, R.A., and Suter, U.W. (1992) Preparation of muscovite with ultrahigh specific surface area by chemical cleavage. *Colloid and Polymer Science*, **270**, 392-398.

- Frost, R.L., Kristof, J., Paroz, G.N., Klopogge, J.T. (1998) Molecular structure of Dimethyl sulfoxide intercalated kaolinites. *Journal of Physical Chemistry, Part B*, **102**, 8519 – 8532.
- Greene-Kelly, R. (1952) Irreversible dehydration in montmorillonite. *Clay Mineral Bulletin* **1**, 221-225.
- Hofmann, U. & Klemen, R. (1950) Verlust der Austauschfähigkeit von Lithiumionen an Bentonit durch Erhitzung. *Zeitschrift für Anorganische Chemie*, **262**, 95 - 99.
- Jasmund, K. and Lagaly, G. (1993) Tonminerale und Tone. Steinkopff Verlag, Darmstadt.
- Jaynes, W.F. and Bigham, J.M. (1987) Charge reduction, octahedral charge and lithium retention in heated, Li-saturated smectites. *Clays and Clay Minerals*, **35**, 440 - 448.
- Kapygin, A., Bulavtsev, V., Zhidkov, A. (1968) Device for delamination of mica crystals. *Sowjet patent* SU 1,217,684.
- Meier, L.P., Shelden, R.A., Caseri, W.R., Suter, W.R. (1994) Polymerization of Styrene with ionically bound high surface area mica: grafting via an unexpected mechanism. *Macromolecules*, **27**, 1637 – 1642.
- Mosser, C., Mestdagh, M., Decarreau, A., and Herbillon, A.J. (1990) Spectroscopic (ESR, EXAFS) evidence of Cu for (Al - Mg) substitution in octahedral sheets of smectites. *Clay Minerals*, **25**, 271 - 282.
- Osman, M.A., Moor, C., Caseri, W.R., and Suter, U.W. (1999a) Alkali metals ion exchange on muscovite mica. *Journal of colloid and interface science*, **209**, 232 - 239.
- Osman, M.A. and Suter, U.W. (1999b) Dodecyl pyridinium/alkali metals ion exchange on muscovite mica. *Journal of colloid and interface science*, **214**, 400 - 406.
- Reichenbach, G. v., H. and C. I. Rich (1969) Potassium release from muscovite as influenced by particle size. *Clays and Clay Minerals*, **17**, 23 – 29.
- Stavely, D.C. (1971) Mica delamination. *US patent* 3,570,775.
- Trillo, J.M., Alba, M.D., Alvero, R., and Castro, M.A. (1993) Reexpansion of collapsed Li-montmorillonites; evidence on the location of Li⁺ ions. *Journal of the Chemical Society - Chemical Communications*, **24**, 1809 - 1811.
- Vempati, R.K., Mollah, M.Y.A., Reddy, G.R., Cocke, D.L., Lauer Jr., H.V. (1996) Intercalation of kaolinite under hydrothermal conditions. *Journal of Materials Science*, **31**, 1255 – 2159.
- Yates, St.F., DeFilippe, I., Gaita, R., Clearfield, A., Bortun, L., Bortun, A. (2000) Process for preparing chemically modified micas for removal of cesium salts from aqueous solution. *US patent* 6,114,269.

CHAPTER 2

MATERIAL PREPARATION

2.1 CHEMICAL DELAMINATION OF MUSCOVITE BY NITRATES OF BI- AND TRIVALENT CATIONS IN AUTOCLAVES

Parts of this chapter were patented under the title “Verfahren zur chemischen Delamination von Glimmer mit zwei- und mehrwertigen Metall-Nitraten in Autoklaven” (Friedrich, F., Weidler, P.G., Nüesch, R.), Deutsches Patentamt München, application number 10327627.0, June 2003.

2.1.1 INTRODUCTION

In a joint project with Merck KgaA the delamination behaviour of muscovites and possibilities for their chemical modification were investigated.

As described in the previous chapter, most of the known delamination techniques lead to strong structural damage in the minerals. On the other hand the treatment with a supersaturated lithium nitrate solution, as described by Caseri *et al.* (1992) and Meier *et al.* (1994), leads to a strong delamination of muscovite. But this set-up does not allow the use of other salts for delamination and intercalation processes.

In the presented method, autoclaves are used as reaction vessels for the chemical modification and partial delamination of muscovite with supersaturated solutions of several nitrate salts. Therewith an advanced temperature range between 100°C and 200°C and increased pressure can be used for the treatment. For the first time this allows the intercalation of di- and trivalent metal cations like Cu, Mg, Zn and Al.

2.1.2 INTERCALATION/DELAMINATION PROCEDURE IN AUTOCLAVES

For the delamination experiments stainless steel autoclaves equipped with teflon compartments were used (Figure 2.1). They were filled with 250 mg of the < 400 μm size fraction of an Indian muscovite obtained by Merck. These muscovite samples were mixed with oversaturated solutions of several nitrates (see Table 2.1). The closed autoclaves then were heated at various temperatures between 140°C and 190°C for different times between 24 and 240 hours. Afterwards the suspensions were filtered by vacuum filtration using cellulose-nitrate filter paper (pore size: 0.45 μm , obtained from Sartorius, Goettingen, Germany).

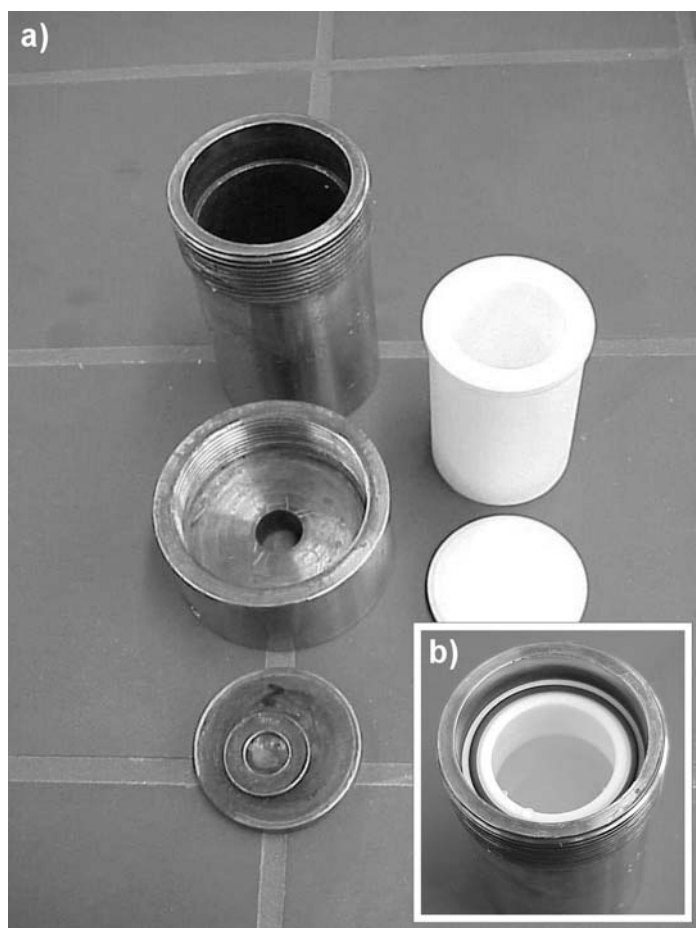


Figure 2.1 a) Components of an autoclave for the nitrate experiments. b) The teflon compartment has a capacity of about 50 ml, it is covered with an o-ring and a teflon lid (here it is filled with a Mg-nitrate solution). Covered with an additional steel plate the sealed autoclave can be stored in an oven at temperatures up to 200°C.

Table 2.1 Nitrate salt solutions for the delamination experiments in autoclaves.

Salt	Amount	Volume H ₂ O	Temperature
Al(NO ₃) ₃ x 9 H ₂ O	52 g	10 ml	150°C
Cu(NO ₃) ₂ x 3 H ₂ O	65 g	15 ml	140°C
LiNO ₃	52 g	20 ml	140°C
Mg(NO ₃) ₂ x 6H ₂ O	50 g	15 ml	190°C
NaNO ₃	65 g	15 ml	170°C
Zn(NO ₃) ₂ x 6 H ₂ O	65 g	10 ml	170°C

Salt that precipitated during cooling was dissolved by adding additional water. Finally the treated samples were washed with 250 ml water and dried at 65°C for 20 h. This procedure supplied a fine-grained, silver shiny powder. Besides the time series several further investigation series were carried out:

1) Reaction time series:

Reaction time: (12 hrs.), 24 hrs, 48 hrs, (65 hrs), 72 hrs, 96 hrs, 120 hrs, 144 hrs, 168 hrs, 192 hrs, 240 hrs, (288 hrs)

Start (Ansatz): 250 mg muscovite + various nitrates + water

Reaction temperature: 130 – 190°C

2) Temperature series:

Reaction temperatures: 110°C, 130°C, 150°C, 170°C, 190°C

Start: 250 mg muscovite + various nitrates + water

Reaction time: 24 – 48 hours

3) Concentration series:

Muscovite concentrations: 20 mg, 50 mg, 100 mg, 300 mg, 500 mg, 800 mg

Start: various muscovite amounts + various nitrates + water

Reaction temperature: 130°C – 190°C

Reaction time: 24 – 48 hours

4) Influence of the grain size:

5 fractions: < 32 µm, 63 – 32 µm, 125 – 63 µm, 200 – 125 µm, > 200 µm

Start: 250 mg muscovite + 52 g Li-nitrate + 20 ml H₂O

Reaction temperature: 140°C

Reaction time: 48 hrs

2.1.3 INTERCALATION/DELAMINATION PROCEDURE IN ROUND BOTTOM FLASKS

For comparison with the autoclave results, additional muscovite samples were treated with the nitrate salt solutions according to the method described by Caseri *et al.* (1992). Here the mica nitrate suspensions were heated in a 100 ml round bottom flask in an oil bath, which merely allowed a maximum reaction temperature of about 135°C (Figure 2.2). To avoid the loss of water during the long treatment times, the round bottom flask was equipped with a water cooler.

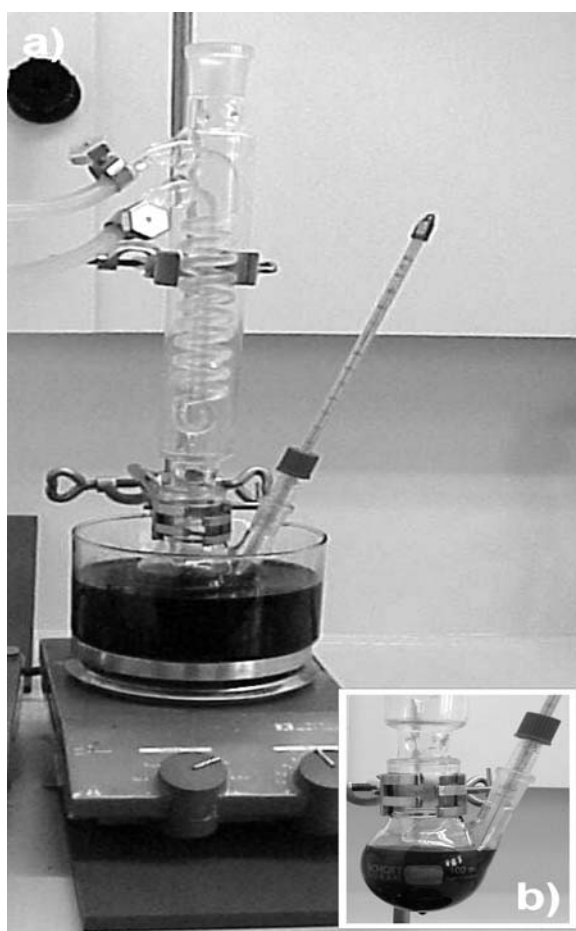


Figure 2.2 Set-up of the delamination experiment in a round bottom flask. b) detailed view on a Cu-nitrate experiment in the round bottom flask.

For these experiments 250 mg muscovite powder was mixed with the nitrate salt solutions shown in Table 2.2. Only the Li- and the Cu-nitrate-experiments reached the maximum temperature of 135°C, the other suspensions boiled at lower temperatures (Al-nitrate: 112°C, Mg-nitrate: 115°C, Zn-nitrate: 119°C).

The washing and drying procedure after the experiments was the same as for the autoclave samples and yielded silver shiny powders, too. Only the Cu-nitrate-treatment supplied a fine-grained powder of bluish to greenish colour.

Table 2.2 Nitrate salt solutions for the delamination experiments in the round bottom flask.

Salt	Amount	Volume H ₂ O	Temperature
Al(NO ₃) ₃ x 9H ₂ O	65 g	31 ml	112
Cu(NO ₃) ₂ x 3H ₂ O	65 g	20 ml	135
LiNO ₃	65 g	25 ml	135
Mg(NO ₃) ₂ x 6H ₂ O	65 g	20 ml	115
NaNO ₃	65 g	15 ml	110
Zn(NO ₃) ₂ x 6H ₂ O	65 g	10 ml	119

2.2 PREPARATION OF DICKITE INTERCALATION COMPOUNDS

The dickite sample used in this study was US-Standard # 15 from San Juanito, Mexico. Dimethylsulfoxide (DMSO, (CH₃)₂SO) and N-methylformamide (NMF, C₂H₅NO) were of analytical reagent-grade and were obtained by Merck and Fluka.

The dickite:dimethylsulfoxide (DMSO) intercalate was prepared in suspension, according to a procedure for the intercalation of kaolinite as described by Heller-Kallai *et al.* (1991). Therefore 3 g of dickite were mixed with 10 ml DMSO and 1 ml H₂O. The suspension was sealed in a polyethylene flask and stored for 72 hours at a temperature of 70°C.

The dickite:NMF intercalate was produced in a similar way by suspending 2 g dickite in 8 ml NMF and 1 ml H₂O and heating it for 72 hours at a temperature of 60°C. In contrast to a method for the intercalation of kaolinite described by Uwins *et al.* (1993) no pre-intercalation with hydrazine was necessary (Olejnik *et al.*, 1971).

Due to their thermal instability, these intercalation compounds require special care in drying the treated suspensions. Rotary drying (SpeedVac, Bachhofer)

was found to be by far the least destructive and the shortest drying technique without any impact on the intercalated material (Friedrich and Nüesch, 2002).

Thus the suspensions were centrifuged in the SpeedVac for 20 min, afterwards the clear solution was decanted and the moist paste was centrifuged for 90 min under a slight vacuum and at a temperature of about 40°C. This supplied a fine grained, white powder.

REFERENCES

- Bakes, St.E. (1973) Delamination of mica by molten salts. *US Patent* 3,770,651.
- Casari, W.R., Shelden, R.A., Suter, U.W. (1992) Preparation of muscovite with ultrahigh specific surface area by chemical cleavage. *Colloid and Polymer Science*, **270**, 392 – 398.
- Friedrich, F. and Nüesch R. (2002) The influence of the drying technique on the stability of Kaolinit:DMSO intercalates. *Contributions of the 18th Meeting of the IMA*, Edinburgh, UK.
- Friedrich, F., Weidler, P.G. and Nüesch, R. (2003) Verfahren zur chemischen Delamination von Glimmer mit zwei- und mehrwertigen Metall-Nitraten in Autoklaven. *Deutsches Patentamt München, application number 10327627.0*
- Heller-Kallai, L., Huard, E., Prost, R. (1991) Disorder induced by de-intercalation of DMSO from kaolinite. *Clay Minerals*, **26**, 245 – 253.
- Jasmund, K. and Lagaly, G. (1993) *Tonminerale und Tone*. Steinkopff Verlag, Darmstadt (Germany). 490 p.
- Kapygin, A., Bulavtsev, V., Zhidkov, A. (1968) Device for delamination of mica crystals. *Sowjet patent* SU 1,217,684.
- Kuzakov, M.G. and Vajnblat, Y.SH. (1990) Method for delamination of mica crystals. *Sowjet patent* SU 1,608,063.
- Meier, L.P., Shelden, R.A., Casari, W.R., Suter, W.R. (1994) Polymerization of Styrene with ionically bound high surface area mica: grafting via an unexpected mechanism. *Macromolecules*, **27**, 1637 – 1642.
- Olejnik, S., Posner, A.M., Quirk, J.P. (1970) The intercalation of polar organic compounds into kaolinite. *Clays and Clay Minerals*, **8**, 421 – 434.
- Osman, M.A., Moor, C., Casari, W.R., and Suter, U.W. (1999a) Alkali metals ion exchange on muscovite mica. *Journal of colloid and interface science*, **209**, 232 – 239.

-
- Osman, M.A. and Suter, U.W. (1999b) Dodecyl pyridinium/alkali metals ion exchange on muscovite mica. *Journal of colloid and interface science*, **214**, 400 – 406.
- Reichenbach, G.v.H. and Rich, C.I. (1969) Potassium release from muscovite as influenced by particle size. *Clays and Clay Minerals*, **17**, 23 – 29.
- Stavely, D.C. (1971) Mica delamination. *US patent* 3,570,775.
- Uwins, P.J.R., Mackinnon, I.D.R., Thompson, J.G., Yago, A.J.E. (1993) Kaolinite:NMF intercalates. *Clays and Clay Minerals*, **41**, 707 – 717
- Yates, St.F., DeFilippe, I., Gaita, R., Clearfield, A., Bortun, L., Bortun, A. (2000) Process for preparing chemically modified micas for removal of cesium salts from aqueous solution. *US patent* 6,114,269.

CHAPTER 3

VIBRATIONAL SPECTROSCOPY

3.1 GENERAL REMARKS

Vibrational spectroscopy involves the use of light to probe the vibrational behaviour of atomic or molecular systems. Vibrational energies of molecules and crystals lie in the approximate energy range of $0 - 60 \text{ kJ mol}^{-1}$ or $0 - 5000 \text{ cm}^{-1}$. As Figure 3.1 shows, this corresponds to the energy of light in the infrared region of the electromagnetic spectrum.

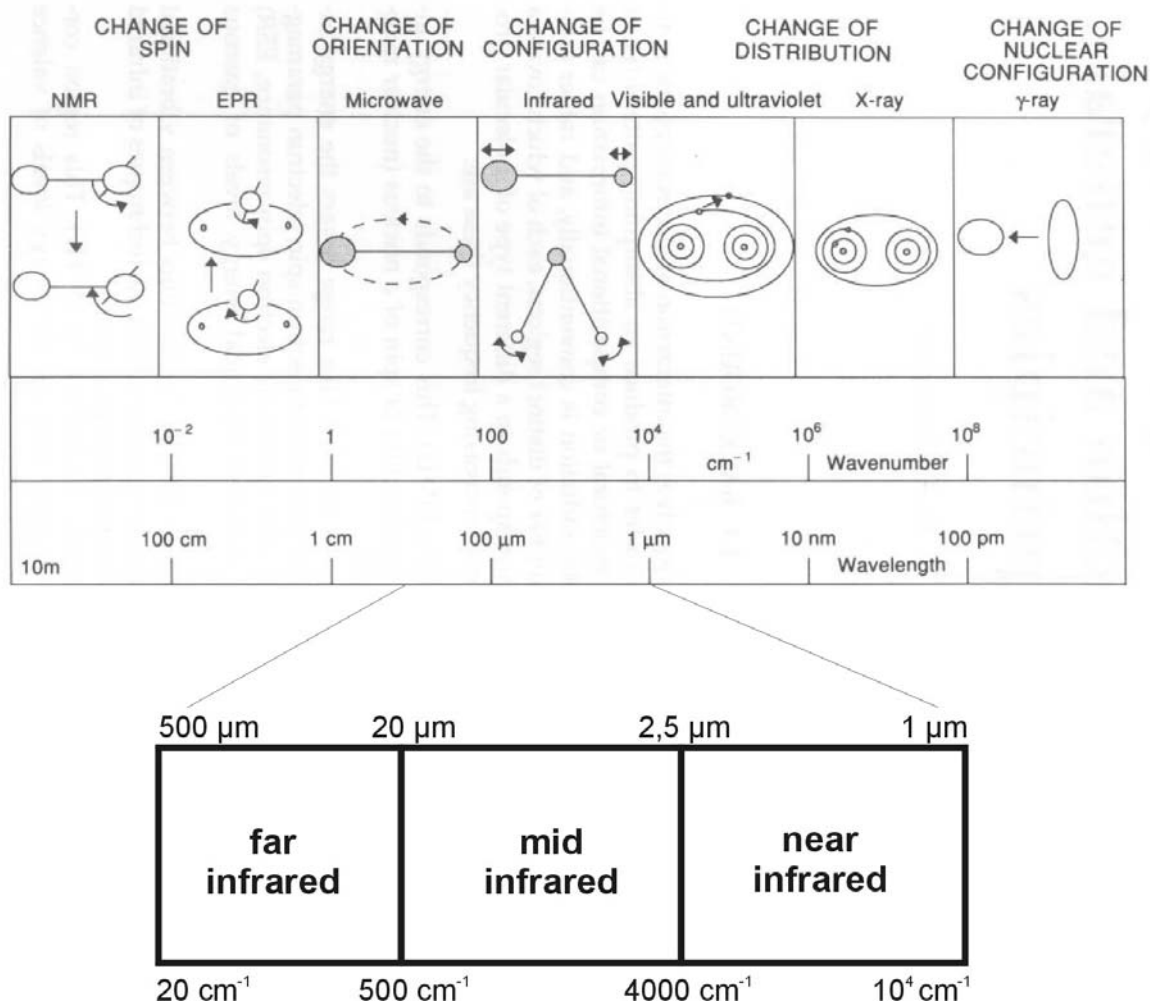


Figure 3.1 Sketch showing the infrared range within the electromagnetic spectrum. (According to Russell and Fraser, 1996)

The relationship between kinetic energy E , frequency ν and wavenumber $\bar{\nu}$ of electromagnetic radiation is shown by the following equations:

$$E = m \cdot c^2 = h \cdot \nu = h \cdot c / \lambda$$

$$\bar{\nu} = 10000 / \lambda$$

E = Energy / eV λ = wavelength / μm ν = frequency / Hz (s^{-1}) $\bar{\nu}$ = wavenumber / cm^{-1}
 m = mass / g h = Planck's constant / $6.6261 \cdot 10^{-34}$ J s c = speed of light / $2.9979 \cdot 10^8$ m s^{-1}

Accordingly energy and frequency are directly proportional. Therefore the ranges of the various kinds of radiation in the electromagnetic spectrum reflect their energies. The highfrequency γ -rays have very high energies, whereas the longwave micro- and radiowaves have low energies. Therefore due to the wavelength the absorption of electromagnetic radiation has different effects on atoms or molecules (Table 3.1).

Table 3.1 Interactions of the radiation wavelength with atoms and molecules. (According to Skoog and Leary, 1992)

Kind of spectroscopy	Wavelength	Wavenumber	Effects on
γ -rays	0,005 – 1,4 Å	-	Atom core
X-ray-absorption, -emission, -fluorescence, -diffraction	0,1 – 100 Å	-	Inner electrons
UV-spectroscopy (vacuum)	10 – 180 nm	10^6 – 50000	Bonding electrons
UV/VIS-Spectrometry	180 – 780 nm	50000 - 10000	Bonding electrons
NIR-Spectroscopy		4000 – 10000	Rotation / vibration of molecules
FTIR-/Raman-spectroscopy		400 – 4000	Rotation / vibration of molecules
FIR-Spectroscopy		20 – 500	Rotation / vibration of molecules
Microwave	0,75 – 3,75 mm	10 – 20	Rotation of molecules
EPR	3 cm	0,3	Electron spin in magnetic fields
NMR	0,6 – 10 m	0,017 – 0,001	Core spin in magnetic fields

Generally we can say, that the absorbed energy is transferred into electron, atom or molecule movement. For example, high energy radiation in the UV/Vis range with short wavelengths ($0.2 - 0.8 \mu\text{m} = 45000 - 12000 \text{ cm}^{-1} = 1.5 - 5 \text{ eV}$)

affects the movement of the electrons in an atom and lifts them into a higher energetic state. Whereas the absorption of IR-radiation with much lower energies ($0.5 - 0.05 \text{ eV} = 2.5 - 25 \text{ }\mu\text{m} = 4000 - 400 \text{ cm}^{-1}$) affects the bonding angles and the bondlengths between the atoms in a molecule. These changes in the bonds can be described mathematically as stretching or deformation vibrations, resulting in spectra with characteristic absorption bands.

This can be reduced to the fact, that a vibrating or rotating group of atoms is able to interact with a moving electric charge. But this interaction is only possible, if the charges of the atoms are not distributed symmetrically in the molecule, or if the charge distribution will become unsymmetrical due to the vibration of the atoms. Thus molecules absorb electromagnetic radiation of appropriate frequency, if the vibrations of the considered group of atoms result in a change of dipole moment.

As the intensities and positions of these bands depend on a) the degree of crystalline order, b) the masses and charges of the atoms, and c) the kind of bonding in a molecule, infrared spectroscopy became a rapid and powerful physical method universally applicable to structural analysis (e.g. Gottwald and Wachter, 1997; Günzler and Gremlich, 2003).

In contrast to the “direct” infrared techniques, Raman spectroscopy is not an absorption, but a scattering method. Visible light (usually a monochromatic laser beam in the visible range) is passed through the sample. Most of it exits the sample without an interaction (Rayleigh scattering). A small fraction of about 10^{-3} of the incident intensity is scattered by the atoms, which absorb parts of the radiation energy to lift the bonding electrons into higher energetic states. The wavelength of the scattered beam thus shifts to a smaller wavelength, reduced exactly by the absorbed amount of energy (Raman shift, Stokes lines), which lies in the range of infrared energies.

The Raman effect can be explained as a collision process between photons of the electromagnetic radiation and the electrons of the valence shell of the atoms in a molecule. Thereby small amounts of the potential energy are adsorbed, which lead to electron transitions into higher energetic states, the

electron shell is polarized. This is the main criteria for Raman-active vibrations and as no change of dipole moment is necessary Raman bands reveal further vibrational information about the molecule structure.

3.2 VIBRATIONAL SPECTROSCOPY OF LAYERED SILICATES

Besides the widespread use in organic chemistry, spectroscopy over the entire infrared range (Wavenumbers from 10000 – 50 cm^{-1}) is more and more used in clay mineralogy and materials sciences (e.g. Hawthorne, 1988). As Table 3.2 shows, the vibrations of layer silicates can be approximately separated into those of the constituent units, like the hydroxyl groups, the tetrahedral silicate layer, the octahedral layer and those of the interlayer cations (Farmer, 1974).

Table 3.2 Vibrational units of layer silicates in the entire infrared range.

Wavenumber / cm^{-1}	<i>Units</i>	Technique
70 – 150	Interlayer cations / interactions with the tetrahedral layer	FIR
200 – 600	Si–O bending vibrations	FIR / MIR / Raman
600 – 950	OH bending vibrations / interactions with octahedral cations	MIR / Raman
700 – 1200	Si–O stretching vibrations	MIR / Raman
1400 – 1600	Organic intercalates (esp. N-H and S-O bonds)	MIR / Raman
2900 – 3200	Organic intercalates / Water	MIR / Raman
3400 – 3700	OH stretching vibrations	MIR / Raman
4200 – 4600	OH combination bands (stretching + bending vibrations)	NIR
4000 – 4700	OH / intercalate combination bands	NIR
7000 – 7300	OH overtones	NIR

Especially mid infrared spectroscopy (MIR: 4000 – 400 cm^{-1}) represents an established tool for the study of the clay framework and of molecules adsorbed on its surface. Several extensive reviews deal with this method (e.g. Farmer, 1974; Russel and Fraser, 1996). In addition to the classical FTIR transmission spectroscopy using sample pellets of pressed halide salts (e.g. KBr, CsJ), in the

last years special techniques like diffuse reflectance infrared spectroscopy (DRIFT) and photoacoustic FTIR spectroscopy (PAS) have been established successfully for the investigation of powdered materials in clay science (Madejova and Komadel, 2001). Additionally, as a complementary technique to spectroscopy in the mid infrared range, Raman spectroscopy reveals further details of the clay lattice structure, (Frost, 1995; McKeown et al., 1999; Frost et al., 2001).

The far infrared region (FIR: $400 - 50 \text{ cm}^{-1}$) provides information on the structure of the interlayers, especially the interactions of the interlayer cations with the SiO_4 -units of clays (e.g. Fripiat, 1981; Diaz et al., 2000). Yet the near infrared spectral range above 4000 cm^{-1} (NIR: $10000 - 4000 \text{ cm}^{-1}$) has not received much attention by clay scientists.

Recently NIR spectroscopy has become more important, because it offers the possibility to investigate the structural environment of the central atoms in the octahedral layers (Petit et al., 1999, 2004) and of the hydration states of the clay interlayers.

3.3 TECHNIQUES

3.3.1 MID INFRARED FTIR-SPECTROSCOPY (MIR: $4000 - 400 \text{ CM}^{-1}$)

KBr-Pellets / Transmission Infrared Spectroscopy

The FTIR spectra were recorded on a Bruker IFS66/S spectrometer equipped with a DTGS detector, using KBr-pellets made of 3 milligrams of powdered sample mixed with 300 milligrams of KBr (for a few samples a ratio of 10 mg sample powder to 500 mg KBr was used). 64 scans in the $4000 - 400 \text{ cm}^{-1}$ spectral range were recorded with a resolution of 4 cm^{-1} .

Diffuse Reflectance Infrared Spectroscopy (DRIFT) and Photoacoustic Spectroscopy (PAS) ($4000 - 400 \text{ cm}^{-1}$)

Additionally DRIFT spectroscopy was used for a detailed measurement especially in the Si-O stretching region ($1200 - 800 \text{ cm}^{-1}$, Figure 3.2). For this sample preparation 10 mg of sample material was slightly ground with 500 mg

KBr, then the powders were poured loosely into a sample cup to obtain a random orientation. The spectra were obtained using a diffuse reflectance accessory from Spectra-Tech Inc., also equipped with a DTGS detector. 64 scans were measured with a scanner velocity of 1.6 kHz and a resolution of 8 cm^{-1} . A polished aluminum disc was used for the background measurement.

Photoacoustic spectra were recorded using a PAS accessory from MTEC photoacoustic Inc. (Ames, Iowa) with the same parameters as for the DRIFT measurements. Carbon black was used for the background measurements. The measurements resulted in very clear spectra with good spectral resolution (Figure 3.3).

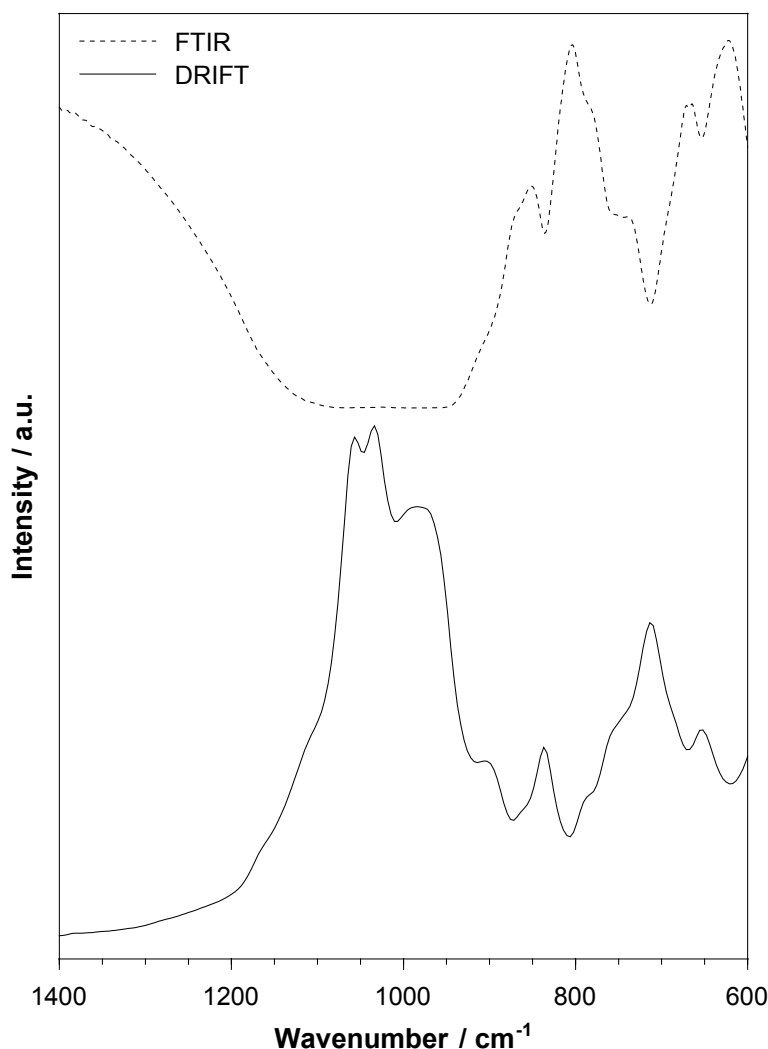


Figure 3.2 Comparison of DRIFT and FTIR spectra of muscovite in the region between 600 and 1200 cm^{-1} .

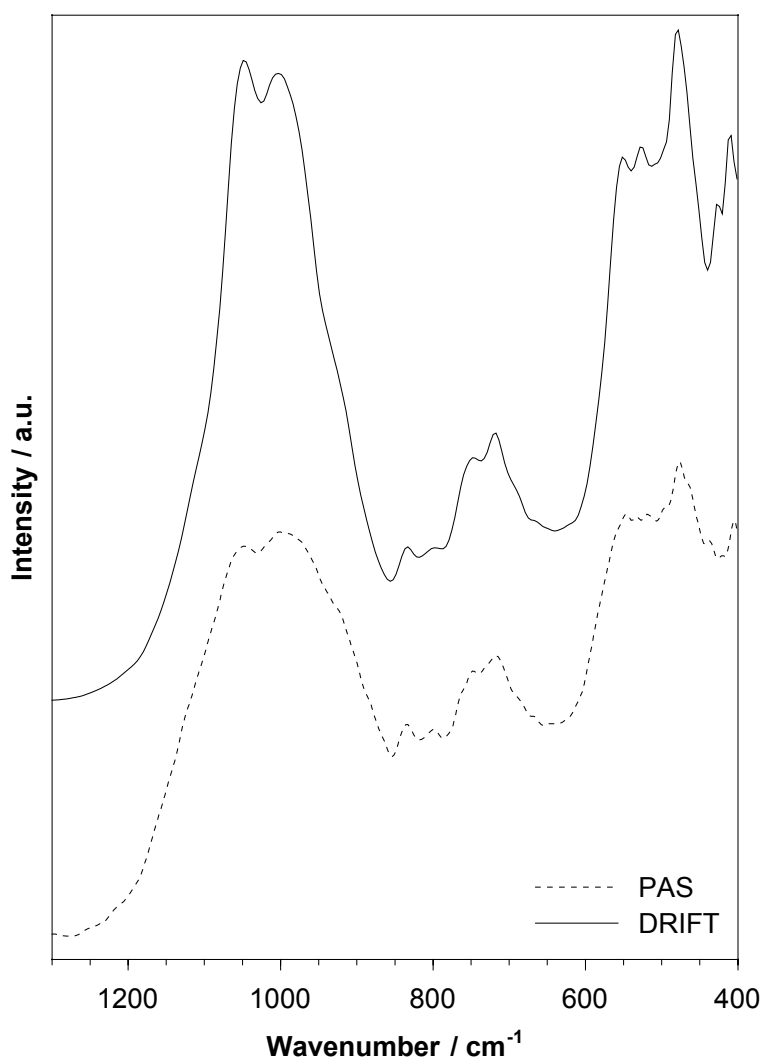


Figure 3.3 Comparison of DRIFT and PAS spectra of Cu-muscovite in the region between 400 and 1200 cm^{-1} .

3.3.2 FAR INFRARED SPECTROSCOPY (FIR: 400 – 50 CM^{-1})

The far infrared spectra were collected at the IR-Beamline (SUL-IR) of the Angstrom Source Karlsruhe (ANKA) at the Forschungszentrum Karlsruhe. Synchrotron radiation was chosen, due to its higher brilliance in comparison to globars or Hg-lamps (Figure 3.4), which led to a much better resolution of the relatively weak vibrational bands in this spectral region.

For the measurements polyethylene pellets were pressed using a ratio of 5 – 8 mg of sample powder to 55 mg of polyethylene. The measurements were obtained in transmission mode using a Bruker IFS66v/S spectrometer operating

under vacuum. The spectrometer was equipped with a Bolometer detector operated at 4.2 K. A 6 μm multilayer beamsplitter (mylar/Si) was used and for intensity attenuation a Si-window was set into the beam behind the sampleholder. With this setup 64 scans in the 700 – 20 cm^{-1} spectral range were recorded with a resolution of 4 cm^{-1} .

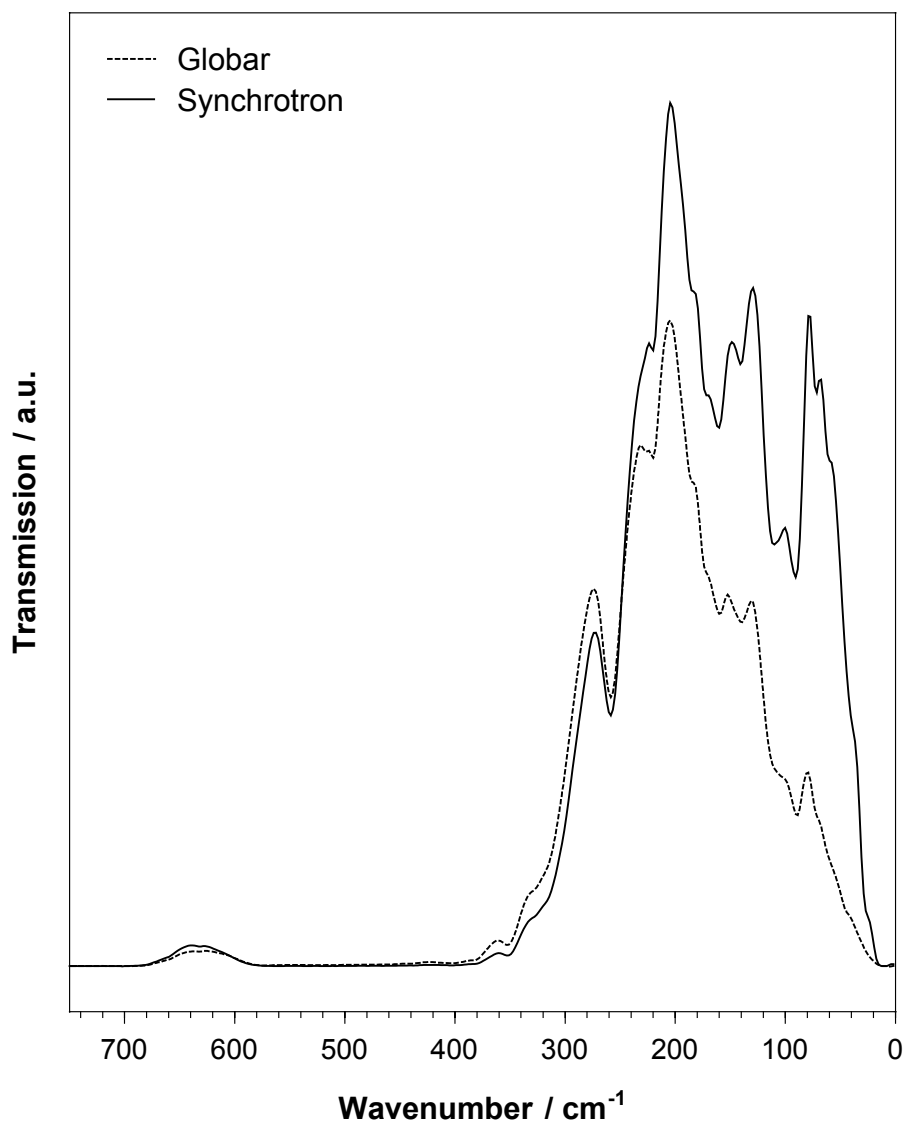


Figure 3.4 Comparison of far infrared sources: synchrotron radiation versus globar.

3.3.3 NEAR INFRARED SPECTROSCOPY (NIR: 8000 – 4000 cm^{-1})

The NIR spectra were obtained using the above mentioned Bruker IFS66/S equipped with the DRIFT accessory from Spectra-Tech. The spectrometer was equipped with a Tungsten source, a mylar beamsplitter and a DTGS detector. The powdered samples were analyzed without any dilution in a KBr matrix. For each sample, 64 scans were recorded in the 10000 – 4000 cm^{-1} range, with a scanner velocity of 5 kHz and a resolution of 4 cm^{-1} . Additionally transmission spectra were scanned, using the same instrument parameters. The KBr pellets were prepared by mixing 3 mg of sample with 500 mg KBr.

3.3.4 FT-RAMAN SPECTROSCOPY

The Raman spectra were obtained using the Bruker IFS66/S FTIR spectrometer equipped with a Bruker Raman FRA106 accessory. This comprised a Nd:YAG laser, operating at a wavelength of 1064 nm (9394 cm^{-1}) and a Raman sampling compartment incorporating a 180 degree optics. The spectrometer contained a CaF_2 beam splitter and a high sensitive germanium detector operated at liquid nitrogen temperature. Under these conditions Raman shifts can be observed in the spectral range 4000 – 120 cm^{-1} .

The spectra were obtained by pressing the sample powder into an aluminium sample holder. Measurement times between 5 and 20 min and variable power densities between 75 and 1100 mW were used to obtain the best signal/noise ratio. The spectra were recorded as single beam spectra with a resolution of 8 cm^{-1} .

Additionally some investigations were carried out on muscovite samples using a diode-laser operating at a wavelength of 785 nm (12740 cm^{-1}). These samples were also used for further measurements with dispersive Raman spectroscopy at Bruker Optics GmbH using a Sentinel spectrometer.

REFERENCES

- Diaz, M., Farmer, V.C., and Prost, R. (2000) Characterization and assignment of far infrared absorption bands of K⁺ in muscovite. *Clays and Clay Minerals*, **48**, 433-438.
- Farmer, V.C. (1974) Layer silicates. pp. 331 – 364, in: *The infrared spectra of minerals*. (V.C. Farmer, editor). Monograph **4**, Mineralogical Society, London.
- Fripiat J.J. (1981) Application of far infrared spectroscopy to the study of clay minerals and zeolites. pp. 191 – 210, in: *Advanced techniques for clay mineral analysis*. (J.J. Fripiat, editor). Developments in Sedimentology, **34**, Elsevier, Amsterdam.
- Frost, R.L. (1995) Fourier transform Raman spectroscopy of kaolinite, dickite and halloysite. *Clays and Clay Minerals*, **43**, 191-195.
- Frost, R.L., Fredericks, P.M., Klopogge, J.T., Hope, G.A. (2001) Raman spectroscopy of kaolinites using different excitations wavelengths. *Journal of Raman Spectroscopy*, **32**, 657-663.
- Gottwald W. und Wachter G. (1997) *IR-Spektroskopie für Anwender*. Verlag Wiley - VCH, Weinheim, 294 S.
- Günzler H. und Gremlich H.U. (2003) *IR-Spektroskopie*. 4. Aufl., Verlag Wiley - VCH, Weinheim, 352 S.
- Hawthorne, F.C. (ed.) (1988) *Spectroscopic methods in mineralogy and geology*. Reviews in mineralogy, **18**, Mineralogical Society of America, Washington, USA.
- Madejová, J. and Komadel, P. (2001) Baseline studies of the clay minerals society source clays: infrared methods. *Clays and Clay Minerals*, **49**, 410-432.
- McKeown, D.A., Bell, M.I. and Etz, E.S. (1999) Vibrational analysis of the dioctahedral mica: 2M1 muscovite. *American Mineralogist*, **84**, 1041-1048.
- Petit, S., Madejova, J., Decarreau, A., Martin, F. (1999) Characterization of octahedral substitutions in kaolinites using NIR Spectroscopy. *Clays and Clay Minerals*, **47**, 103-108.
- Petit, S., Martin, F., Wiewiora, A., De Parseval, P., Decarreau, A. (2004) Crystal-chemistry of talc: A near infrared (NIR) spectroscopy study. *American Mineralogist*, **89**, 319-326.
- Russell, J.D. and Fraser, A.R. (1996) Infrared methods. pp. 11 – 67 in: *Clay Mineralogy: Spectroscopic and chemical determinative methods*. (M.J. Wilson, editor). Chapman & Hall, London.
- Skoog, D.A. and Leary, J.J. (eds.) (1992) *Principles of instrumental analysis*. Saunders College Publishing, Orlando.

CHAPTER 4

ANALYTICAL METHODS

4.1 X-RAY DIFFRACTION

XRD patterns were recorded over the range of 3° to 63° 2 θ , using a Siemens D5000 diffractometer. Counting time was 2 s in 0.015° steps. Heating stage measurements were obtained on a D8 diffractometer (Bruker AXS) equipped with a TC-basic heating stage from mri – Physikalische Geräte GmbH. The heating rate was 5°C per minute in a temperature range from 20 to 1000°C and the patterns were recorded over a range of 3° to 63° 2 θ with 2 s counting time in 0.015° steps. Both diffractometers were equipped with a graphite secondary monochromator and CuK α radiation ($\lambda = 1.5418 \text{ \AA}$) was used for measurement.

4.2 ANALYTICAL CHEMISTRY

Besides the contents of the major elements Al, Si, Mg, Na, K, Ca, Fe, (Mn, P, S) and Ti the amounts of some trace elements were also analysed by X-ray fluorescence (Rb, Cs, Ni, Cu, Zn).

The measurements were done at the laboratory for geochemistry at the RWTH Aachen using an energy dispersive SPECTRO X-Lab 2000 spectrometer, equipped with a nitrogen cooled Si(Li)detector. The spectrometer used three different targets for the polarization of the X-rays (Molybdenum, Al₂O₃, HOPG, Table 4.1). Therefore the voltages varied between 12 and 50 kV and the currents varied between 2 and 12 mA during the measurements.

Due to the small amounts of treated muscovites, the sample preparation was difficult. The best results were obtained by using plastic cylinders covered with a mylar foil.

Table 4.1 Used targets for the excitation of the elements between Na and U.

Target	Type of target	Elements	Voltage
Mo	Secondary	Cr – Y (K), Hf – U (L)	40 kV
Al ₂ O ₃	Barkla	Zr – Ce (K)	55 kV
HOPG	Bragg	Na – V (K)	15 kV

In these cylinders 200 mg of the fine grained sample powder was filled. To stabilize the powder, it was suspended in 1 ml Elvacit solution (40 g Elvacit in 800 ml acetone). To avoid the formation of bubbles during the evaporation of the acetone, the suspensions first were dried one hour at room temperature and then two hours at 40°C.

In addition, pellets of the original muscovite and of the dickite (San Juanito) were produced by mixing and pressing 4 g of sample powder with 0.9 g of HoechstWax (Fluxana BM-0002-1 Licowax C Micropowder PM). They were measured under the same conditions as the Elvacit-samples.

4.3 MICROSCOPIC TECHNIQUES

4.3.1 ELECTRON MICROSCOPY

Environmental Scanning Electron Microscopy (ESEM)

The examination of the changes in particle morphology and of the grain size distribution by the nitrate treatment was carried out by an environmental scanning electron microscope (ESEM) using a Philips ESEM XL 30 FEG. This kind of SEM uses a chamber atmosphere of 1 – 3 Torr water vapour instead of high vacuum. Because the instrument is equipped with a special gaseous secondary electron detector (GSE-detector), sputtering of the samples with conductive material like gold or carbon is not necessary. Therefore it is particularly suitable for the investigation of sensitive samples like intercalated phyllosilicates. In our investigations a chamber atmosphere of 1 Torr and an acceleration voltage of 10 – 15 kV was applied. The investigation of the grain size distribution was done by examination of 60 particles per sample, similar to a method used in sedimentary petrography (point-counting).

High resolution transmission electron microscopy (HRTEM)

Transmission electron microscopy was used to obtain informations about the changes in the arrangement of the layers due to the chemical modification of the samples.

Therefore a special preparation technique was used to achieve oriented phyllosilicate samples (Elsass et al., 1998). First a textured sample was produced by drying a muscovite suspension. Pieces of this sample were fixed in Agar and were saturated in water for two days. The embedding process consisted of 12 successive exchanges, as described in Table 4.2. The first step consisted in replacing the water by immersing the samples in methanol (four times). Then the methanol was progressively replaced by 1,2-propyleneoxide (three baths of different proportions of methanol and propyleneoxide: $\frac{1}{3}$, $\frac{1}{2}$ and $\frac{2}{3}$). This was followed by three exchanges with pure 1,2-propyleneoxide. Afterwards the 1,2-propyleneoxide was half replaced by Spurr resin and stored over night to evaporate the 1,2-propyleneoxide. The last exchange was carried out with pure resin. Then it was filled in TEM-forms and polymerised for 24 hours at 60°C.

Table 4.2 Steps of the TEM embedment procedure for oriented clay samples. (According to Elsass et al. 1998).

Liquid	Exchanges	Time
Water	Initial state	2 days
Methanol	4 exchanges	30 minutes
Methanol / 1,2-propyleneoxide	3 exchanges	30 minutes
1,2-propyleneoxide	3 exchanges	30 minutes
Resin / 1,2-propylene oxide	1 exchange	12 hours
Resin	1 exchange	4 hours
Resin	1 exchange	24 hours, polymerisation at 60°C

The samples were cut into ultra thin sections (100 nm) using a Leica Ultracut UCT microtome. The thin sections were fixed on TEM-nets covered with carbon foils (“Lacey films” on Cu-nets, mesh size: 3.05 mm). Due to the preparation technique, these specimens allowed the observation especially of the (001)-layers of the treated muscovite particles and of possible interstratifications.

At the Laboratory for Electron Microscopy (LEM) in the physics department of the university of Karlsruhe a Philips CM 200 FEG microscope with a super twin lens was employed for HRTEM imaging. The microscope was equipped with a field emission gun, operating at a high tension of 200 kV and spot size 2 was normally chosen for the bright field imaging. The photographs were obtained using the highest possible aperture. To reduce the effects of damage by the electron beam, the specimens were examined at the lowest possible beam intensity. Most images were obtained at magnifications of 300.000x and 380.000x, while the selected area electron diffraction (SAED) patterns were obtained with a camera length of 1.3 m.

As noted by other researchers (Robertson and Eggleton, 1991; Ma and Eggleton, 1999) clay minerals, especially mixed layers are very difficult to work with under the TEM. Therefore the majority of the area recorded on most images does not contain much information, maybe due to an extensive beam damage. Due to this damage, in some cases it was not possible to record both bright field images and electron diffraction patterns from the same area. Hence, good results were obtained by moving across the specimen under HRTEM conditions, finding areas that were aligned to show clear basal lattice fringes, then focusing quickly and recording the image immediately on film. Only then the orientation was checked briefly by electron diffraction patterns.

4.3.2 ATOMIC FORCE MICROSCOPY (AFM)

For the measurement of the particle thickness of original and treated muscovites investigations with an AFM were carried out. The images were made on a Digital Instruments Nanoscope III MultiMode SPM, operating in contact mode. The AFM was operated with Si_3N_4 cantilevers (ESP-CONT W) to obtain images in height- and deflection mode.

The AFM samples were prepared by dispersing 3 mg muscovite powder in 50 ml deionised water (10 min. ultrasound). A small volume of the suspension was dropped on a polished Al_2O_3 disc and dried at 90°C.

4.4 SPECIFIC SURFACE AREA (BET-METHOD)

Information about the degree of delamination of the treated muscovite was obtained from the increase in the specific surface areas of the treated samples. To that the adsorption of nitrogen was performed according to the BET-method, using a Quantachrome Autosorb-1 (e.g. Brunauer, et al. 1932, Gregg and Sing, 1991). 7-point BET were performed, whereas the sorption isotherm was composed of 40 adsorption and 20 desorption points (Outgassing conditions: 24 hours under vacuum at 105°C).

REFERENCES

- Brunauer, S., Emmett, P.H. and Teller, E. (1932) Adsorption of gases in multimolecular layers. *Journal of the American Chemical Society*, **60**, 309-319.
- Elsass, F., Beaumont, A., Pernes, M., Jaunet, A.-M., and Tessier, D. (1998) Changes in layer organisation of Na- and Ca-exchanged smectite materials during solvent exchanges for embedment in resin. *The Canadian Mineralogist*, **36**, 1475 – 1483.
- Gregg, S.J. and Sing, K.S.W. (1991) *Adsorption, surface area and porosity*. 2nd ed., Academic Press, London, 303 pp.
- Ma, C. and Eggleton, R.A. (1999) Surface layer types of kaolinite: a high-resolution transmission electron microscope study. *Clays and Clay Minerals*, **47**, 181 – 191.
- Robertson, I.D.M. and Eggleton, R.A. (1991) Weathering of granitic muscovite to kaolinite and halloysite and of plagioclase-derived kaolinite to halloysite. *Clays and Clay Minerals*, **39**, 113 – 126.

CHAPTER 5

MINERALOGICAL CHARACTERIZATION OF THE METAL-NITRATE TREATED MUSCOVITES

5.1 INTRODUCTION

In this chapter the physical effects of the nitrate treatment on the muscovite crystals are discussed. Moreover the main focus lies on the interactions of the di- and trivalent cations Al^{3+} , Cu^{2+} , Mg^{2+} , Zn^{2+} with the mica structure. This results in the following questions to be answered: Is it possible to intercalate the cations into the interlayers and does this lead to a delamination of the mica sheets?

Therefore several microscopic techniques are used to investigate the morphology of the obtained products and to determine the changes in their grain size distribution. Additionally the results of specific surface area measurements are used to calculate the particle thickness of the delaminated micas. In the second part of this chapter the mineral phases are characterized by X-ray diffraction and HRTEM imaging. Upon the XRD-data, the crystallographic parameters of the new phase are calculated.

5.2 MATERIALS AND METHODS

For the characterization of the treated muscovites several microscopic and analytical methods were used. All of them were described in detail in the previous chapter. Therefore here only a short overview of the used methods is given.

The morphological investigations and the measurement of the grain sizes were done on a Philips ESEM XL 30 FEG and on a Digital Instruments Nanoscope III MultiMode SPM. Specific surface areas (SSA) were measured,

according to the BET method, using a Quantachrome Autosorb-1. The chemical data were obtained by X-ray fluorescence analysis, on a energy dispersive SPECTRO X-Lab 2000 spectrometer.

For structural investigations HRTEM and X-ray diffractometry were used. The XRD patterns were recorded over a range between 3° and 63° 2θ on a Siemens D5000 diffractometer. The HRTEM imaging was done on a Philips CM 200 FEG, equipped with a super twin lens.

Because of the general difficulties in getting useful Rietveld refinements of the clay mineral cell parameters from the XRD-patterns (e.g. Moore and Reynolds 1997), the parameters were calculated with the cell parameters refinement program "CelRef", using single line fitted XRD-data.

The peak fitting was done with the Jandel Peakfit software package. A Voigt function was chosen, with the minimum number of peaks used for the fitting process. A linear 2-point background was chosen and fitting was undertaken until reproducible results were obtained with squared correlations of $r^2 > 0.997$.

CelRef V3 (Laugier and Bochu, 2003) is a least square refinement method. The refinements were undertaken by using at least eight fitted peaks until reproducible results were obtained with mean square deviations < 0.01 . As starting values for the cell parameter calculations those of muscovite ($a = 5.19$ Å, $b = 9.02$ Å, $c = 20.13$ Å, and $\beta = 95.5^\circ$) and of rectorite ($a = 5.13$ Å, $b = 8.88$ Å, $c = 23.85$ Å, and $\beta = 96.3^\circ$) were chosen. The refinements were done in the two space groups C2/c and C2.

5.3 RESULTS AND DISCUSSION

5.3.1 GRAIN SIZE DISTRIBUTION AND STACK THICKNESS

Electron microscopy. The ESEM images in Figure 5.1 illustrate the strong morphological changes of the muscovite particles (Figure 5.1a, MU-0), due to the nitrate treatment (Figure 5.1b-d). Thereby the flakes not only are cleaved parallel to the sheets, but also deep cracks arise on the surfaces with increasing treatment time, which lead to a remarkable grain size decrease (Figures 5.1b,

and 5.1c). Furthermore Figure 5.1d shows, that the margins of the mineral often fan out and roll up (similar to halloysite or hydrated kaolinite). This also contributes to the grain size decrease. The changes in the grain sizes were calculated by measuring the sizes of about 60 particles in the electron microscope (ESEM) for each cation-treatment, similar to the point-counting method in sediment petrography (Figure 5.2).

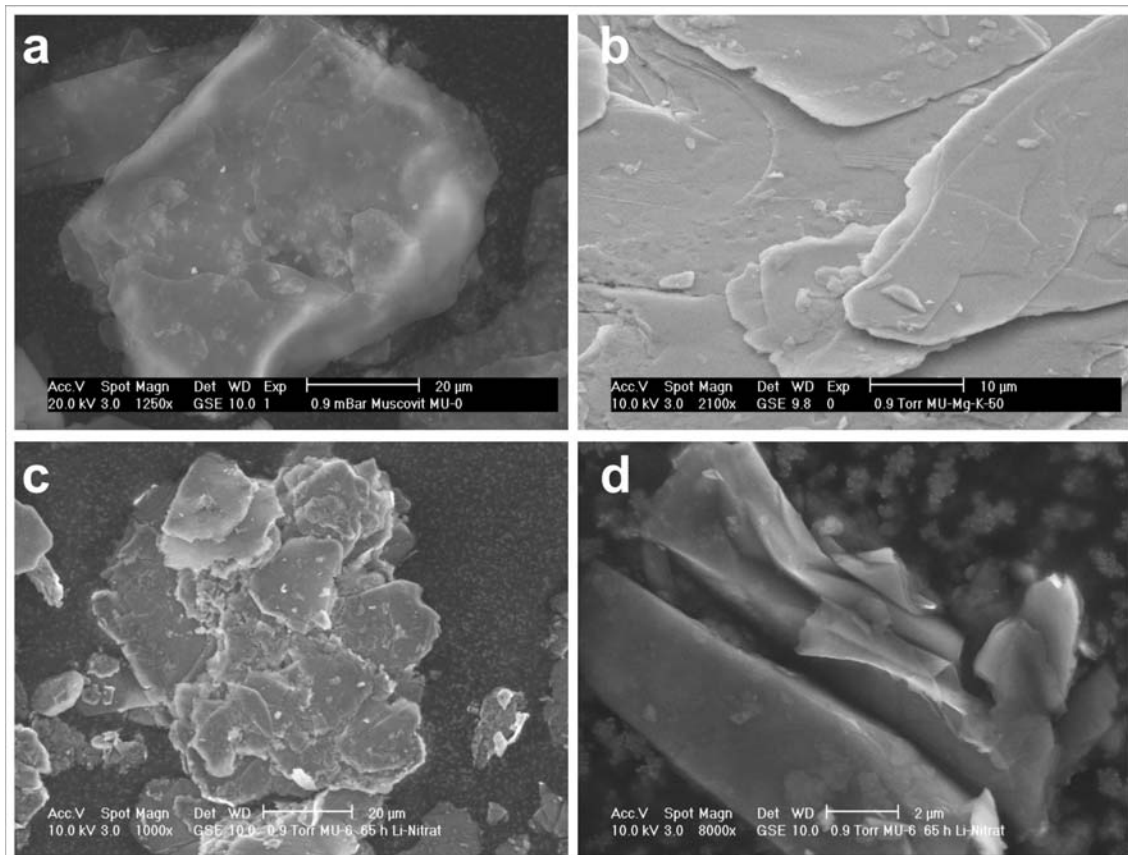


Figure 5.1 ESEM-images showing the morphological changes of the muscovite crystals, due to the nitrate-treatment. a) Original, untreated material (MU-0) with a smooth morphology. Notice the rounded edges and the flat surface. b) Cleaved stacks on the surface of a treated particle. c) Deep cracks through the sheets cause a strong decrease in grain size d) The margins of this small particle fan out and roll up, also leading to a delamination of the particle.

The original muscovite (MU-0) has a medium diameter (median) of about 100 µm and an additional minor maximum at 70 µm. It decreases to 60 µm due to the Mg-nitrate treatment. The median of the Zn-nitrate treated samples decreases to 40 µm and that of the Cu-muscovites to 50 µm. Furthermore the treated muscovites show a very good unimodal sorting of the particles.

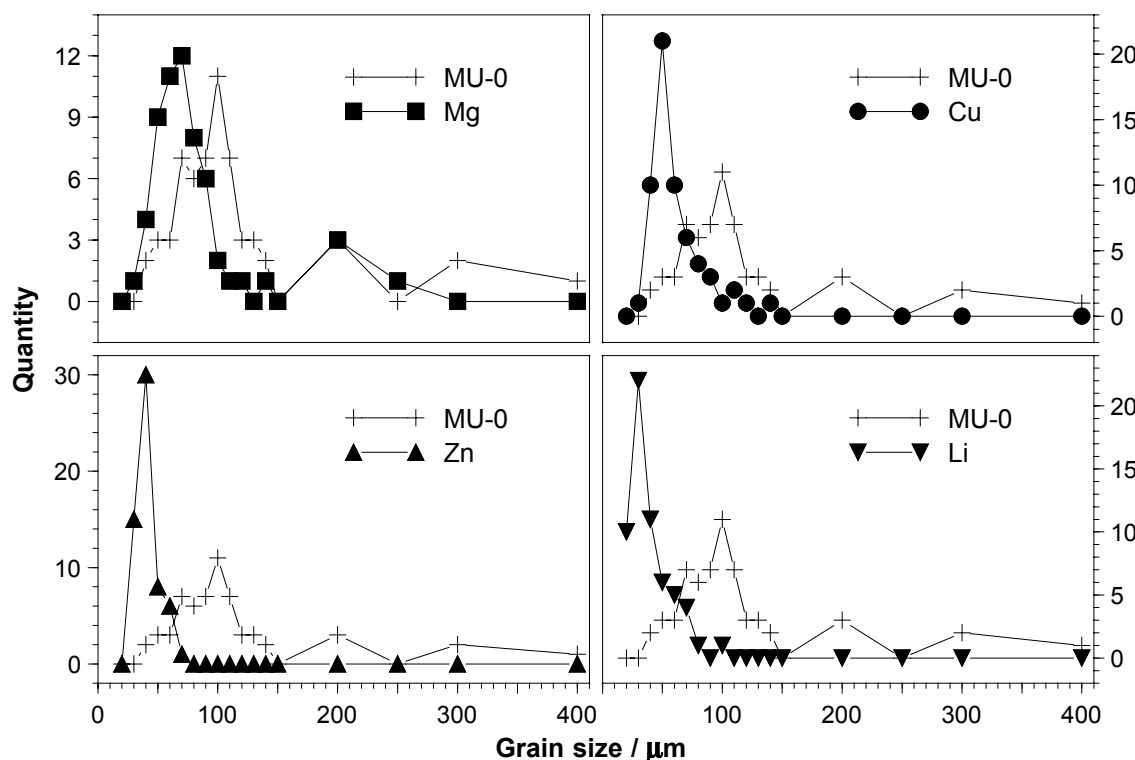


Figure 5.2 Changes in the grain size distributions, due to the treatment with the different nitrates. All the treated muscovites show a remarkable decrease of the medium diameters.

In contrast to this, the original muscovite powders have a broad size spectrum, with some very large crystals ($> 250 \mu\text{m}$) in a matrix of smaller particles.

Atomic force microscopy. The AFM-images (deflection mode) presented in Figure 5.3 show the decrease in particle thickness due to the Mg-nitrate treatment. As it is only possible to measure the smallest fraction of the material (especially of the original muscovites), because of height limitations of the AFM, no systematic investigations of the micas are practicable with this method. Nevertheless, these first measurements clearly show the tendency of the muscovites to decreasing grain sizes and particle thicknesses, due to the nitrate-treatment.

Specific surface areas. N_2 -absorption measurements with the BET-method revealed a strong increase of the specific surface areas due to the nitrate treatments. For example the Mg-nitrate treatment leads to an increase from $8.1 \text{ m}^2 \text{ g}^{-1}$ up to $84.5 \text{ m}^2 \text{ g}^{-1}$ after a treatment time of 280 hours (Figure 5.4). In

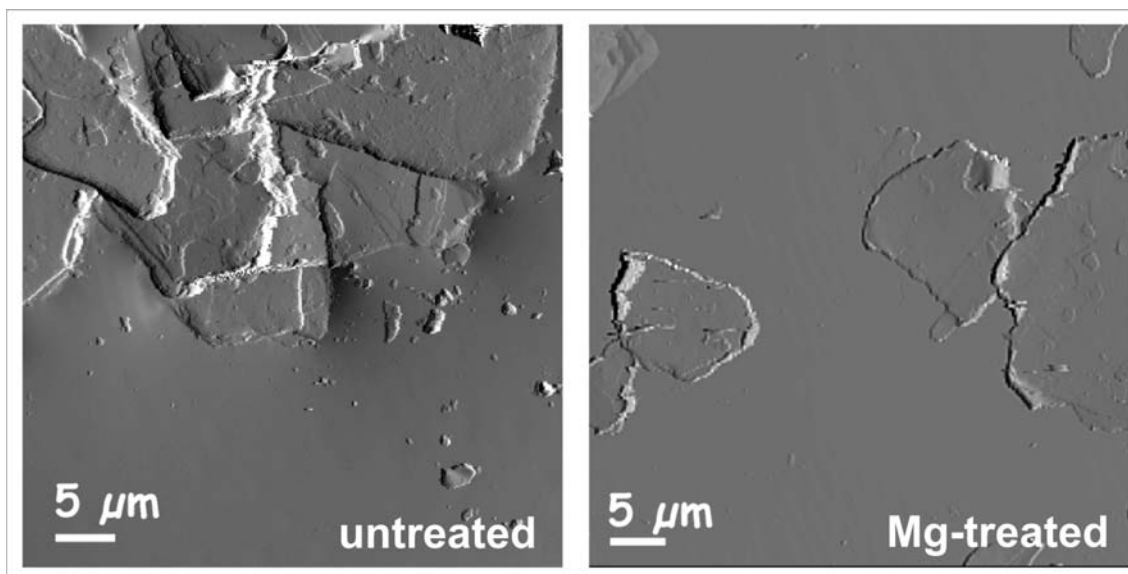


Figure 5.3 AFM-images (deflection mode) of an untreated original muscovite and of a Mg-treated sample showing the decrease in particle height, due to the treatment.

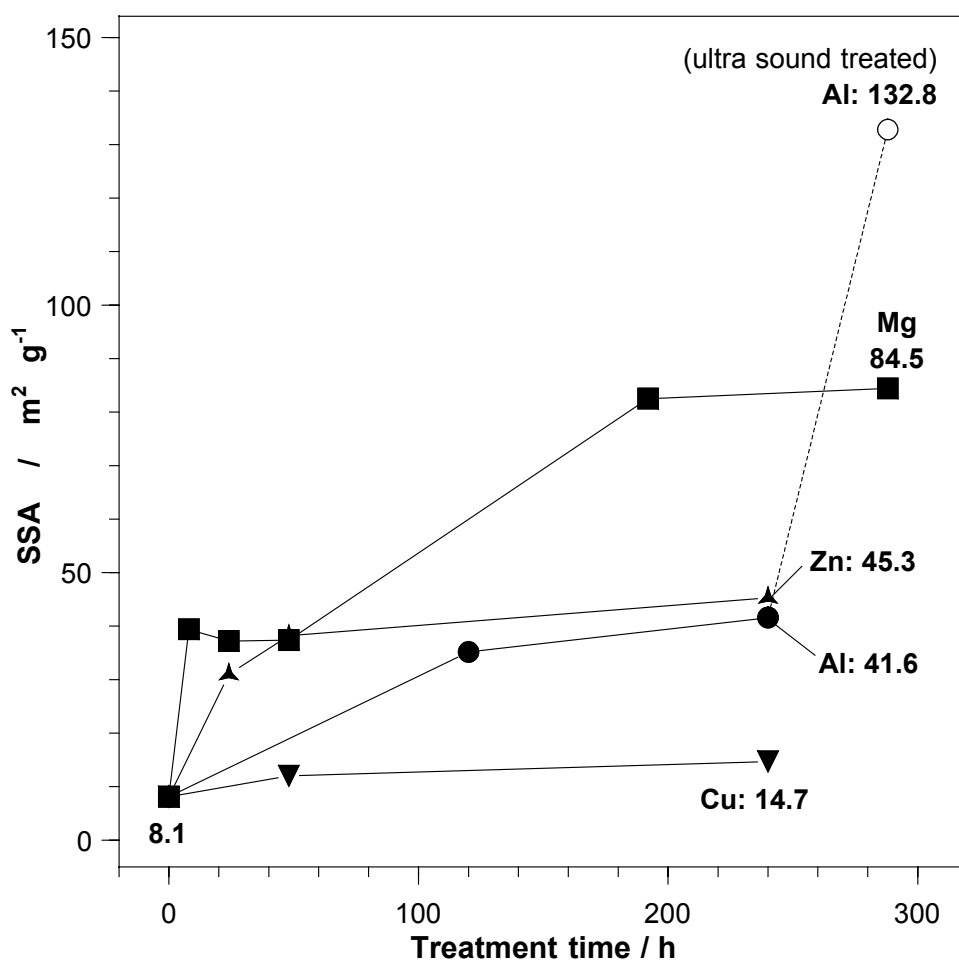


Figure 5.4 Increasing specific surface areas due to the treatment with several nitrate salts. Additional use of ultra sound increases the surface areas drastically.

contrast to that, the Cu-muscovite only shows a much lower increase of the surface area to $14.7 \text{ m}^2 \text{ g}^{-1}$.

The treatment with Al- and Zn-nitrate for 240 hours reveals a remarkably increased SSA of 41.6 and $45.3 \text{ m}^2 \text{ g}^{-1}$, respectively. A further treatment with ultra sound increases the surface area of the Al-muscovite up to $132.8 \text{ m}^2 \text{ g}^{-1}$.

From N_2 -data there are no hints for the existence of micropores. This means that the measured changes in the specific surface areas are only caused by the delamination of the sheets. With this assumption the particle heights can be calculated by transforming some simple equations. For example the aspect ratio (AR) of phyllosilicates is given by:

$$\mathbf{AR = diameter / thickness = AR = d / h} \quad (\text{Equation 1})$$

$$\rightarrow \mathbf{d = AR \times h, \text{ or } h = d / AR}$$

while the specific surface area (SSA) is given by (V = volume, ρ = *specific density* = $2,6 \times 10^6 / \text{g m}^{-3}$):

$$\mathbf{SSA = area / mass = A / M}$$

With mass (M) = volume (V) x specific density (ρ) this reveals:

$$\mathbf{SSA = A / (V \times \rho)} \quad (\text{Equation 2})$$

The surface area (A_0) of a flat cylinder can be used as first approximation for the SSA of a muscovite stack, hence:

$$\mathbf{A_0 = 2 A_G + A_M, \text{ with}} \quad (\text{Equation 3})$$

$$A_G = \text{Area of the cylinder faces} = \pi \times r^2$$

$$A_M = \text{Area of the cylinder sides} = 2 \times \pi \times r \times h \quad r = d / 2$$

$$\rightarrow \mathbf{A_0 = 2 \times \pi \times r^2 + 2 \times \pi \times r \times h = 2 \times \pi \times r^2 \times (r+h)}$$

The volume of a flat cylinder is given by:

$$\mathbf{V_{cyl} = \pi \times r^2 \times h} \quad (\text{Equation 4})$$

Combining with $r = d/2$ and transforming these equations gives Equation 5, which then can be used to calculate the particle height:

$$\mathbf{SSA = (2d + 4h) / d \times h \times \rho} \quad (\text{Equation 5})$$

With this equation the number of layers of the delaminated materials can be estimated. For example the particle thickness of Mg-treated muscovite particles with a SSA of $84,5 \text{ m}^2\text{g}^{-1}$ decreases to 30 nm, respectively 30 layers.

5.3.2 X-RAY DIFFRACTION AND HRTEM

In the following part the results of the autoclave experiments are compared to the results of the treatment in round bottom flasks according to the method of Caseri *et al.* (1992).

Autoclave experiments. The X-ray pattern of the untreated muscovite (MU-0) is shown in Figure 5.5. According to the data presented in Table 5.1, this mica is assigned to a muscovite- $2M_1$, which has a monoclinic symmetry and crystallizes in the space group No. 15 $C2/c$ (Bailey 1980, 1987). Significant for this symmetry is the lack of the d_{001} -peak. Thus, the first peak, which is visible in the range between 3° and $10^\circ 2\Theta$ is the d_{002} at 1.02 nm ($8.8^\circ 2\Theta$). According to this space group the refined cell parameters of the $2M_1$ muscovite are: $a = 5.19 \text{ \AA}$, $b = 9.02 \text{ \AA}$, $c = 20.13 \text{ \AA}$, and $\beta = 95.5^\circ$ (Bailey, 1980).

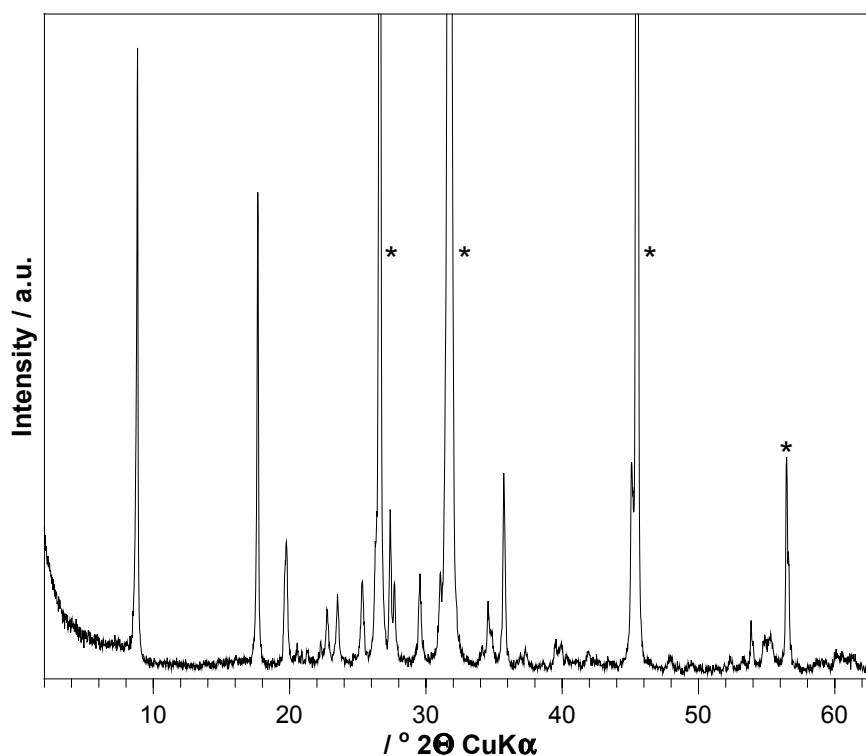


Figure 5.5 X-ray pattern of the untreated muscovite (MU-0) in the range between 2° and $63^\circ 2\Theta$. (*) assign the peaks of NaCl, which was used as internal standard.

Table 5.1 X-ray powder data of the untreated muscovite MU-0 compared to literature data of a $2M_1$ -muscovite. Spacings in nm.

<i>d</i> -spacings		<i>hkl</i>
Brindley and Brown, (1980)	This study	
1.014	1.035	002
0.500	0.502	004
0.448	0.448	110
0.446	0.446	11-1
0.439	-	021
0.429	0.432	111
0.411	0.416	022
0.397	0.399	112
0.389	0.391	11-3
0.374	0.378	023
0.350	0.352	11-4
0.335	0.326	006
0.321	0.322	114
0.299	-	025
0.287	0.288	115
0.280	0.278	11-6
0.259	0.262	13-1
0.258	0.259	116
0.256	-	20-2
0.251	0.251	008
0.246	-	13-3
0.245	0.243	202
0.240	0.241	20-4
0.238	0.233	133
0.225	0.226	040
0.224	0.225	041
0.220	-	221
0.218	0.215	22-3
0.215	-	222
0.213	-	135
0.205	0.209	044
0.201	0.201	00 10
0.198	0.190	13-7
-	0.184	
0.174	0.175	13-9
0.170	0.170	150

The treatment with Al-, Cu-, Mg-, and Zn-nitrate in the autoclaves results in strong changes in the XRD patterns (Figure 5.6). Especially in the range between 3° and $10^\circ 2\theta$ all patterns show the development of two new broad

peaks at around 1.1 and 2.3 nm. The new peaks strongly increase their intensities with increasing reaction time, while at the same time the intensity of the d_{002} -peak of the original muscovite strongly decreases and nearly disappears in the shoulder of the new peak at 1.1 nm ($7.9^\circ 2\theta$). Figure 5.7 shows these changes in a time series of a Cu-nitrate treated sample. Additionally, over the entire range between 3° and 63° most of the original muscovite peaks decrease their intensities and get broader during the treatment, while their 00l-peaks slightly shift positions and decrease their intensities only to a minor degree.

The occurrence of these new peaks and the changes of the 00l-peaks in the XRD-patterns prove, that the treatment with metal-nitrate salts results in a strong increase of the interlayer space. This means, that the metal-ions can not only be adsorbed on the muscovite surfaces. But they are in fact intercalated into the interlayers of the mineral.

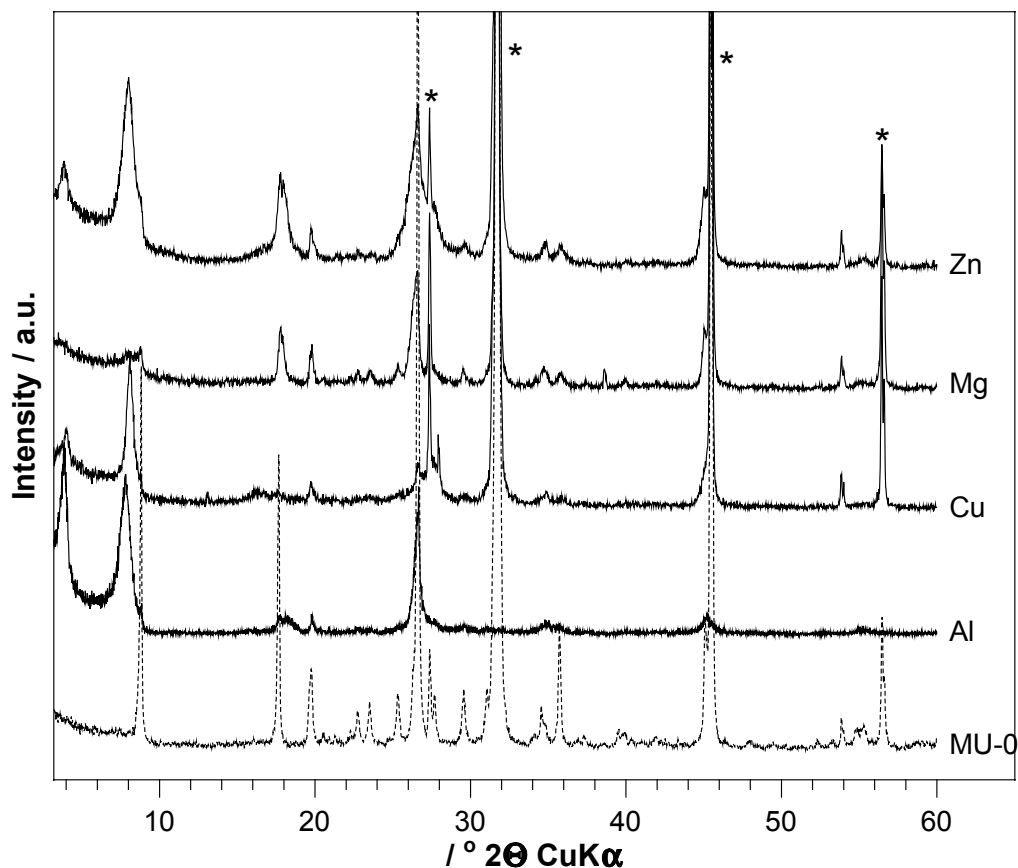


Figure 5.6 Observed changes in the XRD-patterns, due to the autoclave treatment with various nitrate salts. Again the (*) assign the peaks of NaCl.

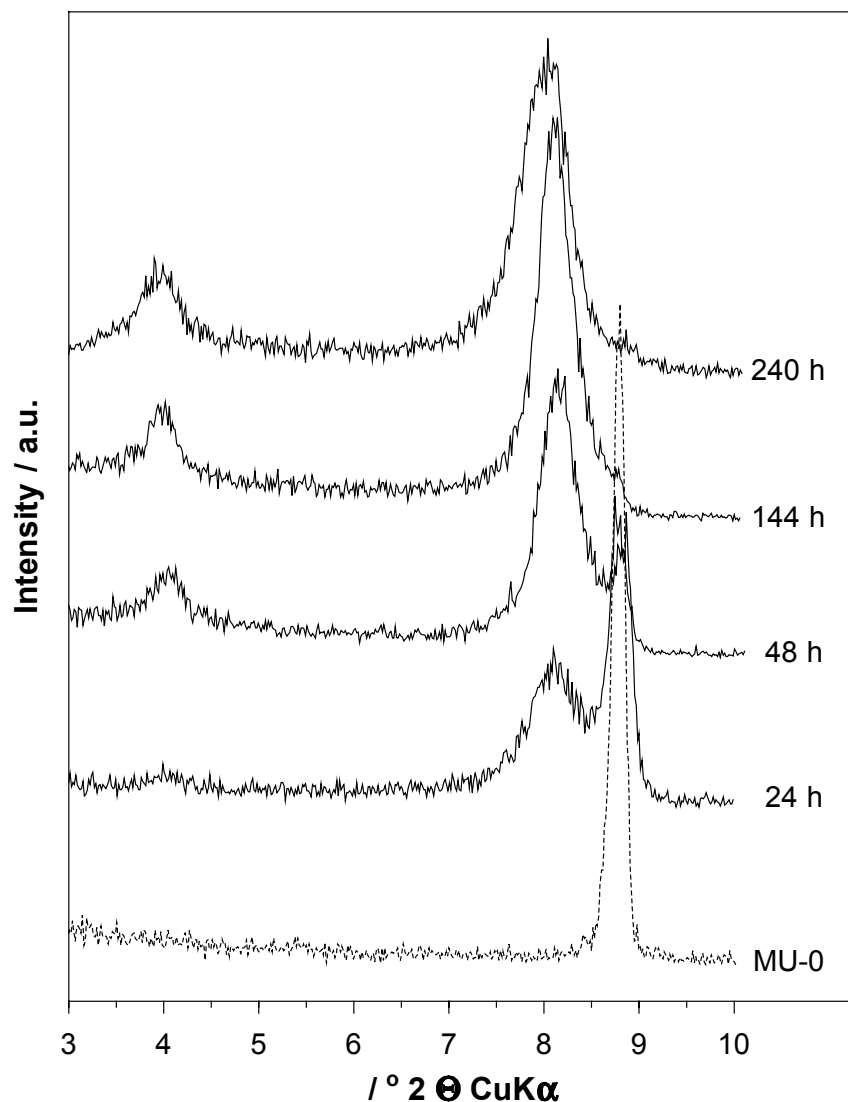


Figure 5.7 The XRD patterns of a Cu-intercalated muscovite show the development of the new peaks at 1.1 nm and 2.1 nm in dependence of the treatment time. At the same time the d_{002} of the original MU-0 strongly decreases.

This results in the formation of a mixed-layer structure, consisting of already intercalated “smectite”-layers and relatively unaffected “original” muscovite-layers. Because the patterns show irrational series of basal reflections, this new phase is assigned to an irregular muscovite-‘smectite’ mixed-layer (Moore and Reynolds, 1997). A chemically similar, regular muscovite-smectite mixed-layer structure is described by several authors as rectorite (e.g. Kodama, 1966; Bailey, 1980; Jakobsen *et al.*, 1995).

As the chemical data in Table 5.2 show, the intercalation of the bi- and trivalent cations is no simple ion exchange mechanism of the interlayer potassium versus the new cations. However, no strong decrease of the

potassium amount is detectable during the treatment. Thus it can be assumed, that the K^+ as well as the Al^{3+} -, Mg^{2+} -, Cu^{2+} -, or Zn^{2+} -ions appear together in the interlayer region, which is one of the main reasons for its expansion.

Table 5.2 Chemical data of the treated muscovites. A comparison of the data after treatment times of 48 and 240 hours show no strong decrease of the potassium amounts.

Treatment time / h	Gew.-%							
	Al ₂ O ₃	K ₂ O	CuO	K ₂ O	MgO	K ₂ O	ZnO	K ₂ O
untreated	38.7	9.2	-	9.2	-	9.2	-	9.2
48	38.5	9.2	0.8	9.1	0.5	9.2	2.1	9.1
240	37.3	8.9	2.2	8.5	1.1	9.1	3.2	8.8

The mixed-layering of the nitrate treated micas can also be shown by high-resolution TEM imaging. Figures 5.8a and 5.8b are examples of lattice fringe images of a Cu-treated muscovite. The treated phases show small domains with fringes having a spacing of 2.2 nm. Between them weaker fringes (with lower contrast) are visible with a spacing of 1.1 nm, resulting in a so called two-layer periodicity (Figure 5.8a). Ahn and Peacor (1986) described such variations in contrast in HRTEM images of mixed-layers either by differences in the structure or in the chemistry of alternate layers. This is consistent with the chemical data presented above. Figure 5.8b emphasizes the irregular interstratification of the layers. Regions with spacings of 2.2 nm are divided by small regions with lattice fringes having spacings of 1.1 nm (arrows).

These new peaks are assigned to the d_{001} and d_{002} of the intercalated mixed-layer phase. This means, that the incorporation of the cations leads to strong changes in the crystal symmetry and therefore in the extinction rules. Thus the calculation of the cell parameters is only possible in a space group of lower symmetry. Accordingly, for the refinement of the parameters shown in Table 5.3 the space group No.5 C2 had to be chosen.

Table 5.3 Results of the CelRef-calculations for the cell parameters of the intercalated mixed-layer phases. (In parenthesis the space groups are given in which the calculations were done.)

Cell-parameter	Muscovite (C2/c)	Cu (C2)	Zn (C2)	Mg (C2)	Al (C2)
<i>a</i>	5.199	5.006	5.011	5.019	5.096
<i>b</i>	9.021	8.925	9.031	9.030	9.032
<i>c</i>	20.134	21.887	22.525	22.335	23.045
β	95.54	93.57	97.40	95.23	93.33

Surprisingly the intercalation not only leads to an expansion along the *c*-axis, but also to a decrease of the *b*-lattice-parameter. While the expansion along the *c*-axis can be explained by the intercalation procedure and the occurrence of both the foreign cations and the potassium in the interlayers, the shrinkage along the *b*-axis possibly occurs due to a distortion and rotation of the tetrahedral layers during the migration of the small cations into the muscovite lattice structure as it is observed for cations like Cu and Li in smectites (e.g. Trillo et al., 1993; Heller-Kallai et al. 1995).

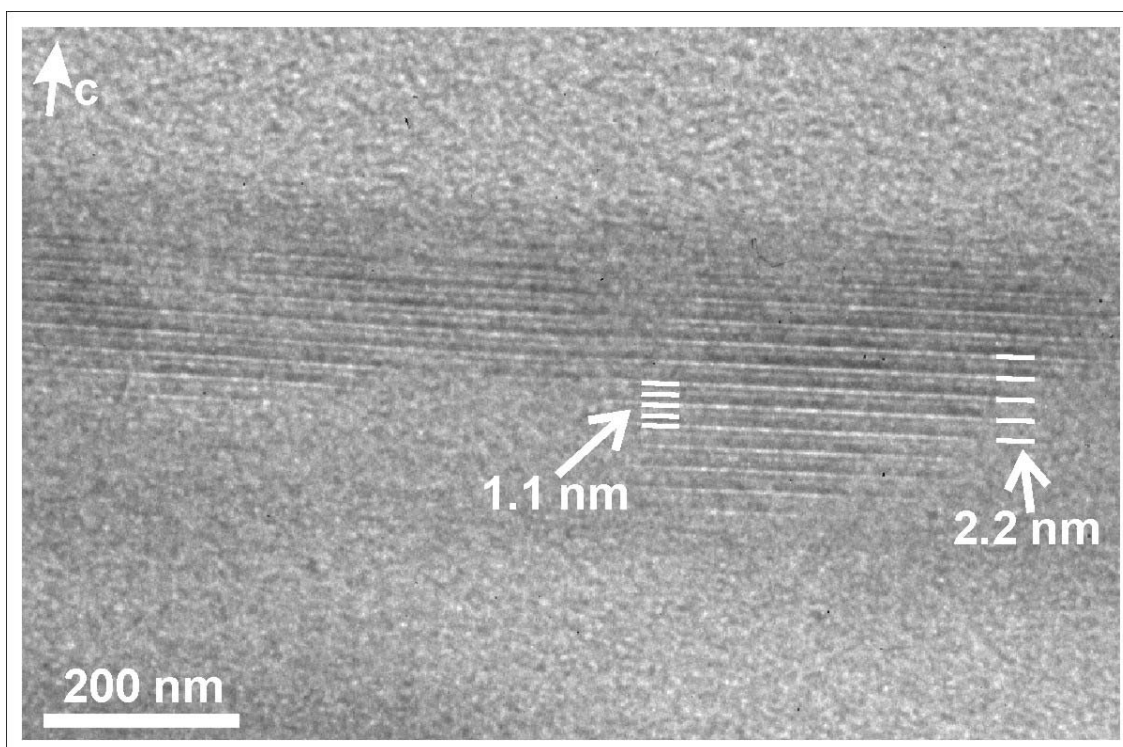


Figure 5.8a HRTEM image of Cu-nitrate treated muscovite showing the expansion along the *c*-axis. The intercalated sample contains domains with a so called two-layer periodicity having lattice fringes with spacings of 2.2 nm, between weaker fringes are visible with spacings of 1.1 nm. (x 380000).

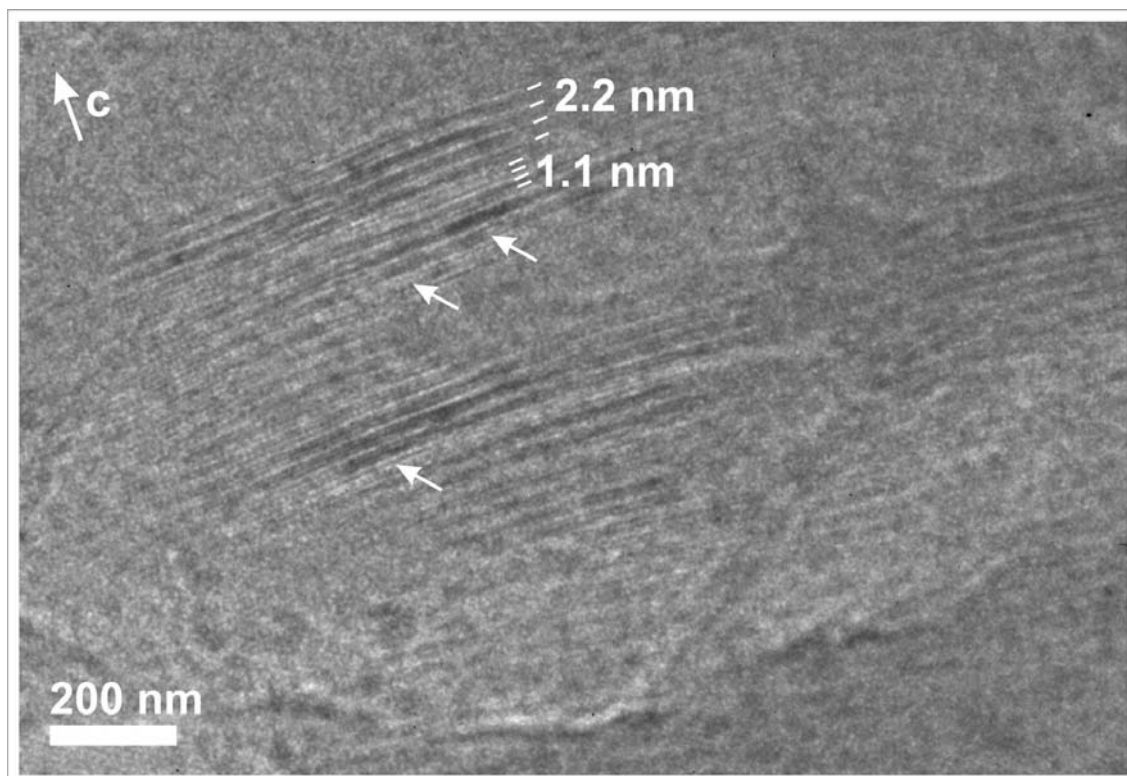


Figure 5.8b This lattice fringe image shows the irregular interstratification of the new mixed-layer phase. Domains with spacings of 2.2 nm are divided by small regions, having spacings of 1.1 nm (arrows). (x 380000).

Round-bottom-flask experiments. In contrast to the autoclave-treatments, the experiments in the round-bottom-flasks, according to the conventional method of Caseri et al. (1992) showed essentially no changes in the XRD-patterns (Figure 5.9). According to Table 5.4 only the treatment with Al- and Cu-nitrate solutions in round-bottom-flasks produced nearly the same changes in peak positions as the autoclave treated samples, but much longer treatment times were necessary (more than two weeks).

In contrast to the autoclave experiments the Cu-nitrate treated samples are of bluish to greenish colour and strongly increased their masses (starting weight: 0.250 g, product weight: 2.6 g). These materials showed additional strong peaks assigned to the copper-nitrate-hydrate gerhardtite $\text{Cu}_2(\text{NO}_3)(\text{OH})_3$, which is naturally formed during the evaporation of copper-nitrate-solutions (Figures 5.10) (Holleman and Wiberg, 1985; Rösler, 1991). Lots of small gerhardtite-needles are formed on the muscovite surfaces, which are impossible to be isolated from the particles (Figure 5.11).

Table 5.4 Comparison of the observed peak positions of autoclave and round bottom flask treated samples in the range between 3° and $10^\circ 2\theta$.

Nitrate	Parameters		XRD-Peaks / nm
	Temperature	Method ²⁾	
Al	$112^\circ\text{C}^{1)}$	RBF	1.03, 1.14, 2.25
	150°C	Auto	1.03, 1.13, 2.27
Cu	135°C	RBF	1.03, 1.11, 2.21
	140°C	Auto	1.03, 1.11, 2.19
Mg	$115^\circ\text{C}^{1)}$	RBF	1.03
	190°C	Auto	1.00, 1.08, 2.31
Zn	$119^\circ\text{C}^{1)}$	RBF	1.05
	170°C	Auto	1.02, 1.17, 2.39

1) At these temperatures the suspensions boiled.

2) RBF = Round-bottom-flask (Caseri et al. 1992), Auto = Autoclave experiments

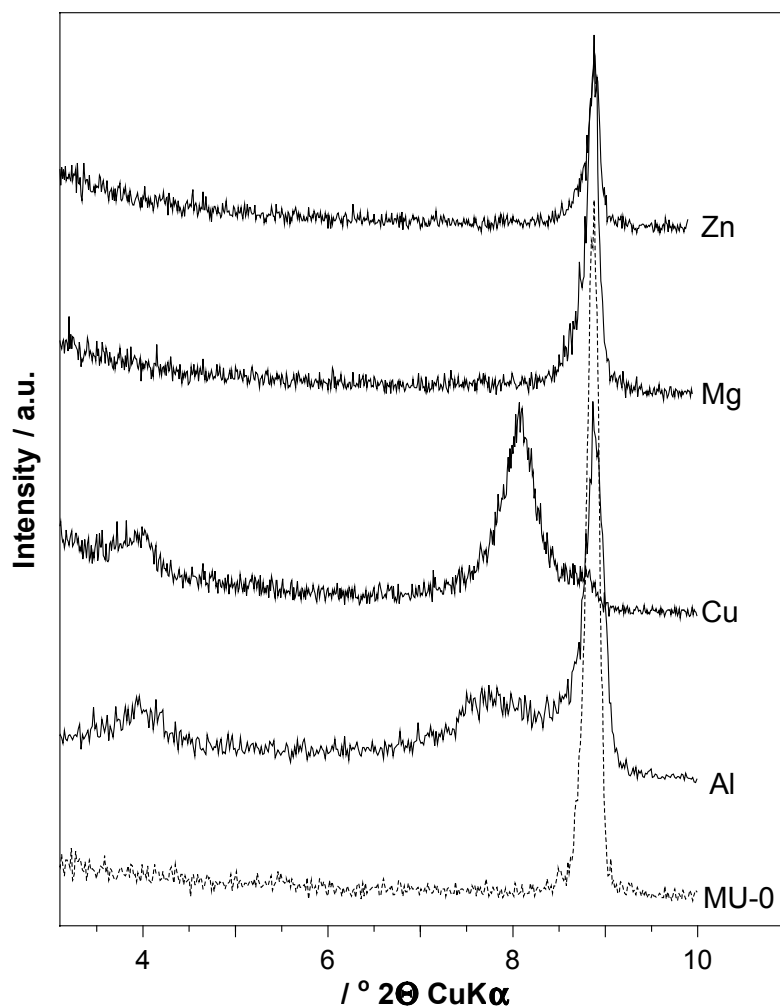


Figure 5.9 Observed changes of the 00l peaks in the range between 3° and $10^\circ 2\theta$, due to the round-bottom-flask treatment with various nitrate salts.

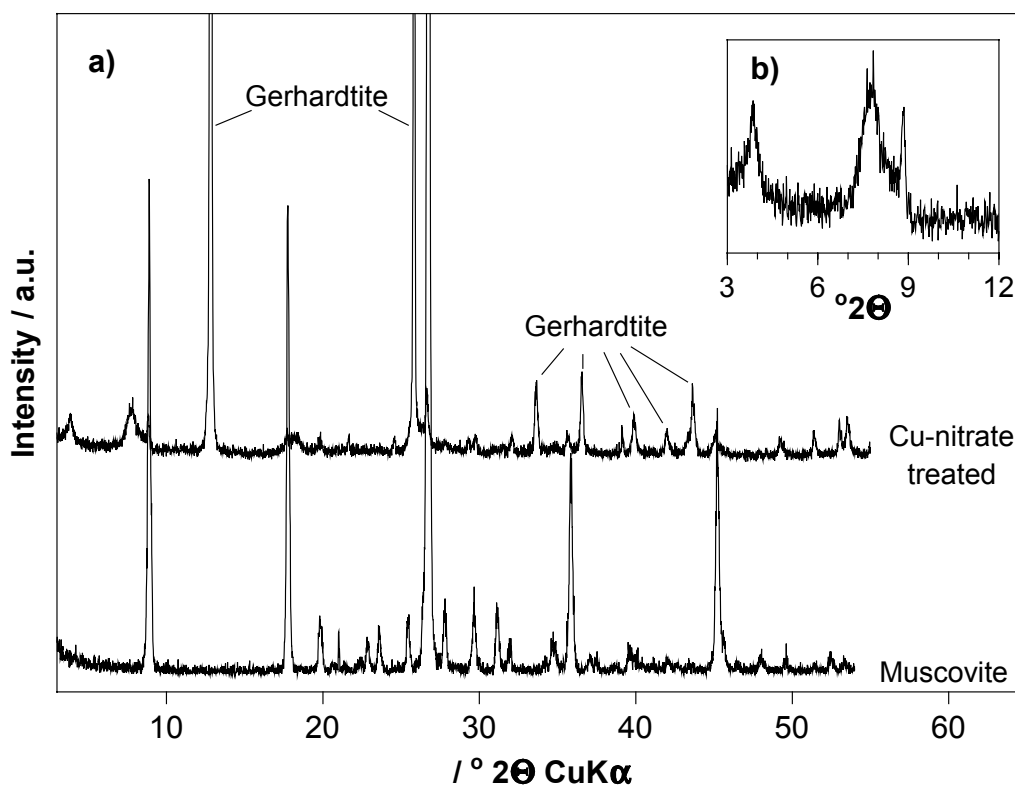


Figure 5.10 XRD pattern of a Cu-muscovite treated in a round-bottom-flask. a) range between 3 and 55° 2 θ with strong gerhardtite ($\text{Cu}_2(\text{NO}_3)(\text{OH})_3$) peaks. b) detailed view on the 001-region showing the new mixed-layer peaks at 1.1 nm and 2.2 nm.

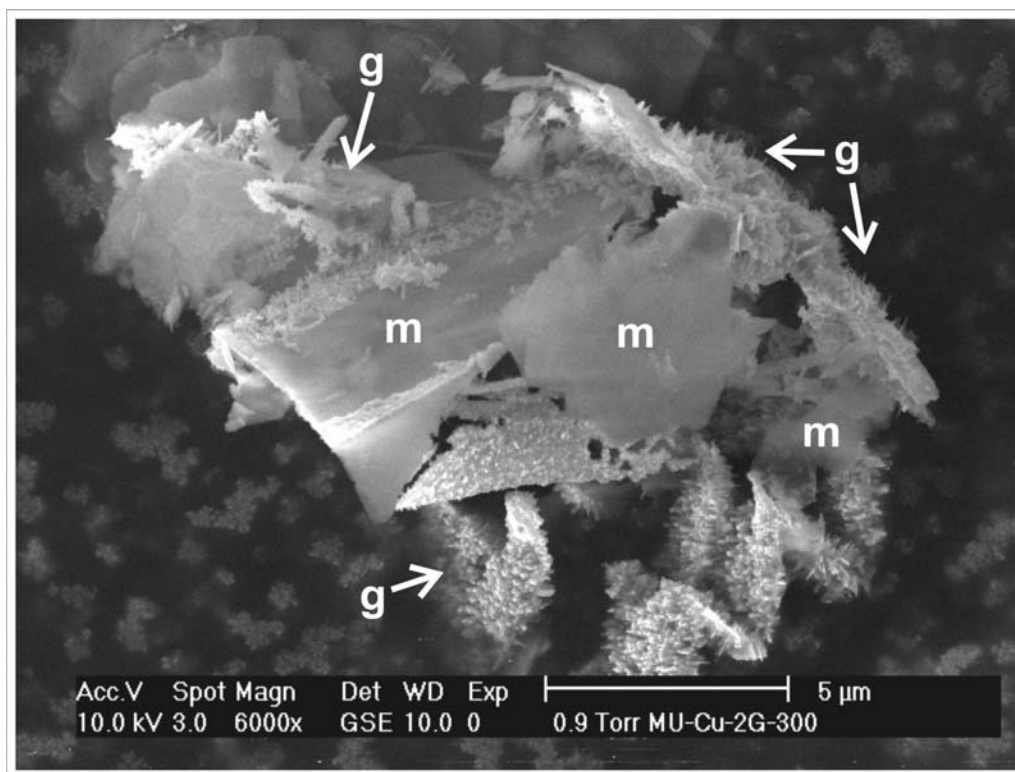


Figure 5.11 ESEM-image showing small needles of gerhardtite ($\text{Cu}_2(\text{NO}_3)(\text{OH})_3$) crystals (g) grown on Cu-nitrate treated muscovite particles (m).

Obviously the use of autoclaves hinders the formation of this additional phase, may be due to the missing oxygen, which would be necessary for the formation of nitrate-hydrates like gerhardtite (Holleman and Wiberg, 1985).

For all the other nitrate treated samples no changes of the 00l-peak positions in the 3° to 10° range are detected. This can be explained by the lower reaction temperatures in the round-bottom-flasks than in the autoclaves, because most of the solutions started to boil at temperatures much below 140°C.

5.4 CONCLUSIONS

The treatment of muscovite with nitrate solutions of di- and trivalent cations in autoclaves leads to strong changes of the structure and the morphology of the mica crystals.

Microscopic investigations show a strong decrease in grain size distribution and particle thickness, which is in accordance with the increasing specific surface areas. This proves the strong delamination of the particles.

Additionally the analysis of XRD data shows that the nitrate treatment leads to the intercalation of the cations. The consequence is an expansion along the c-axis and a contraction along the a-axis. Thus from these data it can be concluded that the entire crystal structure of muscovite is affected by the intercalation. Due to the simultaneous occurrence of the potassium in the interlayer space, it is unclear where the incorporated cations are fixed. To answer this question and to investigate the migration paths of the cations, further methods are necessary. Therefore in the following chapters the results of several vibrational spectroscopic methods are discussed.

In contrast to these results, the intercalation and delamination experiments in round-bottom-flasks revealed mainly no changes of the muscovite. In particular, the XRD patterns showed no changes. One of the main reasons for this are the much lower reaction temperatures around 120°C. Thus, this method is not useful for the intercalation of bi- or trivalent cation.

REFERENCES

- Ahn, J.H. and Peacor, D.R. (1986) Transmission electron microscope data for rectorite: implications for the origin and structure of "fundamental particles". *Clays and Clay Minerals*, **34**, 180-186.
- Bailey, S.W. (1980) Structures of layer silicates. pp. 1-124, in: *Crystal structures of clay minerals and their X-ray identification*. (G.W. Brindley and G. Brown, editors), Monograph **5**, Mineralogical Society, London.
- Bailey, S.W. (1987) Classification and structures of the micas. pp. 1-12. and Crystal chemistry of the true micas. pp. 13-60, in: *Micas* (S.W. Bailey, editor), Reviews in Mineralogy, **13**, 2nd edition, Mineralogical Society of America, Washington.
- Casari, W.R., Shelden, R.A. and Suter, U.W. (1992) Preparation of muscovite with ultrahigh specific surface area by chemical cleavage. *Colloid and Polymer Science*, **270**, 392-398.
- Clementz, D.M., Pinnavaia, T.J. and Mortland, M.M. (1973) Stereochemistry of Hydrated Copper(II) Ions on the Interlamellar Surfaces of Layer Silicates. An Electron Spin Resonance Study. *The Journal of Physical Chemistry* **77**, 196 - 200.
- Heller-Kallai, L. and Mosser, C. (1995) Migration of Cu ions in Cu montmorillonite heated with and without alkali halides. *Clays and Clay Minerals*, **43**, 738 – 743.
- Holleman, A. and Wiberg, E. (1985) *Lehrbuch der anorganischen Chemie*. 91.-100. Aufl., Walter de Gruyter, Berlin, 1451 p.
- Jakobsen, H.J., Nielsen, N.C. and Lindgreen, H. (1995) Sequences of charged sheets in rectorite. *American Mineralogist*, **80**, 247-252.
- Kodama, H. (1966) The nature of the component layers in rectorite. *American Mineralogist*, **51**, 1035-1055.
- Laugier, J. and Bochu, B. (2003) *CELREF V3*. Developed at the Laboratoire des Matériaux et du Génie Physique, Ecole Nationale Supérieure de Physique de Grenoble (INPG), [Http://www.inpg.fr/LMGP](http://www.inpg.fr/LMGP).
- Moore D.M. and Reynolds R.C. (1997) *X-Ray Diffraction and the Identification and Analysis of Clay Minerals*. 2nd ed., Oxford University Press, Oxford, 378 p.
- Trillo, J.M., Alba, M.D., Alvero, R. and Castro, M.A. (1993) Reexpansion of collapsed Li-montmorillonites; evidence on the location of Li⁺ ions. *Journal of the Chemical Society - Chemical Communications*, **24**, 1809-1811.
- Rösler, H. (1991) *Lehrbuch der Mineralogie*. 5. Aufl., Deutscher Verlag für Grundstoffindustrie, Leipzig, 844 p.

CHAPTER 6

INTERCALATION OF CU(II) AND ZN(II) IN MUSCOVITE OBSERVED BY FTIR SPECTROSCOPIC METHODS

Most parts of this chapter have been submitted under the same title “Intercalation of Cu(II) and Zn(II) in muscovite observed by FTIR spectroscopic methods” (Frank Friedrich, Stefan Heissler, Werner Faubel, Rolf Nüesch and Peter G. Weidler) to the magazine *Clays and Clay Minerals* in April 2004.

6.1 INTRODUCTION

In contrast to 2:1 clay minerals like smectites the interlayer cations of micas, especially of muscovite are difficult to access and are not exchangeable under normal conditions (Jasmund and Lagaly, 1993; Osman et al. 1999a, 1999b). Thus a chemical modification of this mineral is complicated and requires increased pressure and temperatures (e.g. Keppler, 1990; Caseri et al., 1992), and up to date no discussion of IR-spectra of divalent cations intercalated into muscovite is available in the literature. The intercalation of cations like Cu^{2+} and Zn^{2+} into the muscovite interlayers as described by Friedrich et al. (2003) allows an extensive investigation of the interaction mechanisms between these new interlayer cations and the muscovite lattice. Therefore the specific aim of this chapter is the investigation of the changes of the lattice vibrations due to the migration of the cations within the muscovite.

6.2 MATERIALS AND METHODS

For the FTIR spectroscopic investigations Cu-nitrate and Zn-nitrate treated muscovite samples are used. A detailed description of the delamination procedure is given in chapter 2.

The FTIR spectra were recorded on a Bruker IFS 66 spectrometer equipped with a DTGS detector, using KBr-pellets made of 3 milligrams of powdered sample mixed with 300 milligrams of KBr. 64 scans in the 4000 – 400 cm^{-1} spectral range were recorded with a resolution of 4 cm^{-1} . In addition, diffuse reflectance infrared fourier transform (DRIFT) spectroscopy was used for a detailed measurement especially in the Si-O stretching region (range of 1200 – 800 cm^{-1}). For this 10 mg of sample material was slightly ground with 100 mg KBr, then the powders were poured loosely into a sample cup to obtain a random orientation. Further spectrometer details are given in chapter 3.

6.3 RESULTS

FTIR transmission spectroscopy

MIR region (1000 and 400 cm^{-1}). In general the spectral features in the MIR region between 1000 and 400 cm^{-1} can be attributed to vibrations of the tetrahedral and octahedral units of phyllosilicates (e.g. Loh, 1973; Farmer, 1974; McKeown et al., 1999a, b). Figure 6.1 and Table 6.2 show this range, in which the spectra of the time dependent treatment with Cu- and Zn-nitrate are compared with that of the original muscovite. Both sets show distinct changes with increasing treatment time. Due to the Cu-nitrate treatment two new vibrations at 529 (band 3) and 627 cm^{-1} (band 5) occur. The intensity of the bands at 555, 653 and 713 cm^{-1} (bands 4, 6, 8) strongly decreases. A smaller decrease of intensity is observed for the band at 836 cm^{-1} (band 11), whereas the 653 cm^{-1} band later disappears completely. After a treatment time of 240 hours a weak shoulder occurs at 687 cm^{-1} in both spectra (band 7a). The intensity of the shoulders at 750 and 789 cm^{-1} (band 9, 10) strongly increases, additionally this band shifts to a higher wavenumber (802 cm^{-1} , band 10a), as well as the band at 529 cm^{-1} , which shifts to 534 cm^{-1} . A comparable set of spectra with very similar changes can be observed for the treatment with Zn-nitrate. Figure 6.1 also shows the occurrence of a new band at 531 cm^{-1} , but it does not shift its position.

The 627 cm^{-1} band appears, too, but only as a very small and broad shoulder. The intensity increase of the shoulders at 750 and 789 cm^{-1} also can be observed for the Zn-muscovite. Like in the Cu-muscovite spectra this band also shifts to a higher wavenumber at about 801 cm^{-1} . The intensity of the band at 653 cm^{-1} strongly decreases, but it does not vanish (Table 6.2).

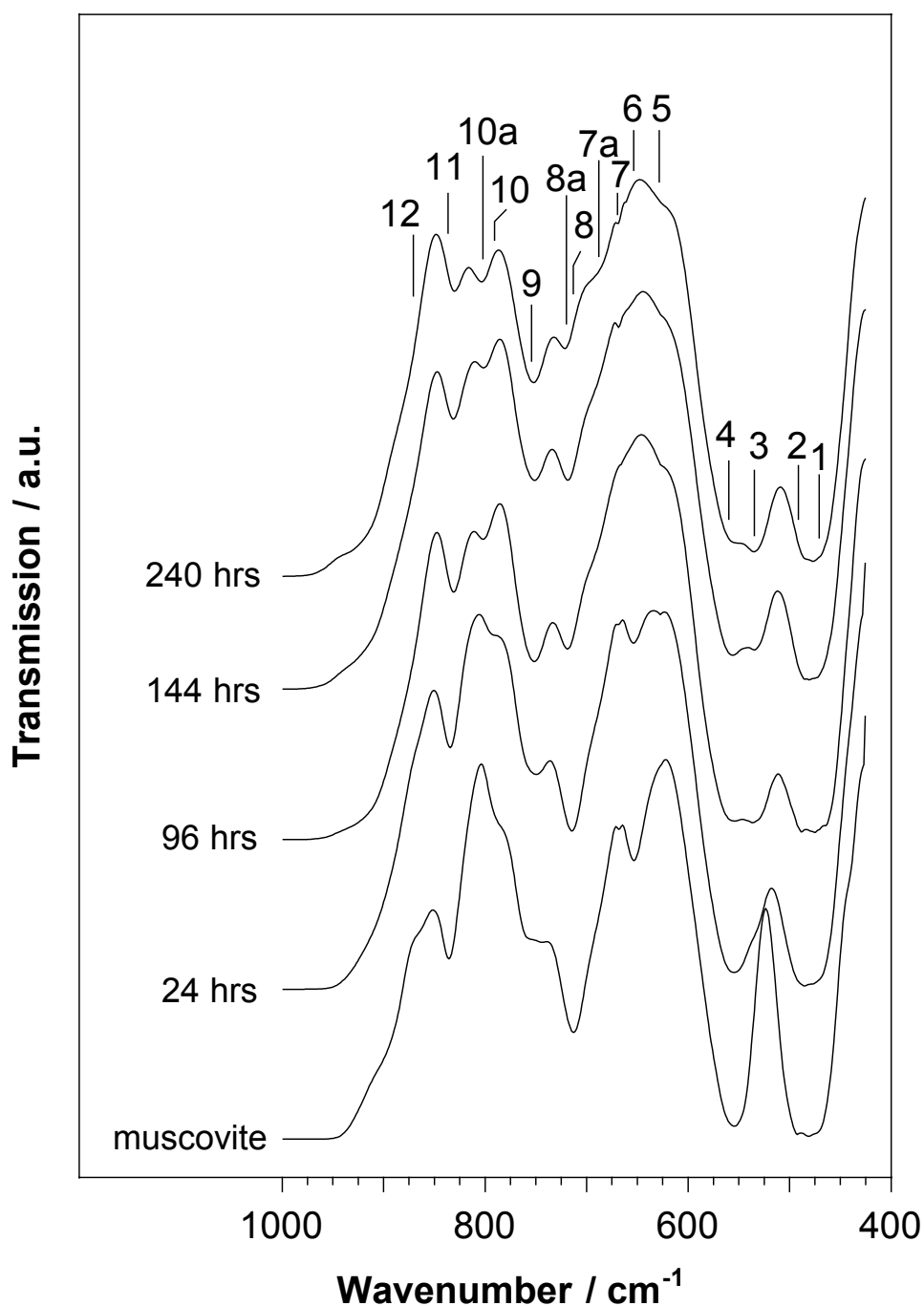


Figure 6.1.a. FTIR-spectra of Cu-intercalated muscovite. (Time series between 0 and 240 hours).

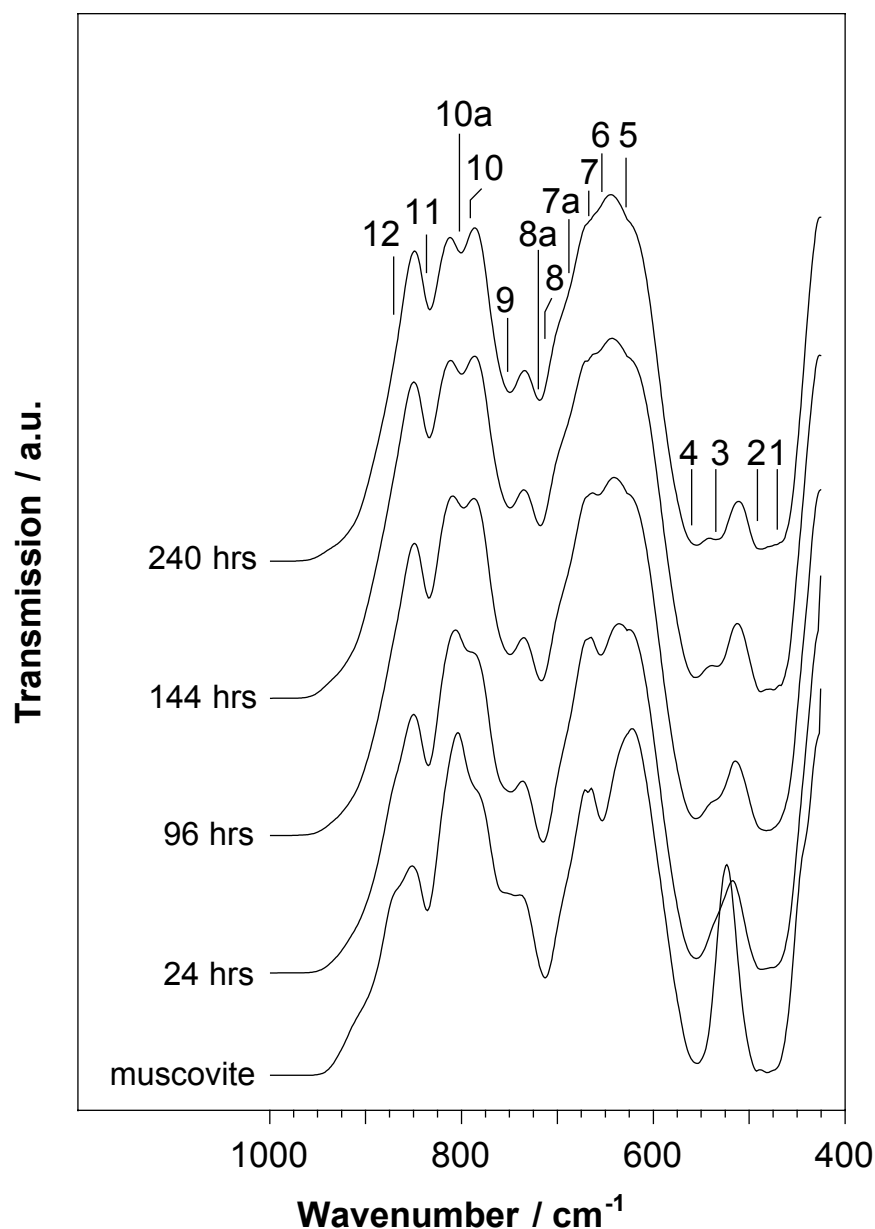


Figure 6.1.b FTIR-spectra of Zn-intercalated muscovite. (Time series between 0 and 240 hours).

OH-stretching region (3700 to 3300 cm^{-1}). The OH-stretching region of muscovite however is only weakly affected by the intercalation of the divalent cations. The broadening of this region may be attributed to a partial dehydration of the original material. For both ions Figure 6.2 shows a band with two maxima, one at 3629 cm^{-1} and the other at 3648 cm^{-1} , which lightly increase in intensity with increasing treatment time, but do not shift their positions. Additionally a very broad band with low intensity occurs in the range of $3500 - 3400 \text{ cm}^{-1}$.

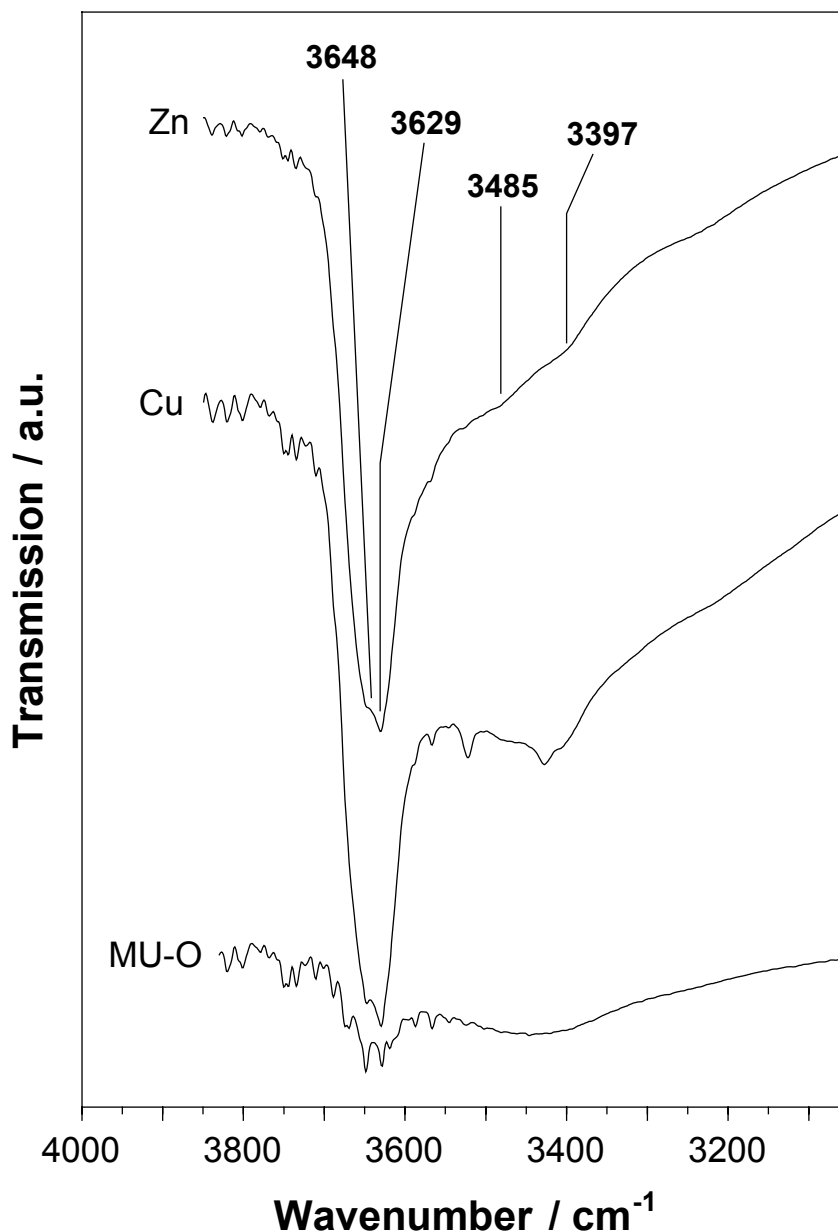


Figure 6.2 FTIR spectra of the OH-region of the Cu- and Zn-muscovites after a treatment of 240 hours.

DRIFT spectroscopy

With DRIFT spectroscopy it is possible to distinguish five bands in the Si–O stretching region between 1200 and 800 cm^{-1} (Figure 6.3). Below 900 cm^{-1} two small bands occur at 836 cm^{-1} (band 11) and a weaker one at 902 cm^{-1} (band 13). The region around 1000 cm^{-1} is dominated by several strong bands, a broad shoulder with a maximum at 979 cm^{-1} (band 14), possibly consisting of two bands and two further maxima at 1033 cm^{-1} and 1056 cm^{-1} (band 15, 16).

Table 6.2a Observed changes of the IR-band positions and intensities due to the Cu-nitrate treatment, and their assignments.

Band No.	orig. muscovite			Cu-treated	
	cm ⁻¹	I	V.A. ^a	observed changes	M.A. ^b
1	476	strong	Si-O	not visible in shoulder of 485	-
2	492	strong	Si-O	shift to 485	rec.
3	-	-	-	new band at 529, shift to 534	Si-O /rec.
4	555	strong	Si-O	intensity decrease	dist. mica
5	-	-	-	shoulder at 627	Al-OH /rec.
6	653	moderate	Si-O	-	-
7	669	weak	phen.	-	-
7a	-	-	-	shoulder at 687	-
8	713	moderate	Al-O ⁻	-	-
8°	-	-	-	shift to 721	Cu-O-Si
9	750	shoulder	Al-O-Si	intensity increase	dist. mica
10	789	shoulder	Al-O-Al	-	-
10a	-	-	-	shift from 789 to 806	dist. mica
11	836	moderate	Al-OH	intensity decrease	dist. OH
12	863	shoulder	-	-	-
13	902	weak	AlAl-OH	-	-
13a	-	-	-	shift to shoulder at 924	dist. OH
14	979	strong	phen.	-	-
14a	-	-	-	shift to 995	-
14b	-	-	-	shift to 1010	rec.
15	1033	strong	Si-O-Si	-	-
15a	-	-	-	shift to 1049	rec.
16	1056	strong	Si-O	disappears in 1049	-
17	1106	shoulder	Si-O	not visible	-

^a V.A. = Vibration Assignment ^b M.A. = Mineral Assignment (rec. = rectorite, phen. = phengite)

Table 6.2.b Observed changes of the IR-band positions and intensities due to the Zn-nitrate treatment, and their assignments.

Band No.	orig. muscovite			Zn-treated	
	cm ⁻¹	I	V.A. ^a	observed changes	M.A.
1	476	strong	Si-O	shoulder at 467	mica
2	492	strong	Si-O	shift to 487	rec.
3	-	-	-	new band at 529, shift to 532	Si-O /rec.
4	555	strong	Si-O	intensity decrease	dist. mica
5	-	-	-	shoulder at 628	Al-OH /rec.
6	653	moderate	Si-O	weak shoulder	mica
7	669	weak	Phen.	weak shoulder	mica
7a	-	-	-	-	-
8	713	moderate	Al-O ⁻	-	-
8a	-	-	-	shift to 720	Zn-O-Si
9	750	shoulder	Al-O-Si	intensity increase	mica
10	789	shoulder	Al-O-Al	-	-
10a	-	-	-	shift from 789 to 801	dist. mica
11	836	moderate	Al-OH	intensity decrease	dist. OH
12	863	shoulder		-	-
13	902	weak	AlAl-OH	-	-
13a	-	-	-	shift to shoulder at 925	dist. OH
14	979	strong	Phen.	-	-
14a	-	-	-	-	-
14b	-	-	-	shift to 1002	rec.
15	1033	strong	Si-O-Si	-	-
15a	-	-	-	shift to 1049	rec.
16	1056	strong	Si-O	disappears in 1049	-
17	1106	shoulder	Si-O	-	-

^a V.A. = Vibration Assignment ^b M.A. = Mineral Assignment (rec. = rectorite, phen. = phengite)

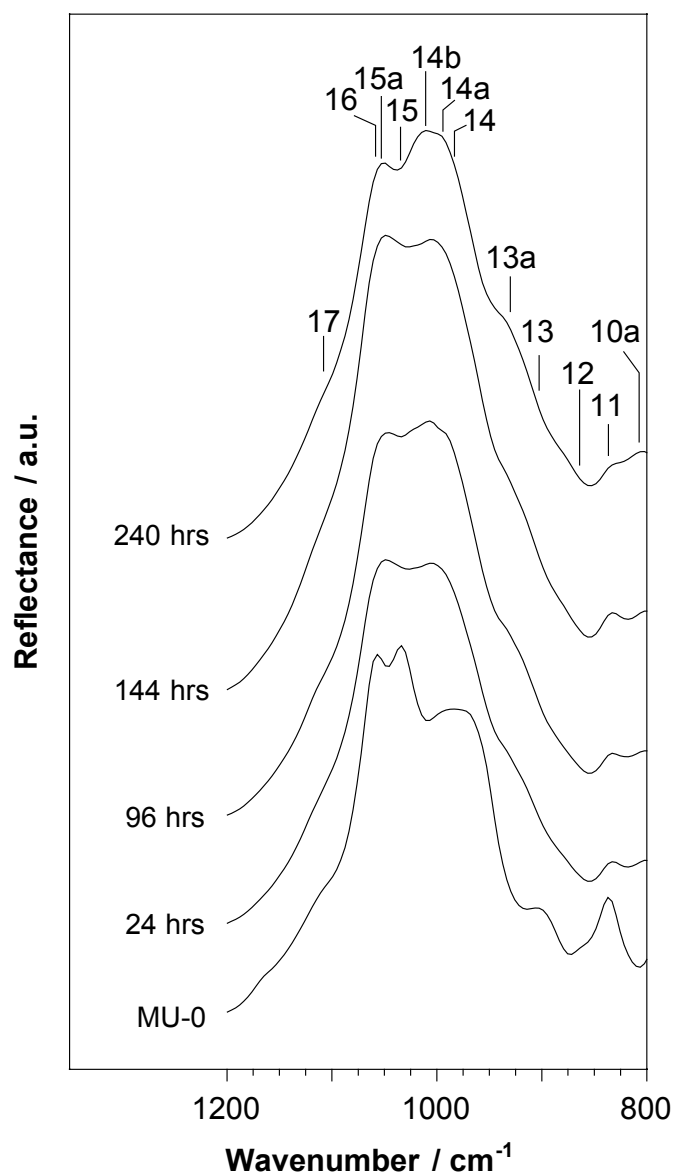


Figure 6.3.a DRIFT-spectra of Cu-treated muscovite samples in the spectral range around 1000 cm^{-1} . Comparison of untreated muscovite (MU-0) with samples after several treatment times.

As shown in the FTIR spectra the position of the 836 cm^{-1} band is not affected by the nitrate treatment, only its intensity slightly decreases. The band at 902 cm^{-1} disappears already after 24 hours of treatment and a shoulder at about 920 cm^{-1} (band 13a) occurs with slightly increasing intensity (Figure 6.4). The intensity of the shoulder at about 979 cm^{-1} increases and its position strongly shifts to higher wavenumber at 995 and 1010 cm^{-1} (bands 14a, 14b) due to the Cu-nitrate treatment and to 1002 cm^{-1} during the Zn-nitrate treatment. Here no band at 995 cm^{-1} exists.

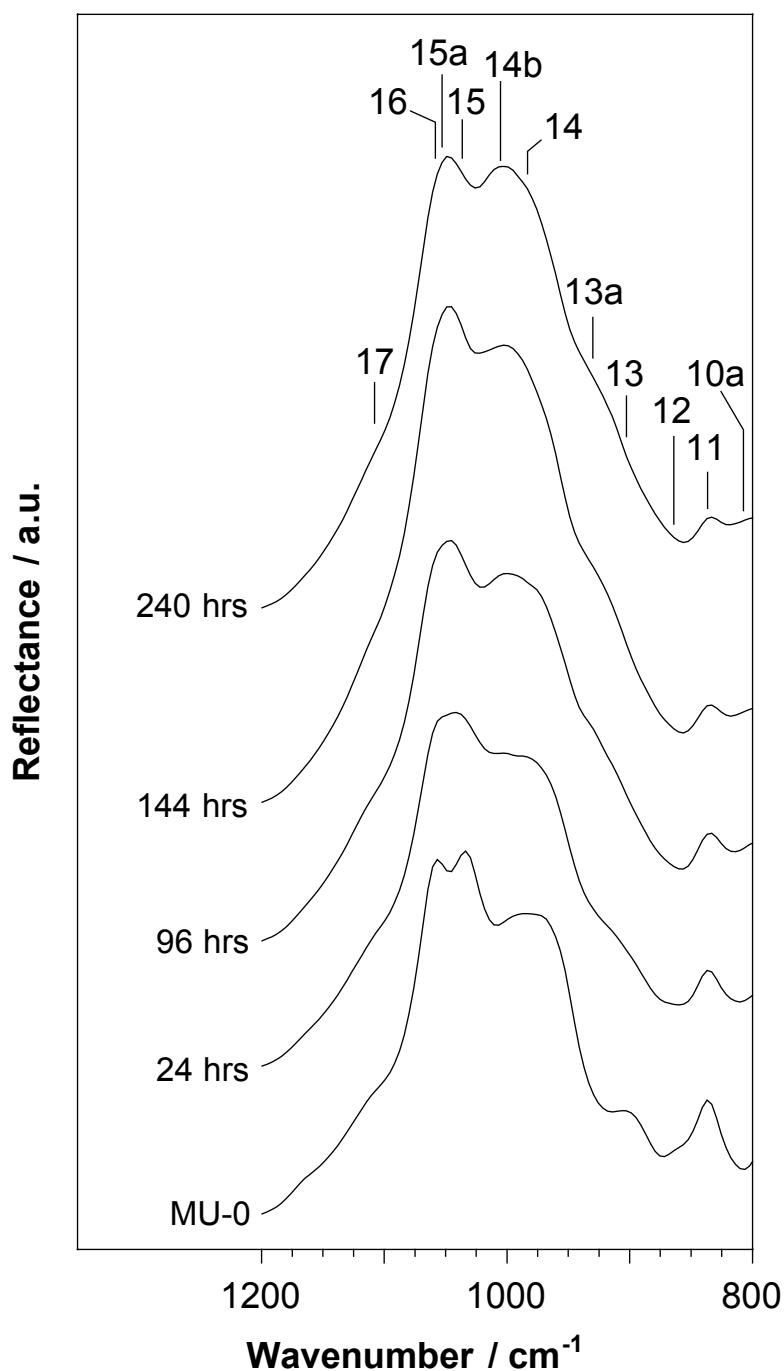


Figure 6.3.b DRIFT spectra of Zn-treated muscovite samples in the spectral region around 1000 cm^{-1} . Comparison of untreated muscovite (MU-0) with samples after several treatment times.

The band at 1033 cm^{-1} also shows a significant shift of its position to about 1047 cm^{-1} (band 15a) for both nitrates, while the band at 1056 cm^{-1} as well as the shoulder at 1106 cm^{-1} (band 17) slowly disappear into the shoulder of the shifted 1047 cm^{-1} band during the nitrate treatment.

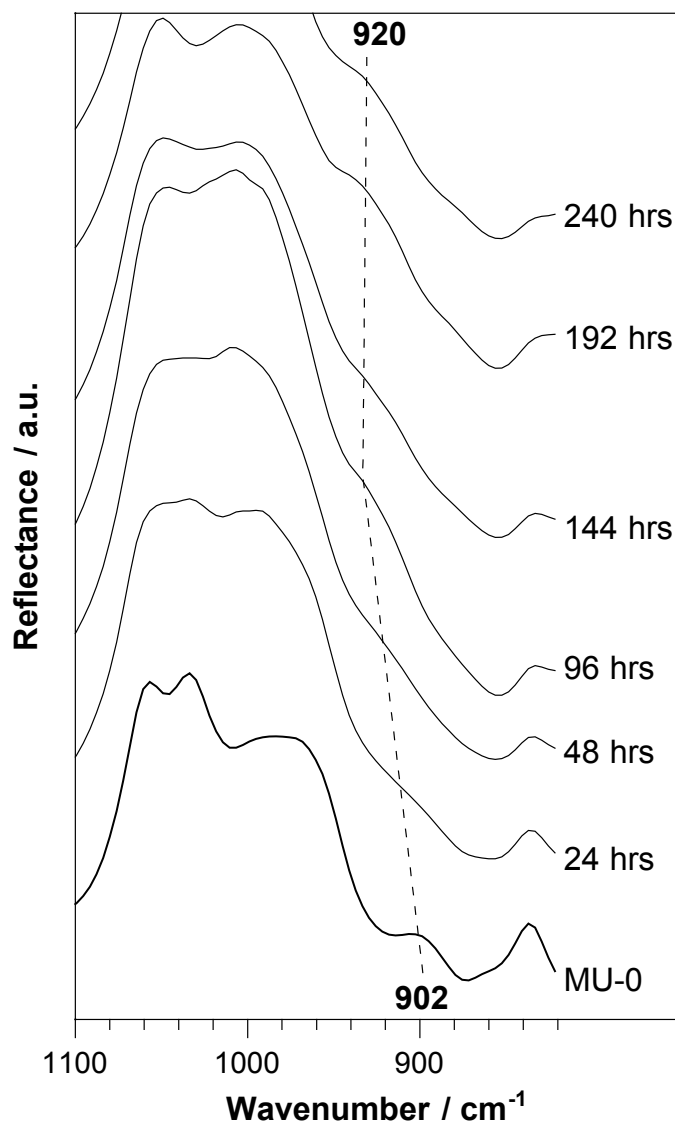


Figure 6.4 Detailed view on the DRIFT spectra of Cu treated muscovite showing the changes in intensity and position of band 13 at 902 cm^{-1} .

6.4 DISCUSSION

General remarks. The spectroscopic investigation of the untreated muscovite yields two vibrations ($669, 979\text{ cm}^{-1}$ and 1106 cm^{-1} ; bands 7, 14, 17), which give hints to an additional, small phengitic component (Figure 6.1, Table 6.2). All the other bands are assigned to muscovite vibrations (Farmer, 1974; McKeown et al., 1999). The phengite vibrations behave similar to the muscovite bands during the experiments. With increasing treatment time their intensity decreases and finally they shift or disappear.

We can assume that all the observed changes in the spectra can be attributed exclusively to changes in the molecular structure of the muscovite, due to the diffusion of the cations into the layers. For example the formation of copper silicates like chrysocolla during the treatment can be excluded by the obtained results. Apart from the lack of characteristic peaks in the XRD patterns, the infrared spectra of Cu treated samples do not show new bands around 820 or 677 cm^{-1} (Mosser *et al.* 1997; Kelm *et al.* 2001). Another possible chrysocolla mode near 720 cm^{-1} (band 8a) occurs in all the spectra independent of the used metal nitrate and is discussed later in detail (Figure 6.1). The existence of metal oxides or nitrates can be excluded likewise, because none of the spectra shows the characteristic bands of these compounds in the 1600 – 1300 cm^{-1} region (e.g. Nyquist and Kagel, 1971).

Farmer and Russell (1971) pointed out, that the Si–O stretching vibrations in clay minerals and micas are very sensitive to distortions in the tetrahedral layers. On the other hand Farmer and Russell (1966) showed that the lattice vibrations do not depend on the distance of the single layers and whether they are separated by a layer of water or other polar molecules. Therefore changes in the interlayer space, for example by the intercalation of cations with different radii and charge should only then affect these bonds, when the cations diffuse to the surfaces of the tetrahedral sheets and move into the ditrigonal holes of these layers as described by the Hofman-Klemen effect in smectites (Hofman and Klemen, 1950; Greene-Kelly, 1952). Then the consequence is, that the observed changes in the spectra of the nitrate treated muscovites are not caused by a simple intercalation of the divalent cations into the interlayers, as proved by our XRD results, but the ions in fact need to migrate into the structure of the mineral. This behaviour is well known for Li or Cu in smectites (e.g. Tettenhurst, 1962; Heller-Kallai and Mosser, 1995), but has never been reported for muscovite.

Si–O vibrations. The development of a Si–O bending vibration as a shoulder at 529 cm^{-1} (band 3) and its shift to 534 cm^{-1} during the nitrate treatment can be attributed to a distortion of the tetrahedral layer (Figure 6.1), due to the movement of the divalent cations into the ditrigonal cavities of the layers

(Farmer 1974; McKeown *et al.* 1999). On the other hand the position of the Si–O vibration at 555 cm^{-1} (band 4) is not affected, only its intensity decreases. Generally an intensity decrease and a broadening of all bands in the $600 - 400\text{ cm}^{-1}$ region is due to the simultaneous occurrence and the overlap of both new rectorite-like vibrations and original mica vibrations (Srasra *et al.*, 1994; Russell and Fraser, 1996).

Similarly, the development of the rectorite-like structure is indicated by the shift of the Si–O stretching band 15 at 1033 cm^{-1} in all spectra (Figure 6.3). With increasing treatment time it moves to higher wavenumbers, approaching the frequency at which rectorite absorbs (band 15a). In comparison with that the Si–O stretching band of muscovite at 1056 cm^{-1} strongly decreases. In both spectra it finally disappears in the shoulder of the shifting rectorite band after a treatment time of about 144 hours. Moreover, the bands become broader, indicating the structural changes and the decreasing structural quality of the mixed-layer mineral. The light shift of the Si–O bending vibration from 492 to about 485 cm^{-1} (band 2) also matches the similarity to the rectorite structure. The shift and broadening of the Si–O–Si stretching band 14 from 979 to about 1010 cm^{-1} is attributed to the distortion of the tetrahedra due to the diffusion of the cations into the ditrigonal holes.

OH-bending region. While the bands at 627 and 653 cm^{-1} are often shown in the literature, they are rarely assigned to specific vibrations. There only exist a few general descriptions of the vibrations in this region as hydroxyls connected to the octahedral Al (Farmer, 1974; Velde, 1978). The decrease of their intensities is probably attributable to the repulsive forces on the proton of the OH group exerted by cations, which are settled deep within the ditrigonal holes of the tetrahedral layers. The disappearance of band 13 and the occurrence of a shoulder at about 920 cm^{-1} (band 13a) also speak in favour of this influence on the OH-groups (Figure 6.4). A reason for this is, that in dioctahedral phyllosilicates the OH-groups are slightly directed to the octahedral vacancies. Therefore the increasing repulsive forces on the protons during the movement of the small cations into the ditrigonal holes result in a strong decrease of the intensity of the Al–Al–OH vibration at 902 cm^{-1} . Madejová *et al.* (1999)

suggested that these repulsive forces change the direction of the dipole moment of the OH groups in smectites and therefore perturb their deformation vibration. As the direction of the OH groups strongly depends on the localization of these additional cations (Bookin and Drits, 1982), one can assume, that the migration of the cations leads to a switching of the hydroxyls into a position perpendicular to the *ab*-plane. This opens possibilities for the cation diffusion into the octahedral sheet. As a mode at about 920 cm^{-1} occurs in illites and rectorites, where octahedral Al is partly substituted versus divalent cations like Mg (Mosser et al., 1990), one can suggest a local movement of the Cu or Zn ions into these octahedral sites to obtain a rectorite-like dioctahedral structure. This is confirmed by the shift and intensity change of the Al–O–Si band at 713 cm^{-1} to a higher wavenumber at 723 cm^{-1} for Cu-muscovite and to a lesser amount for Zn-muscovite. Possibly this shift mirrors the change to a Cu–O–Si respectively a Zn–O–Si stretching vibration, similar to a mode observed in chrysocolla (Kelm et al., 2001). Nevertheless no further hints for the presence of the intercalated cations within the octahedral layer could be observed in the spectra. Especially in the OH-stretching region several authors postulated additional vibrations for Cu exchanged smectites (Madejová et al., 1996; Mosser et al., 1997). Neither Cu–OH or Zn–OH vibrations at about 3640 cm^{-1} , nor absorptions due to a trioctahedral environment of OH groups at about 3680 cm^{-1} were observed (Figure 6.2). This implies, that only a small portion of the divalent cations migrate into the octahedral layer. However, they do not move into the vacant octahedral sites, causing a local trioctahedral environment, but in accordance to Mosser et al. (1990) they possibly substitute for Al. As the Al–O–Si vibration at 750 cm^{-1} increases in intensity and the Al–O–Al mode shifts from 789 to 806 cm^{-1} , a strong distortion of the octahedron is suggested. This distortion is probably related to the Jahn-Teller effect (Mosser et al., 1990), so that Cu is better stabilized in phyllosilicates whose octahedral cavities are not all occupied. The few known natural Cu-phyllosilicates show this phenomena too, all of them are dioctahedral.

An additional effect can be responsible for the occurrence of the absorption at 920 cm^{-1} . As Jaynes and Bigham (1987) and Williams et al. (1991) showed

for smectites, the interactions between migrating cations and the OH groups can cause a partial deprotonation which leads to the fixation of Cu and Zn ions at sites very close to the octahedra. Therefore this fixation should affect all OH-bending vibrations, but it fails to explain the strong influence on all the other absorptions of the octahedral layer. Therefore we assume a combination of both discussed effects.

To obtain further information about these migration paths and the local environment of the intercalated cations, especially Cu, investigations in the far infrared region (FIR) and electron paramagnetic resonance spectroscopy (EPR) are carried out at present.

6.5 CONCLUSIONS

The results of this investigation show that the intercalation of the divalent cations Cu^{2+} and Zn^{2+} leads to the fixation of these ions within the treated muscovites transforming it to a rectorite-like structure. The changes in the XRD and IR spectra suggest that Cu and Zn occupy four different sites in the structure: (a) Simultaneous fixation with potassium in the interlayers, based on the higher d-values in the XRD-patterns shown in chapter 5. (b) Migration into the ditrigonal cavities of the tetrahedral sheet, based on the formation and shift of the Si–O bending vibration at 529 cm^{-1} and the intensity changes of the 555 and the 493 cm^{-1} bands. (c) Movement and fixation in octahedral sites also lead to a rectorite-like structure, due to the substitution of aluminium by divalent ions in these sites. This is based on the shift of the band at 713 to 723 cm^{-1} , which mirrors the vibration of an octahedral Cu–O bond similar to a chrysocolla band. The changes of the bands at 750 and $789 - 806\text{ cm}^{-1}$ show the strong distortion of the octahedra, due to the incorporation of Cu and Zn. (d) The two cations substitute protons in the OH groups, based on the decrease of the OH-bending bands and the disappearance of the band at 902 and its remarkable shift to 920 cm^{-1} .

REFERENCES

- Alba, M.D., Alvero, R., Beccerro, A.I., Castro, M.A., and Trillo, J.M. (1998) Chemical behaviour of lithium ions in reexpanded Li-montmorillonites. *Journal of Physical Chemistry B*, **102**, 2207 – 2213.
- Alvero, R., Alba, M.D., Castro, M.A., and Trillo, J.M. (1994) Reversible migration of lithium in montmorillonites. *Journal of Physical Chemistry*, **98**, 7848 – 7853.
- Bookin, A.S. and Drits, V.A. (1982) Factors affecting orientation of OH-vectors in micas. *Clays and Clay Minerals*, **30**, 415 – 421.
- Calvet, R. and Prost, R. (1971) Cation migration into empty octahedral sites and surface properties of clays. *Clays and Clay Minerals*, **19**, 175 – 186.
- Casari, W.R., Shelden, R.A. and Suter, U.W. (1992) Preparation of muscovite with ultrahigh specific surface area by chemical cleavage. *Colloid and Polymer Science*, **270**, 392 – 398.
- Clementz, D.M., Pinnavaia, T.J., and Mortland, M.M. (1973) Stereochemistry of hydrated copper(II) ions on the interlamellar surfaces of layer silicates. An electron spin resonance study. *Journal of Physical Chemistry* **77**, 196 – 200.
- Farmer, V.C. (1974) Layer silicates. Pp. 331 – 364, in: *the infrared spectra of minerals*. (V.C. Farmer, editor). Monograph **4**, mineralogical society, London.
- Farmer, V.C. and Russell, J.D. (1966) Effects of particle size and structure of the vibrational frequencies of layer silicates. *Spectrochimica Acta*, **22**, 389 – 398.
- Farmer, V.C. and Russell, J.D. (1971) Interlayer complexes in layer silicates. *Transactions of the Faraday Society* **67**, 2737 – 2749.
- Friedrich, F., Weidler, P.G. and Nüesch, R. (2003) Chemical delamination of muscovite by nitrates of di- or trivalent metal cations in autoclaves. – Euroclay 2003, Modena, Italy, June 22 – 26, 2003.
- Greene-Kelly, R. (1952) Irreversible dehydration in montmorillonite. *Clay Mineral Bulletin*, **1**, 221 – 225.
- Heller-Kallai, L. and Mosser, C. (1995) Migration of Cu ions in Cu montmorillonite heated with and without alkali halides. *Clays and Clay Minerals*, **43**, 738 – 743.
- Hofmann, U. and Klemen, R. (1950) Verlust der Austauschfähigkeit von Lithiumionen an Bentonit durch Erhitzung. *Zeitschrift für Anorganische Chemie*, **262**, 95 – 99.
- Jakobsen, H.J., Nielsen, N.C. and Lindgreen, H. (1995) Sequences of charged sheets in rectorite. *American Mineralogist*, **80**, 247 – 252.

- Jasmund, K. and Lagaly, G. (1993) *Tonminerale und Tone*. Steinkopff Verlag, Darmstadt. 490 pp.
- Jaynes, W.F. and Bigham, J.M. (1987) Charge reduction, octahedral charge and lithium retention in heated, Li-saturated smectites. *Clays and Clay Minerals*, **35**, 440 – 448.
- Karakassides, M.A., Madejová, J., Arvaiová, B., Bourlinos, A., Petridis, D. and Komadel, P. (1999) Location of Li(I), Cu(II), Cd(II) in heated montmorillonite: evidence from specular reflectance infrared and electron spin resonance spectroscopy. *Journal of Material Chemistry*, **9**, 1553 – 1558.
- Kelm, U., Sanhueza, V., Madejová, J., Sucha, V., Elsass, F. (2001) Evaluation of identification methods for chrysocolla – a Cu-smectite-like hydrous silicate: implications for heap-leaching extraction of copper. – *Geologica Carpathica*, **52**, 111 – 121.
- Keppler, H. (1990) Ion exchange reactions between dehydroxylated micas and salt melts and the crystal chemistry of the interlayer cation in micas. *American Mineralogist*, **75**, 529 – 538.
- Loh, E. (1973) Optical vibrations in sheet silicates. *Journal of Physics C: Solid State Physics*, **6**, 1091 – 1104.
- Madejová, J., Bujdak, J., Gates, W.P. and Komadel, P. (1996) Preparation and infrared spectroscopic characterization of reduced-charge montmorillonite with various Li contents. *Clay Minerals*, **31**, 233 – 241.
- Madejová, J., Arvaiová, B., and Komadel, P. (1999) FTIR spectroscopic characterization of thermally treated Cu²⁺, Cd²⁺, and Li⁺ montmorillonites. *Spectrochimica Acta A*, **55**, 2467 – 2476.
- McKeown, D.A., Bell, M.I. and Etz, E.S. (1999) Vibrational analysis of the dioctahedral mica: muscovite-2M₁. *American Mineralogist*, **84**, 1041 – 1048.
- Moore D.M. and Reynolds R.C. (1997) *X-ray diffraction and the identification and analysis of clay minerals*. Second edition, University Press, Oxford, 378 pp.
- Mosser, C., Mestdagh, M., Decarreau, A., and Herbillon, A.J. (1990) Spectroscopic (ESR, EXAFS) evidence of Cu for (Al - Mg) substitution in octahedral sheets of smectites. *Clay Minerals*, **25**, 271 – 282.
- Mosser, C., Michot, L.J., Villieras, F., and Romeo, M. (1997) Migration of cations in copper(II)-exchanged montmorillonite and laponite upon heating. *Clays and Clay Minerals*, **45**, 789 – 802.
- Nyquist, R.A. and Kagel, R.O. (1971) *Infrared spectra of inorganic compounds*. Academic Press, New York, 495 pp.

-
- Osman, M.A., Moor, C., Caseri, W.R., and Suter, U.W. (1999a) Alkali metals ion exchange on muscovite mica. *Journal of colloid and interface science*, **209**, 232 – 239.
- Osman, M.A. and Suter, U.W. (1999b) Dodecyl pyridinium/alkali metals ion exchange on muscovite mica. *Journal of colloid and interface science*, **214**, 400 – 406.
- Russell, J.D. and Fraser, A.R. (1996) Infrared methods. Pp. 11 – 67 in: *Clay Mineralogy: Spectroscopic and chemical determinative methods*. (M.J. Wilson, editor). Chapman & Hall, London.
- Sposito, G., Prost, R. and Gaultier, J.-P. (1983) Infrared spectroscopic study of adsorbed water on reduced-charge Na/Li-montmorillonites. *Clays and Clay Minerals*, **31**, 9 – 16.
- Srasra, E., Bergaya, F. and Fripiat, J.J. (1994) Infrared spectroscopy study of tetrahedral and octahedral substitutions in an interstratified illite-smectite clay. *Clays and Clay Minerals* **42**, 237 – 241.
- Tettenhurst, R. (1962) Cation migration in montmorillonites. *American Mineralogist*, **47**, 769 – 773.
- Trillo, J.M., Alba, M.D., Alvero, R. and Castro, M.A. (1993) Reexpansion of collapsed Li-montmorillonites; evidence on the location of Li⁺ ions. *Journal of the Chemical Society - Chemical Communications*, **24**, 1809 – 1811.
- Vedder, W. and McDonald, R.S. (1963) Vibrations of the OH ions in muscovite. *Journal of Chemical Physics*, **38**, 1583 – 1590.
- Velde, B. (1978) Infrared spectra of synthetic micas in the series muscovite-MgAl celadonite. *American Mineralogist*, **63**, 343 – 349.
- Williams, J., Prurnell, J.H. and Ballantine, J.A. (1991) The mechanism of layer charge reduction and regeneration in Li⁺-exchanged montmorillonite. *Catalysis Letters*, **9**, 115 – 120.

CHAPTER 7

FAR INFRARED SPECTROSCOPY OF INTERLAYER VIBRATIONS OF NITRATE TREATED MUSCOVITE

Parts of this chapter have been submitted under the title “Far infrared spectroscopy of interlayer vibrations of Cu(II), Mg(II), Zn(II), and Al(III) intercalated muscovite” (Frank Friedrich, Biliana Gasharova, Yves-Laurent Mathis, Rolf Nüesch and Peter G. Weidler) to the magazine Applied Spectroscopy in September 2004.

7.1 INTRODUCTION

The intercalation and migration of cations into phyllosilicates is extensively investigated by mid infrared spectroscopy (e.g. Loh, 1973; Farmer, 1974; Madejova et al., 1999). As the vibrational modes in the MIR region (4000 – 400 cm^{-1}) only display the effects of migrating cations on the structure of phyllosilicates, vibrations in the far infrared reveal direct information about the interactions of the interlayer cations with the layer lattice (e.g. Ishii, et al., 1967; Velde and Couty, 1985; Prost and Laperche, 1990). However, thus far only the vibrations of potassium and other alkaline metals in micas have been investigated (Tateyama et al., 1977; Schroeder, 1990; Laperche and Prost, 1991; Badreddine et al. 2002).

The possibility to intercalate cations like Cu^{2+} , Mg^{2+} , Zn^{2+} into the muscovite interlayers as suggested by Friedrich et al. (2003) allows an extensive investigation of the interaction mechanisms between these higher charged cations and the muscovite lattice.

Thus in this chapter the FIR spectra of Al-, Cu-, Mg-, and Zn-nitrate treated muscovites are presented. The changes due to the cation migration are investigated and are compared to the results of the mid infrared spectroscopy presented in chapter 6.

7.2 MATERIALS AND METHODS

The nitrate treated muscovite samples used in this FIR study are produced by heating muscovite powders in oversaturated Al-, Cu-, Mg-, Zn-nitrate solutions using autoclaves. The details of this preparation procedure are described in chapter 2.1.

The far infrared spectra were collected at the SUL-IR Beamline at ANKA. For these measurements pellets were produced by pressing 8 mg sample powder with 50 mg polyethylene. All the spectrometer details are extensively described in chapter 3. Spectral manipulation such as matrix subtraction and normalisation due to the slightly decreasing synchrotron beam current had to be performed, using the OPUS software package (Bruker Optics GmbH). Band component analysis was undertaken using the Jandel Peakfit software package, which enabled the type of fitting function to be selected and allows specific parameters to be fixed or varied accordingly. Band fitting was done using a Voigt function, with the minimum number of component bands used for the fitting process. A linear 2-point background was chosen and fitting was undertaken until reproducible results were obtained with squared correlations of $r^2 > 0.9994$.

7.3 RESULTS

Figure 7.1 shows the far infrared spectra of the pure muscovite (MU-0) and of Cu-, Mg-, Zn, and Al-nitrate treated samples in the spectral region between 60 and 400 cm^{-1} . In all spectra the main broad feature occurs around 100 cm^{-1} . It is obvious, that this broad and strong feature does not consist of only one vibrational mode.

In the lowest frequency range all spectra show two very weak shoulders at 68 and 78 cm^{-1} , which are almost invisible in Figure 7.2. The center of the broad main feature is located at 96 cm^{-1} in the original muscovite, but the shape of that feature can not be explained by this band alone, further peaks are necessary. Thus a band component analysis was undertaken, which revealed several additional bands in the entire range for all spectra.

As can be seen in Table 7.1, the band component analysis revealed three more bands at 89, 104 and 110 cm^{-1} . These additional bands appear in all spectra nearly without shifting their positions. But the nitrate-treatments lead to strong changes in the band intensities.

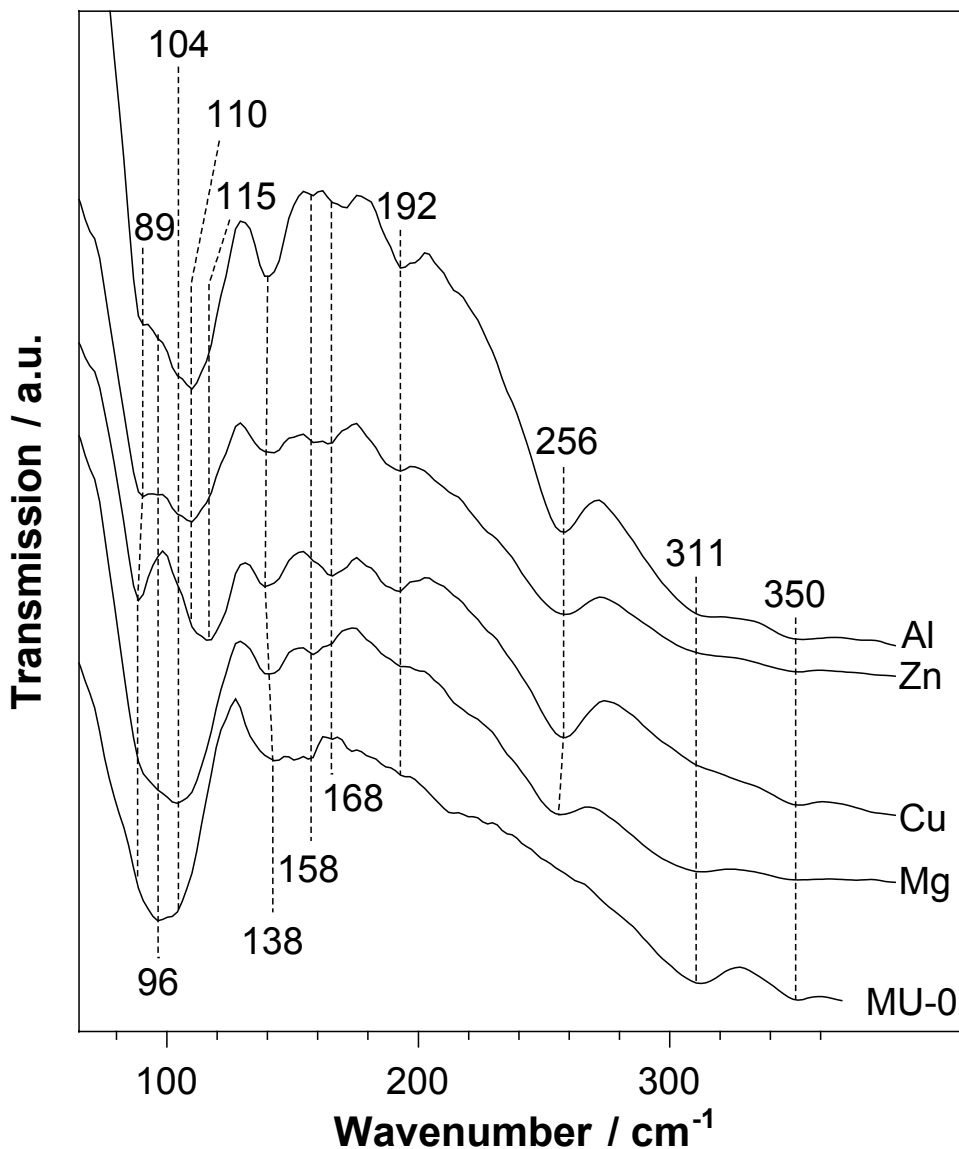


Figure 7.1 Far infrared spectra of muscovite (MU-0) and of Mg-, Cu-, Zn- and Al-nitrate treated samples in the range between 65 and 380 cm^{-1} .

The Mg-nitrate muscovite shows the smallest changes, only the center of the broad feature shifts from the 96 cm^{-1} mode to the band at 104 cm^{-1} . In contrast to this the Cu-nitrate sample shows two strong maxima at 88 and at 115 cm^{-1} . This band also appears at nearly the same position (117, 118 cm^{-1}) in the Zn-

and Al-nitrate samples. The other vibrations appear in Cu-nitrate muscovite as weak shoulders at 95, 102 and 110 cm^{-1} . In the Zn- and Al-nitrate muscovite spectra the two maxima are not as marked as in the Cu-muscovite.

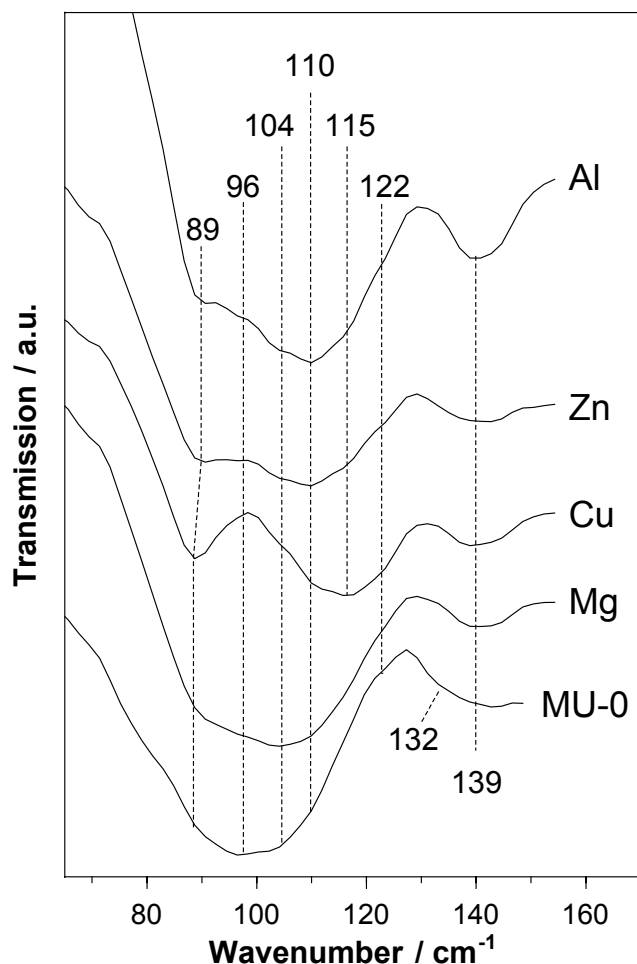


Figure 7.2 Detailed view on the far infrared spectra of muscovite (MU-0) and Mg-, Cu-, Zn- and Al-nitrate treated samples, showing the region of the main K-O band around 100 cm^{-1} .

Here the major bands appear at 89 and 110 cm^{-1} , surrounded by shoulders at 96 , 103 and 117 cm^{-1} in Zn-nitrate muscovite and at 96 , 101 and 118 cm^{-1} in Al-muscovite. A further weak shoulder appears at about 122 cm^{-1} in all spectra, without shifting or changing intensity. The band at 132 cm^{-1} is almost invisible in the spectra, but it is necessary to describe the shape of the curve. It is discussed, later if this band has physical reasons, or if it has to be excluded, due to being a fitting artefact. The next strong mode is located at about 140 cm^{-1} in all spectra except the muscovite spectrum. Here the band component analysis showed two close bands at 139 and 143 cm^{-1} . Notice, that this band is very broad in the muscovite spectrum, possibly due to the existence of the mode at

132 cm^{-1} . Two weak bands appear at 155 and 168 cm^{-1} , another band at 190 cm^{-1} is almost invisible in the muscovite spectrum, but increases in intensity in the series $\text{Mg} < \text{Cu} < \text{Zn} < \text{Al}$. Upon the nitrate treatment a new band appears at 256 cm^{-1} , but its position is not affected by the kind of cation. At 311 and 350 cm^{-1} two broad peaks appear, which are weakend in all treated samples and nearly disappear in the Mg-nitrate spectrum.

Table 7.1 Far infrared band positions of the pure muscovite (MU-0) and the nitrate treated samples obtained by band component analysis. (Results with squared correlations of $r^2 > 0.9995$)

Muscovite cm^{-1}	Mg-treated cm^{-1}	Cu-treated cm^{-1}	Zn-treated cm^{-1}	Al-treated cm^{-1}
66	67	67	68	68
78	78	78	78	76
89	90	88	89	89
96	94	95	96	96
104	104	102	103	101
111	109	110	108	109
-	-	115	117	118
121	123	122	123	124
-	138	137	139	139
143	143	143	143	-
155	156	158	-	-
168	165	168	165	165
190	194	195	193	195
-	254	257	257	256
311	312	310	313	313
350	350	350	351	350

7.4 DISCUSSION

Ishii et al. (1967) and Tateyama et al. (1977) have been among the first researchers to study absorption spectra of micas down to 60 cm^{-1} . On the basis of frequency and K-O distance calculations the observed bands were assigned to Si_2O_5 and octahedral layers. Concurring with each other several authors attributed the bands in the lowest spectral range to motions of the interlayer cations (Fripiat 1981, Schroeder 1992, Badreddine et al. 2002). Especially the potassium vibrations have been intensively investigated (e.g. Prost and Laperche 1990, Laperche and Prost 1991, Diaz et al. 2002). In general the bands at 108 cm^{-1} and 143 cm^{-1} are assigned as the diagnostic modes for K^+ interlayer vibrations (Ishii et al. 1967, Prost and Laperche 1990). Some

additional bands at 99, 190 and 211 cm^{-1} have also been assigned to K-O vibrations, and to motions of the entire interlayer region, respectively (Ishii *et al.* 1967). Surprisingly all these authors did not discuss the strong asymmetry of the 108 cm^{-1} band in most of the presented spectra. Moreover, they attributed band shifts upon cation exchange experiments to vibrational modes of the incorporated foreign cations, although the “new” bands are located at the same positions as the former asymmetric shoulders in the 108 cm^{-1} band (Fripiat 1981, Prost and Laperche 1990, Badreddine *et al.* 2002).

In contrast to this, the untreated muscovite in this study shows a maximum at 96 cm^{-1} (Figure 7.2). Only the band component analysis reveals additional band positions, including the 110 cm^{-1} mode. Upon the nitrate treatment this mode strongly increases its intensity. After 240 hours of Al- and Zn-nitrate treatment the maximum shifted to 109 and 108 cm^{-1} (Figures 7.3b and 7.4a).

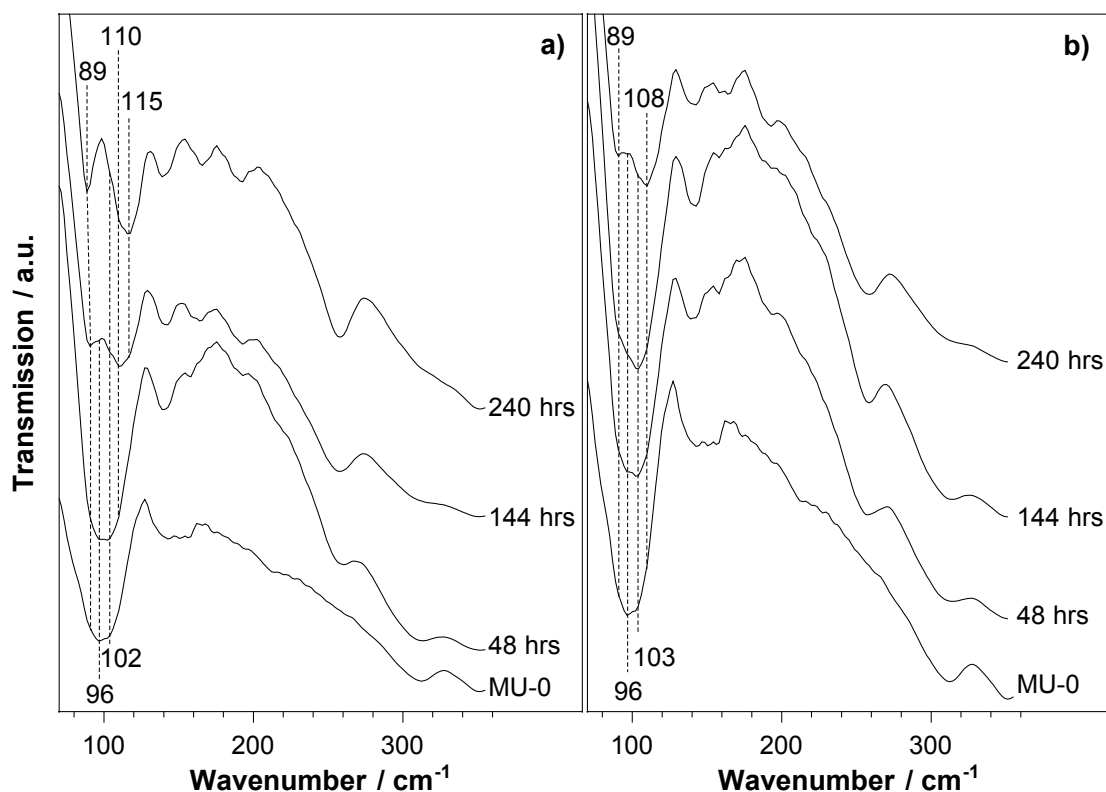


Figure 7.3 Far infrared spectra of nitrate treated muscovites as a function of treatment time between 48 and 240 hours. a) Cu-nitrate treated sample, b) Zn-nitrate treated sample.

In the Cu-muscovite spectra it appears as a strong shoulder in a new formed mode at 117 cm^{-1} (Figure 7.3a), the Mg-nitrate treatment affected the bands to

a minor degree, therefore the 110 cm^{-1} band is a broad maximum together with the band at 96 cm^{-1} (Figure 7.4b).

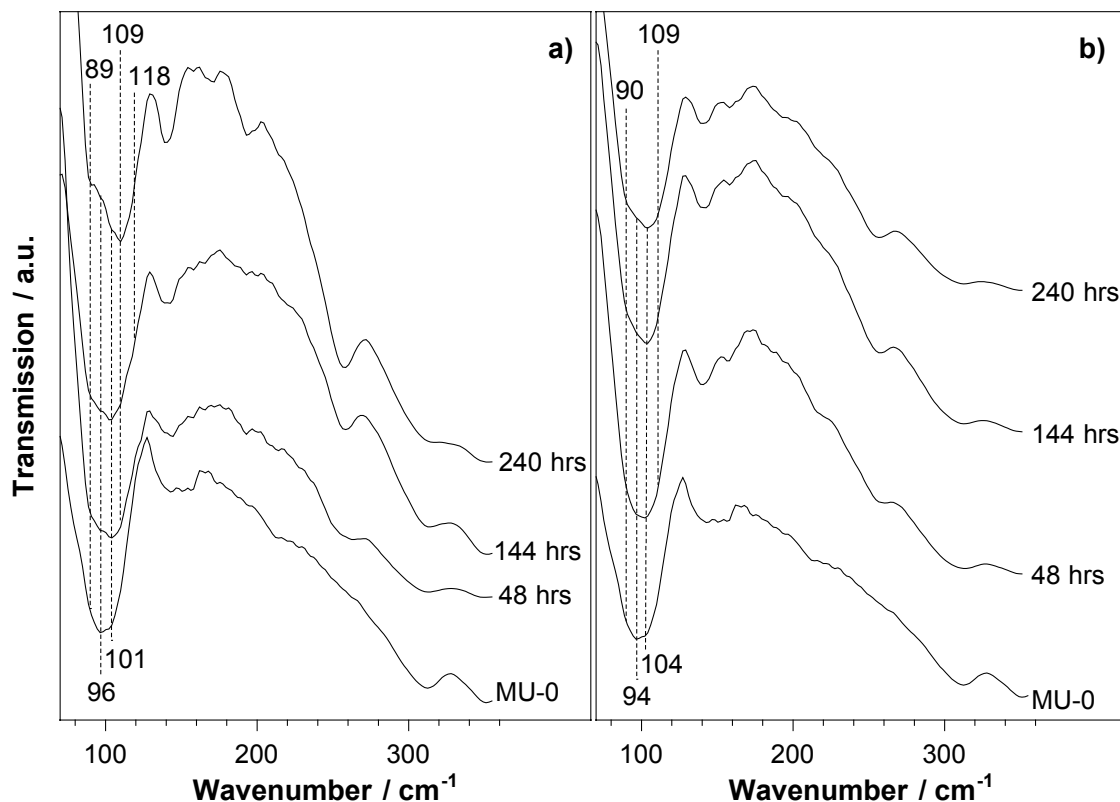


Figure 7.4 Far infrared spectra of nitrate treated muscovites as a function of treatment time between 48 and 240 hours. a) Al-nitrate treated sample, b) Mg-nitrate treated sample.

A possible explanation for these unusual band positions is given by Prost and Laperche (1990). They observed a shift of the K-absorption band at 110 cm^{-1} to 97 cm^{-1} during heat treatment and explained this with an increasing K-O(H) distance due to the loss of protons during dehydroxylation.

Figure 7.5 shows the DRIFT spectra of the original muscovite used in this study (MU-0) compared with a muscovite sample from Ploemeur, France (MU-F). Due to the remarkably lower intensity of the OH stretching bands of MU-0 at 3626 and 3648 cm^{-1} , it can be assumed, that this muscovite is partly dehydroxylated. This explains the occurrence of both bands at 96 and 110 cm^{-1} in the spectrum.

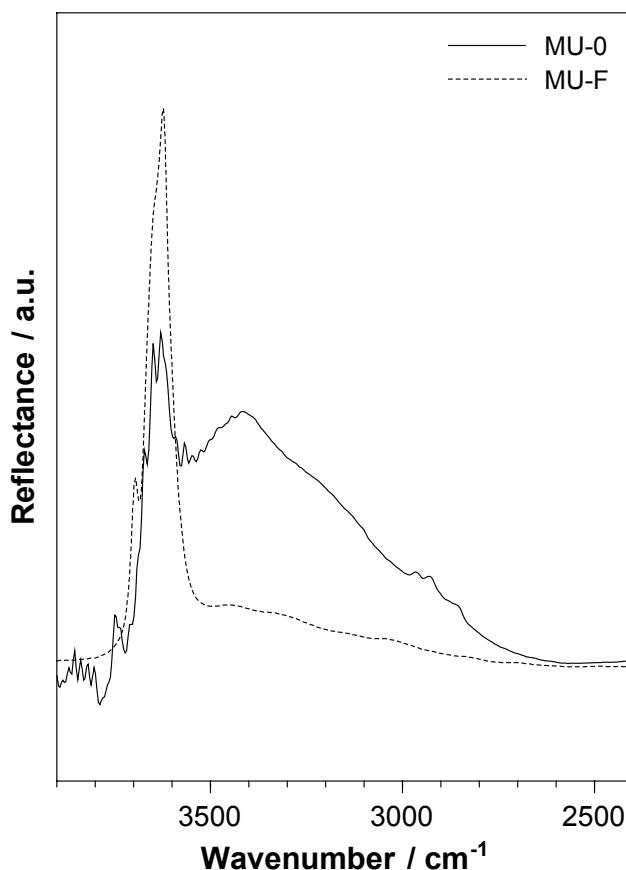


Figure 7.5 DRIFT spectra of the OH stretching region of the muscovite sample used in this study (MU-0) compared to a muscovite sample from Ploemeur, France (MU-F).

The appearance of the 110 cm^{-1} band and the strong decrease of the 96 cm^{-1} band due to the Cu-, Zn- and Al-nitrate treatment probably can be attributed to a slow rehydration of the muscovite layers during the migration of these ions into the interlayer and further into the ditrigonal holes of the tetrahedral layer. Figures 7.4a and b show the time dependence of the process for the Cu- and Zn-nitrate treatment. This supports the results, obtained from the mid infrared study introduced in the preceding chapter. Also the minor changes in the Mg-muscovite spectra, especially the lack of a strong band at 110 cm^{-1} , is in good agreement with the MIR results, implying that the magnesium ions do not migrate as deep into the structure, as the other three cations. But the occurrence of further bands at 89 , 104 and 115 cm^{-1} and the strong changes in their intensities due to the nitrate treatment can not be explained by dehydroxylation and rehydration processes alone.

Instead the occurrence of a band at 115 cm^{-1} in the Cu-muscovite and of the somewhat weaker shoulders at 117 and 118 cm^{-1} in the Zn- and Al-nitrate samples are assumed to appear due to the migration of the foreign cations into the interlayers. The simultaneous occurrence of all the bands in this range can be attributed to the formation of an irregular mixed-layer phase upon the nitrate treatment, consisting of “untreated” muscovite-like layers and some more smectite-like layers with additional cations in the structure. Hence, according to the XRD results presented in chapter 5, the formation of a rectorite-like mineral phase is suggested. The presented spectra are in good agreement with far infrared data of several mixed-layer illite-smectites, showing two bands at $84 - 90\text{ cm}^{-1}$ and $108 - 115\text{ cm}^{-1}$ (Diaz et al. 2002). In the spectrum of a potassium rich rectorite the bands were located at 87 and 113 cm^{-1} , with an additional broad band at 136 cm^{-1} . A similar weak band is also observed at 143 cm^{-1} in our muscovite spectrum, which slightly shifts its position to 138 cm^{-1} upon the nitrate treatment. Diaz et al. (2002) assigned this band to the K-O out-of-plane vibration in an illitic mica, while the other modes are attributed to K^+ fixed in illitic interlamellar spaces of rectorite. Schroeder (1992) attributed these bands to the existence of K^+ in two different environments. The high wavenumber band was assigned to K^+ in a high charge, Al-rich environment, whereas the low wavenumber band resulted from K^+ in a lower charge Fe- and Mg-rich site. Thus the occurrence of the splitted bands in the Cu- and Zn-nitrate, and to a minor degree the Al-nitrate treated samples (Figures 7.4 and 7.5a) possibly suggests the migration of these cations into the TOT structure of the mineral, forming a low charge Cu- or Zn-rich site.

The modes above 140 cm^{-1} are more difficult to assign, because the bands in this spectral range are assumed to be not only due to simple stretch vibrations. The study of Velde and Couty (1985) showed, that the bands in that region are present in most of the investigated phyllosilicates (di- and trioctahedral, with and without interlayer ions) and therefore they suggested that a major component of these bands are vibrations of the Si-O sheet lattice which is common to all of the structures. Nevertheless it is interesting that these lattice vibrations are affected by the nitrate treatment. The reasons for this behaviour again should be the migration of the foreign cations into the interlayer region

and into the ditrigonal holes of the tetrahedral sheet. This is reflected a) by the increasing intensity and the splitting of the broad area around 150 cm^{-1} into better resolved bands, and b) by the strong decrease of the vibrations at 311 and 350 cm^{-1} . As all these modes can be assigned to vibrations dominated by the Si_2O_5 units, this contrary behaviour seems to be inconsistent, but it can be explained by different kinds of lattice motions: The bands at 311 and 350 cm^{-1} are attributed to an “ideal” hexagonal Si_2O_5 unit (Ishii et al. 1967, Farmer 1974). Their intensities decrease due to the migration of additional cations, leading to distortions of the siloxane rings (Badreddine et al. 2002). In contrast to this, additional components affect the Si_2O_5 vibrations at 158 , 168 , 192 and 258 cm^{-1} . Therefore, the bands at 158 and 192 cm^{-1} are assigned to combined vibrations of the siloxane sheets and the interlayer cations (Diaz et al. 2002). Furthermore the band at 168 cm^{-1} has an additional OH related component (Velde and Couty 1985). The increasing intensities of these interlayer vibrations probably can be assigned to a stronger fixation of the interlayer cations within the structure. A possible explanation is given by Badreddine et al. (2002), who showed that the incorporation of additional Ca^{2+} into the interlayers of vermiculites does not only result in expanded interlamellar spaces in the mixed-layer phase, but also induces an expansion along the b dimension and a change in α , the angle of rotation of the tetrahedra. These changes in α induce an opening of the ditrigonal cavity. This has the two observed effects. On the one hand the interlayer cations migrate into the holes and hence will be fixed by strong bonds leading to an increase of the corresponding vibrational modes. On the other hand vibrations of “ideal” Si_2O_5 units are disturbed and their intensities decrease.

7.5 CONCLUSIONS

The far infrared spectrum of the muscovite sample from Merck KgAa shows an unusually low main K-O band at 96 cm^{-1} . At the normal position (110 cm^{-1}) only a very weak shoulder appears. In accordance to DRIFT spectra of the OH-stretching region this is attributed to a partial dehydroxylation of this mineral.

The Al-, Cu-, Mg- and Zn-nitrate treatment of this muscovite shows several effects:

- (1) The intensities strongly change due to the treatment. Especially the weak shoulder at 89 cm^{-1} strongly increases and after a treatment time of 240 hours it appears as one of two major bands in the Cu-, Zn-, and to a minor degree in the Al-spectra. At the same time the band at 96 cm^{-1} strongly decreases.
- (2) A new band occurs at 115 cm^{-1} in the Cu-, Zn- and Al-spectra and
- (3) The intensity of the very weak shoulder at 110 cm^{-1} increases in all spectra.

The simultaneous occurrence of all these bands suggests the formation of a mixed-layer phase similar to rectorite. This means, the foreign cations migrate into the structure, expanding the interlamellar spaces and along the *a*-axis. The additional changes in α induce an opening of the ditrigonal cavity, and thus migration paths are open for the intercalated cations.

Although no element specific shifts of interlayer-vibrations could be observed, this far infrared study provides evidence for the movement of cations into muscovite interlayers and their migration into the ditrigonal cavities.

REFERENCES

- Badreddine, R., Le Dred, R. and Prost, R. (2002) A far infrared study of K^+ ions during $\text{K}^+ - \text{Ca}^{2+}$ exchange in vermicullite. *Clay Minerals*, **37**, 59 - 70.
- Diaz, M., Laperche, V., Harsh, J., Prost, R. (2002) Far infrared spectra of K^+ in dioctahedral and trioctahedral mixed-layer minerals. *American Mineralogist*, **87**, 1207 - 1214.
- Farmer, V.C. (1974) Layer silicates. Pp. 331 - 364 in: *The infrared spectra of minerals*. (V.C. Farmer, editor), Monograph **4**, Mineralogical Society, London.
- Friedrich, F., Weidler, P.G. and Nüesch, R. (2003) Chemical delamination of muscovite by nitrates of di- or trivalent metal cations in autoclaves. Euroclay 2003, Modena, Italy, June 22 – 26, 2003.

-
- Fripiat, J.J. (1981) Application of far infrared spectroscopy to the study of clay minerals and zeolites. Pp. 191 – 210, in: *Advanced techniques for clay mineral analysis*. (J.J. Fripiat, editor), Developments in Sedimentology, **34**, Elsevier, Amsterdam.
- Ishii, M., Shimanouchi, T. and Nakahira M (1967) Far-infrared absorption spectra of layer silicates. *Inorganica Chimica Acta*, **1**, 387 – 392.
- Laperche, V. and Prost, R. (1991) Assignment of the far-infrared absorption bands of K in micas. *Clays and Clay Minerals*, **39**, 281 - 289.
- Loh, E (1973) Optical vibrations in sheet silicates. *Journal of Physics C: Solid State Physics*, **6**, 1091 - 1104.
- Madejova, J., Arvaiova, B. and Komadel, P. (1999) FTIR spectroscopic characterization of thermally treated Cu²⁺, Cd²⁺, and Li⁺ montmorillonites. *Spectrochimica Acta A*, **55**, 2467 – 2476.
- Prost, R. and Laperche, V. (1990) Far-infrared study of potassium in micas. *Clays and Clay Minerals*, **38**, 351 - 355.
- Schroeder, P.A. (1990) Far-infrared, X-ray powder diffraction, and chemical investigation of potassium micas. *American Mineralogist*, **75**, 983 - 991.
- Schroeder, P.A. (1992) Far-infrared study of the interlayer torsional-vibrational mode of mixed-layer illite/smectites. *Clays and Clay Minerals*, **46**, 81 - 91.
- Tateyama, H., Shimoda, S. and Sudo, T. (1977) Estimation of K-O distance and tetrahedral rotation angle of K-micas from far-infrared absorption spectral data. *American Mineralogist*, **62**, 534 - 539.
- Velde, B. and Couty, R. (1985) Far Infrared Spectra of Hydrated Layer Silicates. *Physics and Chemistry of Minerals*, **12**, 347 - 352.

CHAPTER 8

RAMAN SPECTROSCOPY OF PHYLLOSILICATES

8.1 INTRODUCTION

This chapter is divided into two parts. First the difficulties in obtaining Raman spectra of muscovite powders are investigated and the reasons for the appearance of strong fluorescence and background features are discussed. Thus, in the second part the well investigated clay mineral dickite was used as a reference material for the measurement of FT-Raman spectra on clay minerals. Additionally the changes in the dickite spectra due to the intercalation of DMSO and NMF are discussed.

8.2 MATERIALS AND METHODS

The muscovite powder and the Cu- and Zn-nitrate treated samples used in this Raman study, are the same that were chosen for the infrared measurements discussed in the preceding chapters. Their preparation is described extensively in chapter 2.1. Additional measurements were done on large single crystals of the original Merck muscovite. These flakes are approximately 1 cm in diameter.

The intercalation procedures for dickite:DMSO and dickite:NMF using the dickite of San Juanito are described in detail in chapter 2.2. The dry powders were measured without further preparation, only by pressing them into aluminum holders.

Several sampling techniques were used for the spectroscopy of the muscovite samples. First the sample powder was pressed into Al holders and was then measured, using the 180° optics. Furthermore the sample powders

were spread on a Raman mapping stage and then were measured without further preparation. For Surface Enhanced Raman Scattering (SERS) measurements single crystals were fixed on, or powder suspensions were dried on gold or silver coated mirrors and were clamped in the sample holder of the 180° optics. This technique also was used for the single crystal measurements by squeezing them together with the gold mirror into the sample holder.

The Bruker IFS66/S spectrometer equipped with a Bruker Raman FRA106 accessory was used for the FT-Raman measurements. Two lasers operating at wavelength of 1064 and 785 nm were at our disposal. The whole setup is described in chapter 3.

Additionally dispersive Raman measurements were carried out on the muscovite powders at Bruker Optics GmbH, using a SENTINEL spectrometer.

Chemical measurements were obtained by X-ray fluorescence analysis on pressed pellets using an energy dispersive SPECTRO X-Lab 2000 spectrometer. A detailed description of the measurement conditions can be found in chapter 4.

8.3 RAMAN SPECTROSCOPY OF MUSCOVITE

8.3.1 RESULTS

The results of the FT-Raman measurements using an excitation wavelength of 1064 nm are shown in Figure 8.1. Due to the possibly low thermal stability of the material against this long wave radiation, at first a low laser power of 100 mW was chosen. This results in a spectrum with remarkably increasing thermal background above 200 cm^{-1} and with a few peak-like features at wavenumbers above 1800 cm^{-1} (1831, 2224, 2502 cm^{-1}). Increasing the laser power does not improve the quality of the spectra, but the intensity of the background strongly increases with increasing power, on the contrary it is leading to a very intense and broad maximum at wavenumbers around 3000 cm^{-1} at a laser power of 800 to 1100 mW. In the 800 mW spectrum again some very weak band-like features

appear at 245, 395, 689, 762 and 1831 cm^{-1} , which are not visible in all the other spectra, except for the band at 1831 cm^{-1} .

To identify possible errors resulting from the sample preparation, in addition to the powdered samples (pressed into an Al-sample holder), KBr pellets were measured in the sampling compartment with the 180° lens optics. Furthermore unpressed powder was measured on a mapping stage. But all these measurement methods do not have any effect on the spectra, nor do attempts to decrease the noise by varying the number of scans between 30 and 720.

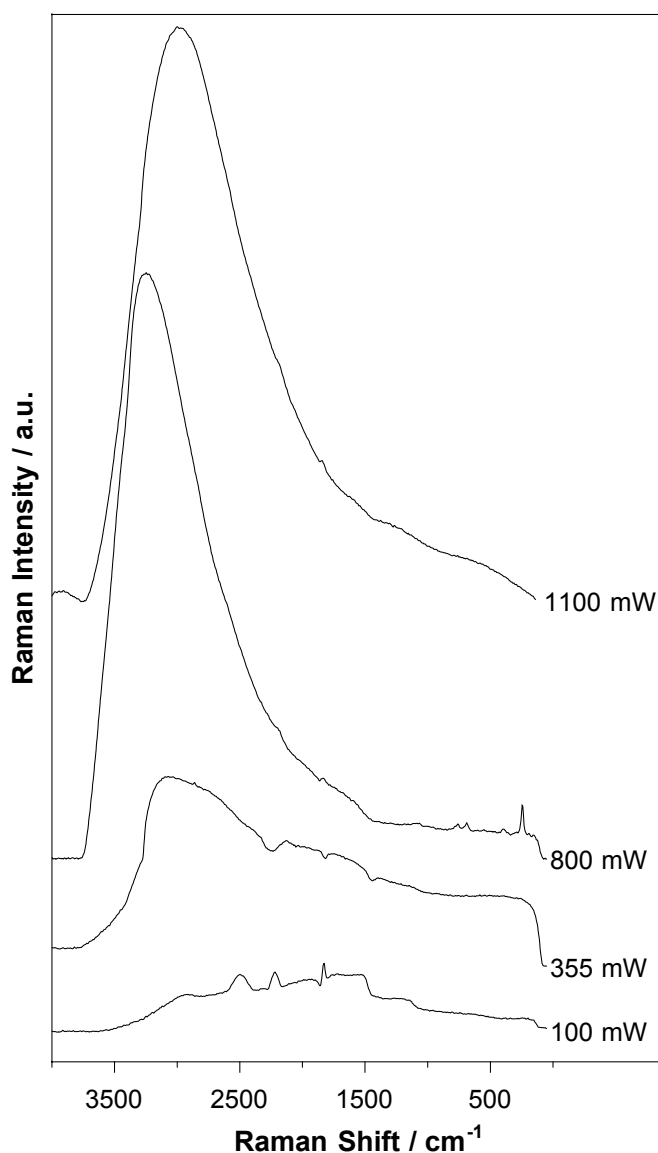


Figure 8.1 Comparison of FT-Raman spectra of a fine-grained muscovite sample in the range between 4000 and 250 cm^{-1} , using an excitation wavelength of 1064 nm. The thermal background strongly increases with increasing laser power.

Measurements using a laser with a lower wavelength at 785 nm reveal the same kind of spectrum, also showing a few broad peaks at 171, 1382, 1906 and 3276 cm^{-1} with an almost lower background (Figure 8.2).

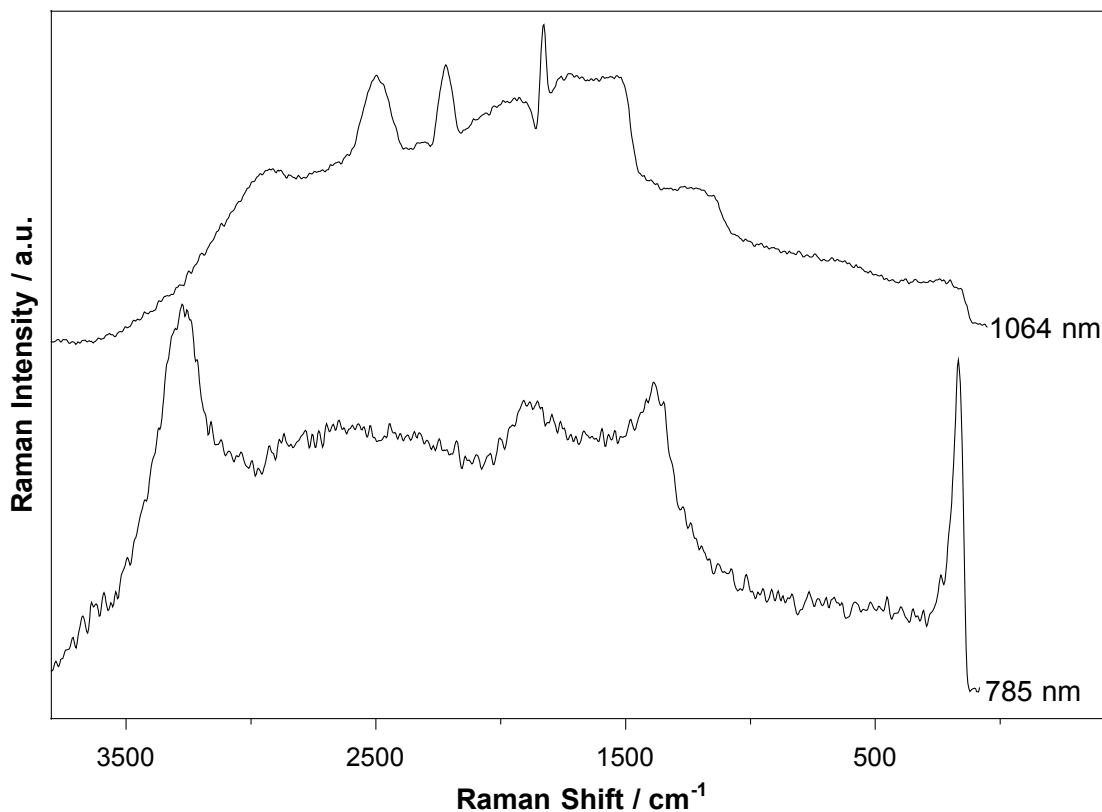


Figure 8.2 FT-Raman spectra of a fine grained muscovite sample ($4000 - 250 \text{ cm}^{-1}$). Comparison of two excitation wavelengths of 1064 and 785 nm.

Also the use of a dispersive Raman technique results in no utilisable spectra (Figure 8.3). Similar to the FT-Raman spectra they are dominated by a strong thermal background and they show a number of peak-like features. But Figure 8.3 also shows differences in the spectra, depending on the measured samples. While, for example, the spectrum of the original muscovite has a very regular wave like structure without assignable bands, the Cu-muscovite spectrum shows a much lower background and some sharp bands at 1063, 1127, and 1295 cm^{-1} . A weaker triplet appears at 1419, 1441 and 1461 cm^{-1} .

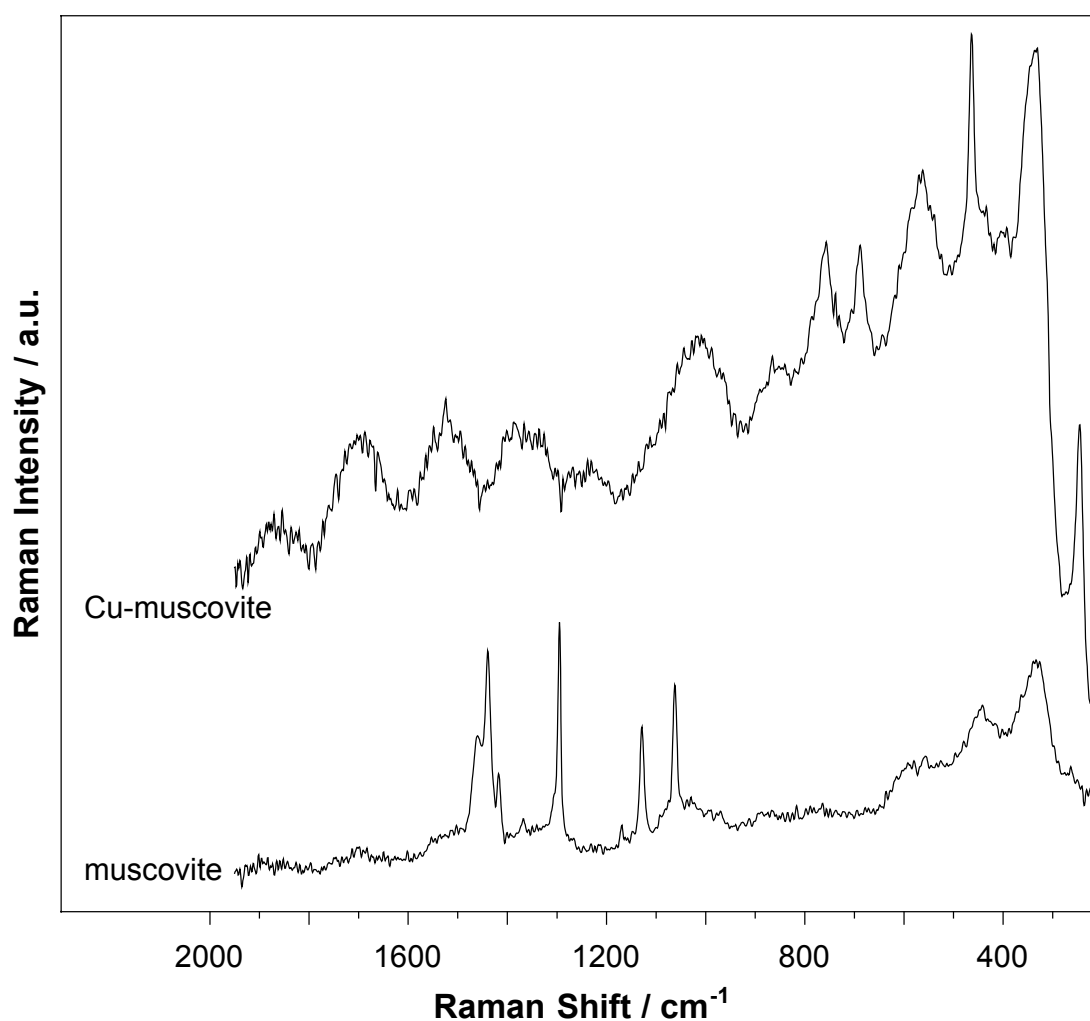


Figure 8.3 Dispersive Raman spectra of fine grained muscovite and a Cu-nitrate treated muscovite in the range between 2000 and 200 cm^{-1} .

8.3.2 DISCUSSION

One of the main problems of Raman spectroscopy is the very weak intensity of the vibrational bands (0.1% of the incident intensity). Therefore they can be superimposed very easily by distortions due to additional interactions of the specimens with the excitatory radiation.

Surprisingly the very rare literature data on Raman spectroscopy of micas (Haley *et al.*, 1982; McKeown *et al.*, 1999a, 1999b) do not report any difficulties during the measurements. To the contrary, they show very clear spectra, without intense backgrounds and fluorescence features. While the technical set-ups are very similar to our system, the only difference is assumed to be the use

of large single crystals instead of powders to collect the spectra, due to the lack of precise descriptions of sample preparation in the mentioned articles.

However, the muscovite spectra presented in Figures 8.1 – 8.3 only show strong backgrounds without interpretable Raman bands, independent of the chosen Raman method. Most spectra show two major kinds of features:

a) a very broad and intense band at Raman shifts of about 3000 cm^{-1} (Figure 8.1) and b) an intense thermal background over the whole spectral range, with protruding peaks of some band like features. Feature a) is in accordance with the fact that an intense fluorescence background is very often encountered with dispersive instruments, when visible light is used for excitation (e.g. Kohlrausch 1972). However, Varetti and Baran (1994) found that fluorescence still can be an important feature in FT-Raman spectroscopy, when exciting powdered samples with infrared radiation, especially for inorganic compounds like Al_2O_3 , phosphate minerals, rare earth minerals, catalysts or zeolites (Hendra et al. 1991, Tanner et al. 2002).

Besides, some additional effects possibly cause the high background especially in the lower wavenumber regions (feature b). For example the diffuse scattering of the primary beam at the particle surfaces in muscovite powder results in an increasing background over the entire spectral range, as well as an increasing sample temperature, which is caused by its interaction with the excitatory radiation at higher laser powers (Kohlrausch 1972). This is in accordance with my observations, that measurements with high laser powers above 800 mW cause visible damages in the pressed sample powders (change of colour, small craters).

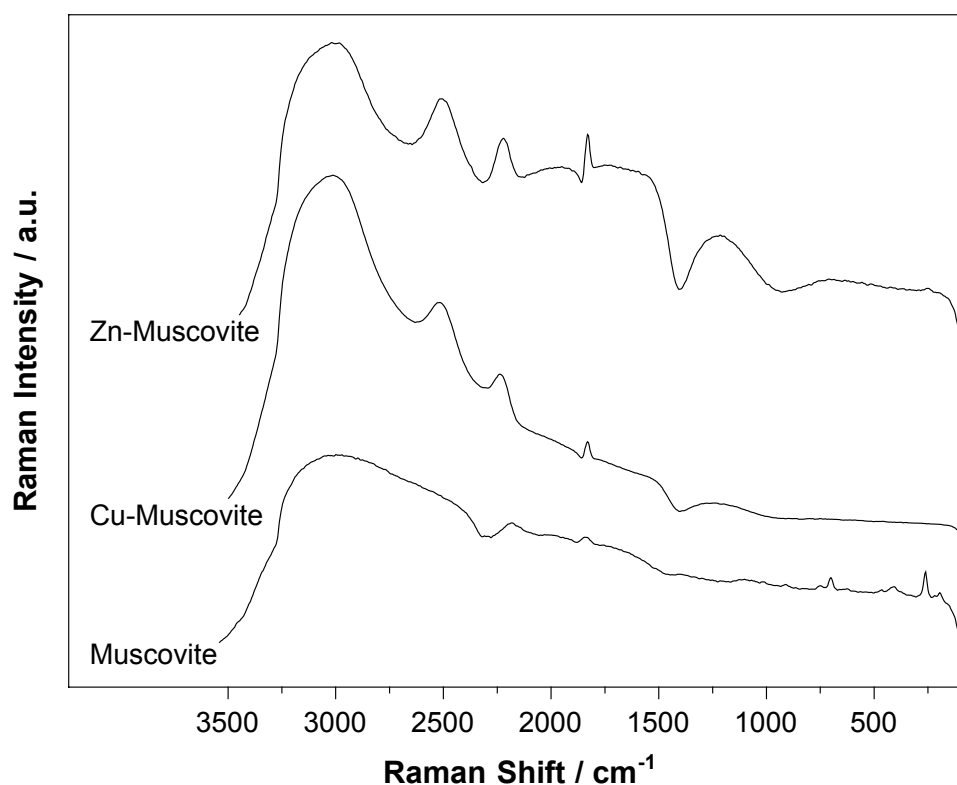


Figure 8.4 FT-Raman spectra of a fine grained muscovite sample in the range between 3500 and 100 cm^{-1} . The intercalated metal cations Cu and Zn increase the strong disturbing features, but the high fluorescence background even exists in the untreated muscovite.

Distortions in anomalously high backgrounds like those observed in the 100 mW spectrum in Figure 8.1 or in the 1064 nm spectrum in Figure 8.2 can be explained by diffuse reflection and scattering of the particle surfaces, which does not appear during the measurement of single crystals. Tanner *et al.* (2002) and Varetti and Baran (1994) showed that similar effects are caused in compounds like Al_2O_3 by “activator cations” of the transition metal groups, especially by Fe(III). As the muscovite samples contain a relatively high amount of iron (Table 8.1), the spectra in Figure 8.4 show no fundamental differences between the original muscovite and the Cu- and Zn-nitrate treated samples.

Table 8.1 Element analysis (wt. %) of the original muscovite (MU-0) and dickite (San Juanito).

Major elements / wt. %	Muscovite	Dickite
Na ₂ O	0,69	< 0,03
MgO	< 0,02	< 0,02
Al ₂ O ₃	33,69	38,31
SiO ₂	48,96	46,86
P ₂ O ₅	0,05	0,61
SO ₃	0,04	0,86
K ₂ O	9,46	0,05
CaO	0,06	0,29
TiO ₂	0,24	0,14
MnO	0,02	< 0,01
Fe ₂ O ₃	1,90	0,20
LOI	0,91	14,60
Total	96,04	101,98

Trace elements / ppm		
Ni	22	< 2
Cu	5	3
Zn	60	4
Ga	67	31
Zr	18	79
Rb	936	2
Cs	102	4
Sr	16	1078
Ba	356	491

But the already existing high background increased with the intercalation of these two transition metal group elements. Additionally occurring broad features between 2500 and 1400 cm⁻¹ and the shift of the strong and very broad peak at 3053 cm⁻¹ to about 3000 cm⁻¹ are also influenced by these cations. The relative similarities in the Cu- and Zn-spectra may be attributed to the neighbourhood of copper and zinc in the periodic system, having very similar masses, radii and electronic structures (Cu: Ar 3d¹⁰ 4s¹; Zn: Ar 3d¹⁰ 4s²).

However, obviously these disturbing effects can not be removed from the spectra by the use of an excitation radiation with a lower wavelength (785 nm). Partly this may be attributed to the remarkably lower laser power of maximum 230 mW, but Figure 8.2 shows that the background is still much too high to obtain an interpretable spectrum.

In fact spectra collected with dispersive Raman technique also showed an intense background (Figure 8.3), but surprisingly especially in the pure muscovite spectrum. In contrast to this, the background in the Cu-treated sample spectrum is remarkably lower. Therefore a few Raman bands appear, whose assignment is very difficult, due to the lack of data about Raman bands above wavenumbers of 1200 cm^{-1} for mica minerals. McKeown *et al.* (1999b) assigned two modes at 1063 cm^{-1} and at 1120 cm^{-1} to stretching vibrations of the Si-O tetrahedra in muscovite. If we assume in accordance with Haley *et al.* (1982) and McKeown *et al.* (1999b) that the positions of the Raman bands are in the same regions as the IR-active vibrations of the structural units in muscovite, the mode at 1295 cm^{-1} also can be assigned to a stretching vibration of Si-O. Raman and IR-bands in the spectral region around 1400 cm^{-1} are very uncommon in phyllosilicate spectra. Therefore they possibly have to be assigned to vibrational modes of $\text{Cu}(\text{NO}_3)_2$, which has not completely been removed after the autoclave treatment.

It is obvious that the use of aluminium sample holders for the measurement of muscovite powders increases the background drastically, especially at higher wavenumbers (Figure 8.5a). While spectra of unpressed powders on a mapping stage show a much lower background, this feature suggests, however, an interaction between the electronic states of the aluminium of the holder and of the muscovite samples.

A further decrease of noise and an improvement of the vibrational bands is obtained using Surface Enhanced Raman Scattering (SERS) of muscovite suspensions dried on aluminium or gold coated mirrors (Figure 8.5b). But the best results are obtained by SERS measurements of large muscovite crystals. Figure 8.6 shows a clear and reproducible spectrum in the range between 150 and 1200 cm^{-1} .

Furthermore, Table 8.2 shows the strong correspondence of these spectra to the assignments of McKeown *et al.* (1999b). The single crystal bands are stronger and, at the same time partly shifted to higher wavenumbers, than the

features in the powder spectrum. But in fact Figure 8.5b shows a clear spectrum of a fine grained muscovite for the first time.

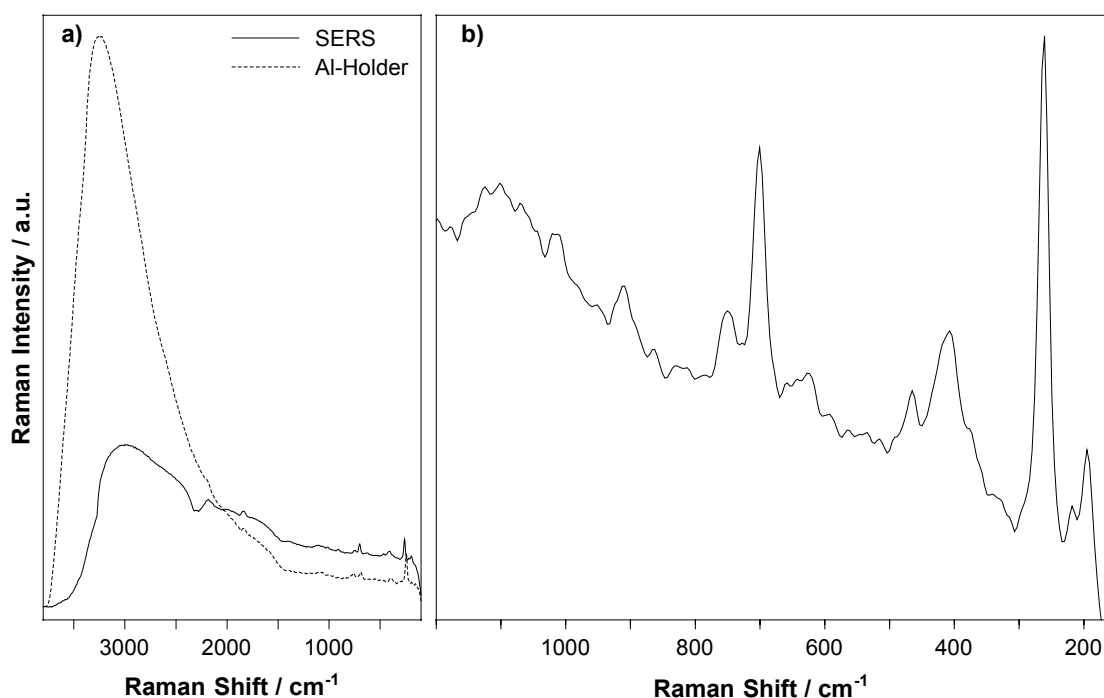


Figure 8.5 Spectra obtained by several sampling techniques. a) Comparison of spectra using a mapping stage and an aluminium sample holder. b) SERS spectrum of a dried suspension of fine muscovite on a gold coated mirror.

Thus these results suggest, that the background and fluorescence features in the spectra of muscovite strongly depend on the grain size of the material. As in literature only Raman spectra of large mica crystals are available, it is not certain yet, if FT-Raman spectroscopy is a useful technique for the study of fine grained phyllosilicates.

To understand the reasons for this very different behaviour, it is necessary to verify the influence of the spectrometer parameters. Therefore in the following part the well investigated phyllosilicate dickite and its intercalation compound dickite:DMSO are used as reference samples. Furthermore with this set-up FT-Raman measurements at dickite:NMF are carried out for the first time, and a structural analysis is performed to investigate the influence of the incorporated molecules on the dickite interlayer space and on the adjacent tetrahedral and octahedral sheets.

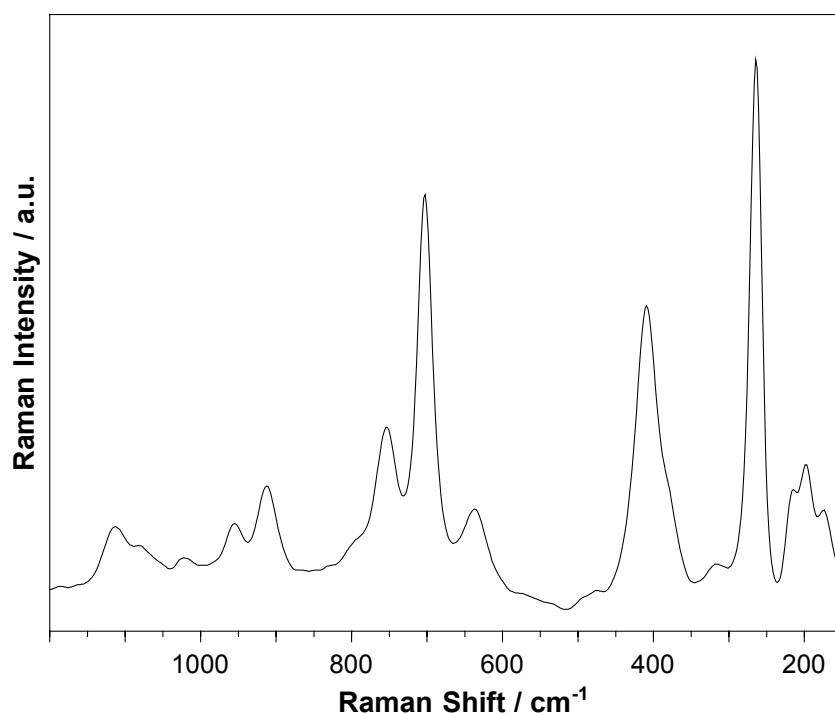


Figure 8.6 SERS spectrum of a muscovite single crystal on a gold coated mirror.

Table 8.2 Observed Raman bands of a powdered and a single crystal muscovite compared to the calculated frequencies of McKeown *et al.* (1999b).

Observed / cm ⁻¹		Calculated / cm ⁻¹	Suggested assignments
Single crystal	Powder	McKeown <i>et al.</i> (1999)	
174	-	177	Al-OH stretching
199	195	193	Al-OH stretching + O _T translation
216	218	214	OH-Al-OH + Al-O
265	260	272	OH + K-O translation
318	-	316	Al-OH + Al-O stretching + tetrahedral rotation
380	376	380	Al-O translation
409	407	405	K-O translation
478	465	483	Al-O stretching + tetrahedral rotation
532	534	540	Si-O-Si bending
573	-	573	Si-Oi translation + K translation
636	627	659	O _T translations
702	700	702	Al-O translation + O _T translations
754	754	754	O-Al-O bending
796	-	-	Al-O-Al (?)
827	827	820	Si-O bending
912	912	-	distorted Al-OH (?)
956	951	970	Si-O stretching
1022	1012	1017	Si-O stretching
1082	1070	1097	Si-O stretching
1115	1102	1118	Si-O stretching

8.4 RAMAN SPECTROSCOPY OF DICKITE AND ITS INTERCALATES

8.4.1 MEASUREMENT OF USEFUL SPECTRA

The FT-Raman spectra of dickite and its intercalates using an excitation wavelength of 1064 nm exhibit very clear spectra with a lot of sharp bands especially in the region around 3200 cm^{-1} and below 1500 cm^{-1} (Figure 8.7). The best spectra are those using a laser power of 600 mW, only the region between 2600 and 1500 cm^{-1} shows a low fluorescence background.

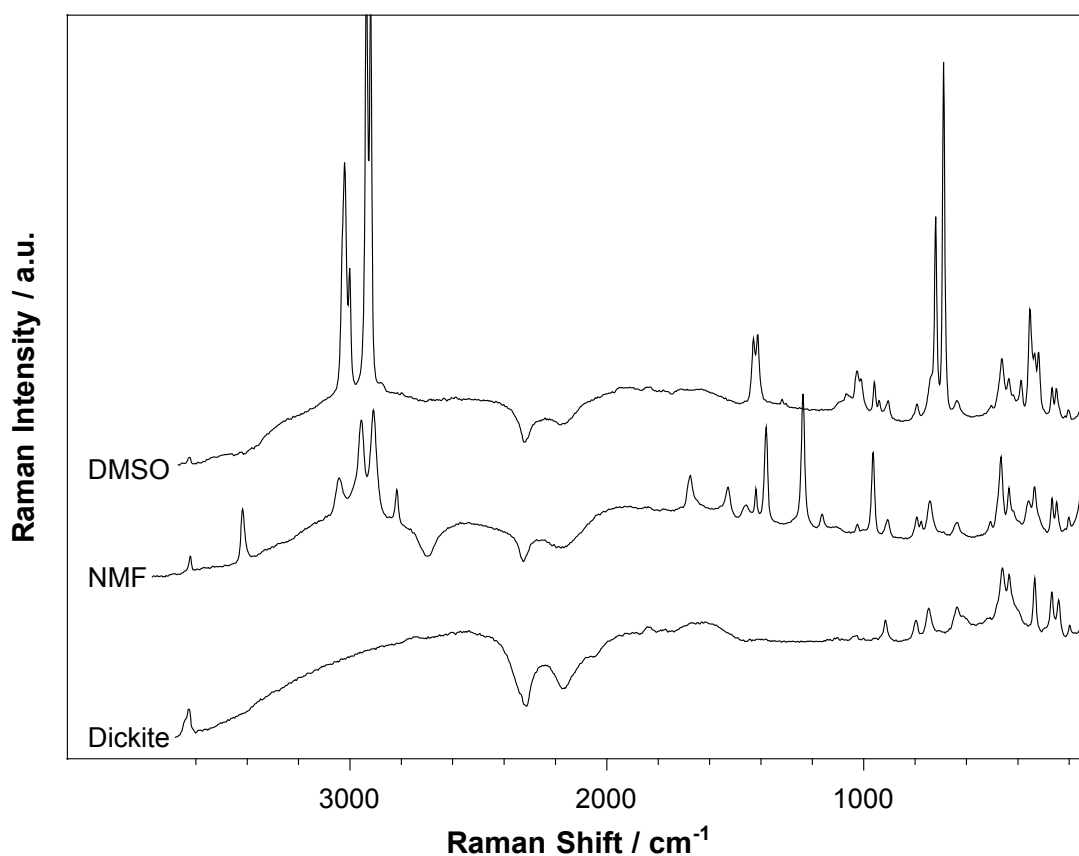


Figure 8.7 FT-Raman spectra of dickite and its intercalates dickite:DMSO and dickite:NMF in the range of 3800 to 150 cm^{-1} .

Similar to the muscovite spectra, variations in the laser power lead to the appearance of background features and to a strong increase of fluorescence (Figure 8.8).

The reason for this very different behaviour of muscovite and dickite powders upon excitation with near infrared laser radiation is difficult to explain (Figure 8.9).

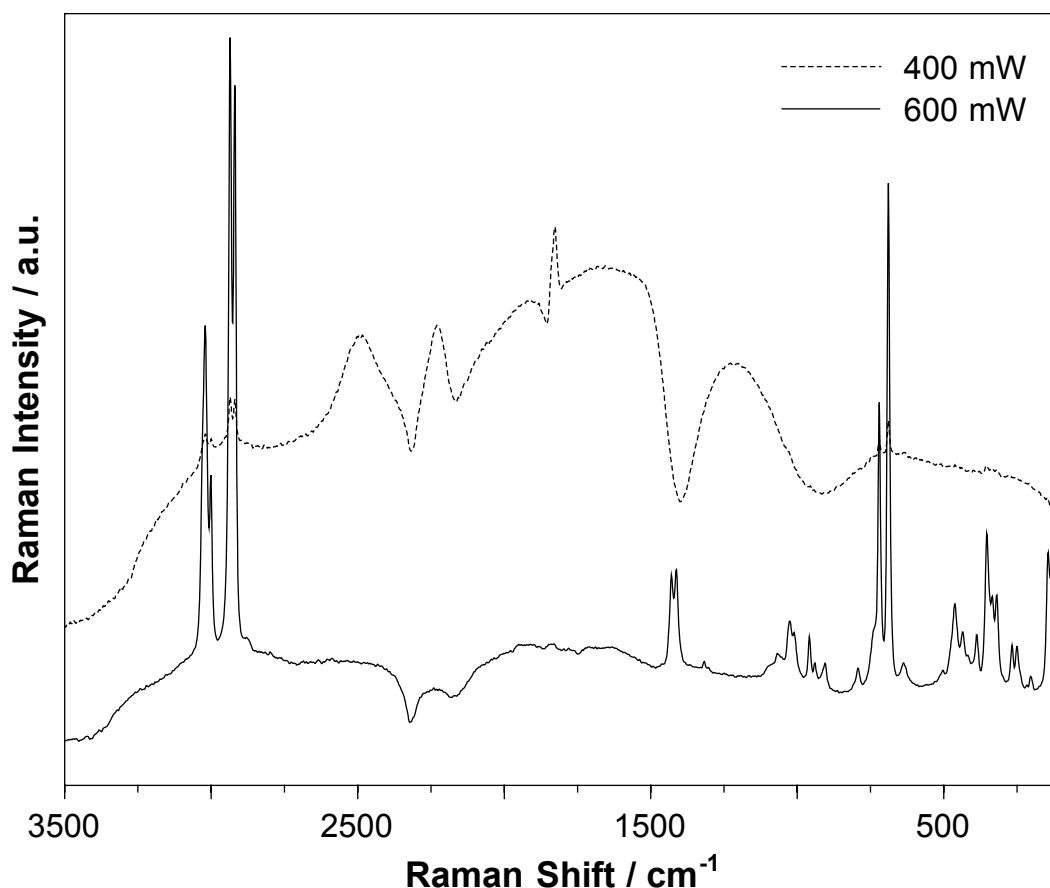


Figure 8.8 FT-Raman spectra of dickite:DMSO with the use of an excitation wavelength of 1064 nm operating at laser powers of 400 and 600 mW.

Possibly the remarkably lower Fe contents of the dickite samples are the main reason for the lack of disturbing background features in the dickite spectra (Table 8.1). Mortensen *et al.* (1991) reported an increasing fluorescence background with increasing Fe contents in Al_2O_3 . At the same time, smallest variations in the Fe concentrations cause dramatic changes in the background intensity. Already Aminzadeh (1997) proposed, that the only possible source for high fluorescence background in Al_2O_3 spectra is Fe^{3+} .

In contrast to the muscovites, no grain size effect can be observed during the measurements of the dickite samples. Although their grain sizes are remarkably smaller ($< 50 \mu\text{m}$) than those of the mica powders (maximum at $400 \mu\text{m}$), it is much easier to obtain spectra of good quality for the dickite samples than for the muscovite powders and even for the single crystals. However, no sample holder dependent background features are observed. Probably they

also occur, due to the remarkably higher Fe contents of the muscovites. Thus no further preparation and measurement techniques are necessary to obtain high quality spectra of the dickite compounds. Therefore a structural analysis of the spectra is possible, which is discussed in the following.

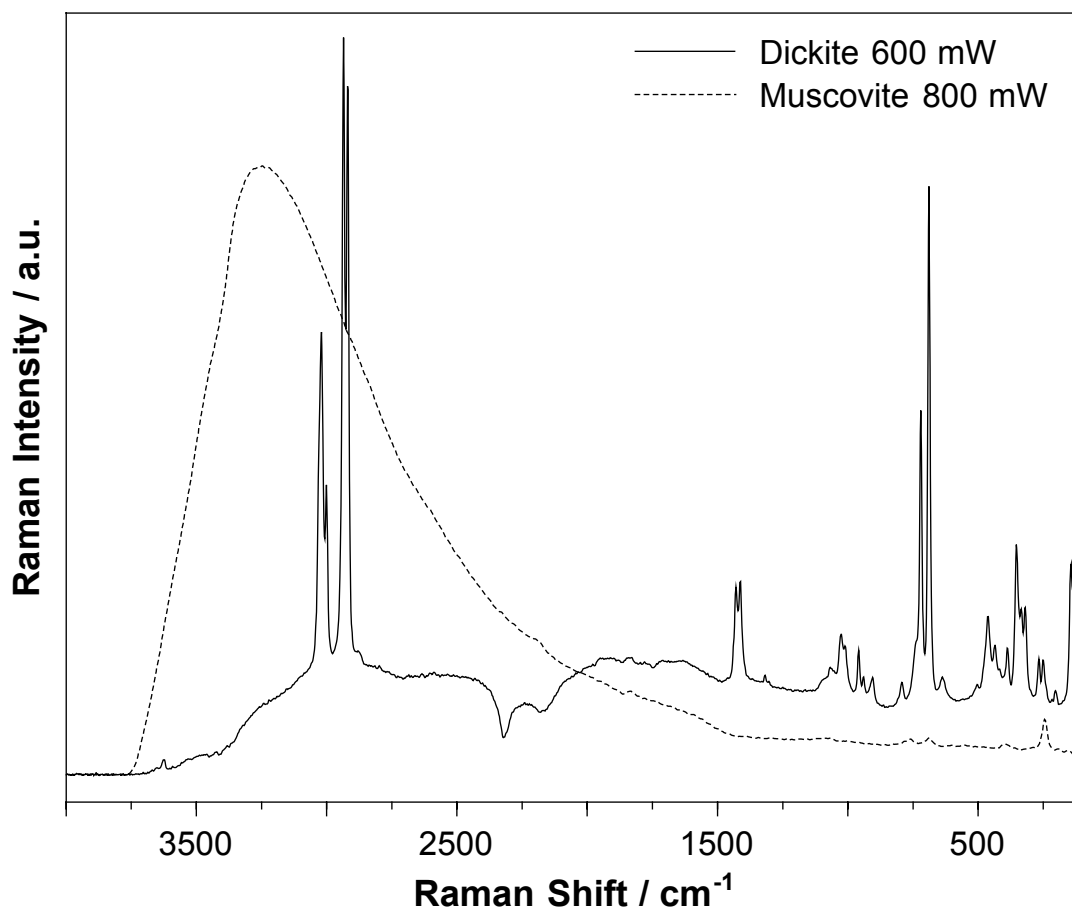


Figure 8.9 Comparison of FT-Raman spectra of muscovite and dickite:DMSO using an excitation wavelength of 1064 nm, operating at 800 mW (muscovite) and 600 mW (dickite:NMF).

8.4.2 STRUCTURAL ANALYSIS OF THE DICKITE RAMAN SPECTRA

OH stretching region. In general vibrational spectra of the OH stretching region of phyllosilicates give information about structural disorder and the incorporation of molecules and cations into the interlayer region. While four OH bands at 3620, 3639, 3652 and 3700 cm^{-1} are reported for the San Juanito dickite (Frost *et al.* 1993, 1995), in this study only two small bands appear at 3627 and 3645 cm^{-1} together with a very broad and weak elevation at about 3700 cm^{-1} (Figure 8.10, Table 8.3 and 8.4). The band at 3627 cm^{-1} can be assigned to the inner

hydroxyl groups of the dickite, whereas the two higher frequency vibrations are assigned to the inner surface OH-groups, which point into the interlayer region. Only the band at 3627 cm^{-1} still remains with decreased intensity after the intercalation of NMF and DMSO. According to Frost et al. (1998a) a possible explanation for these weak intensities and the later lack of most of these bands is the strong crystal orientation dependence of these vibrations. Moreover Frost et al. (2000) pointed out, that in formamide intercalated kaolinite these bands disappear too, and only the 3620 cm^{-1} band still exists after the intercalation. They attributed this to the fact, that the hydrogen bonding patterns are regenerated upon intercalation, which gives a strong hint, that the dickite is nearly fully intercalated.

Low frequency region. Another means of studying the changes in the structure of dickite upon intercalation is the study of the hydroxyl deformation modes (Figure 8.11). These bands are centered at 916 cm^{-1} and 936 cm^{-1} (Frost et al. 1998a). They are assigned to librational modes of the inner surface OH groups. Their shifts (906 and 941 cm^{-1}) and intensity variations during intercalation can be attributed to changes in the polarization of the hydroxyls, due to the formation of hydrogen bondings to the S=O in DMSO or to the C=O of the NMF (Frost et al. 1998a, 2000).

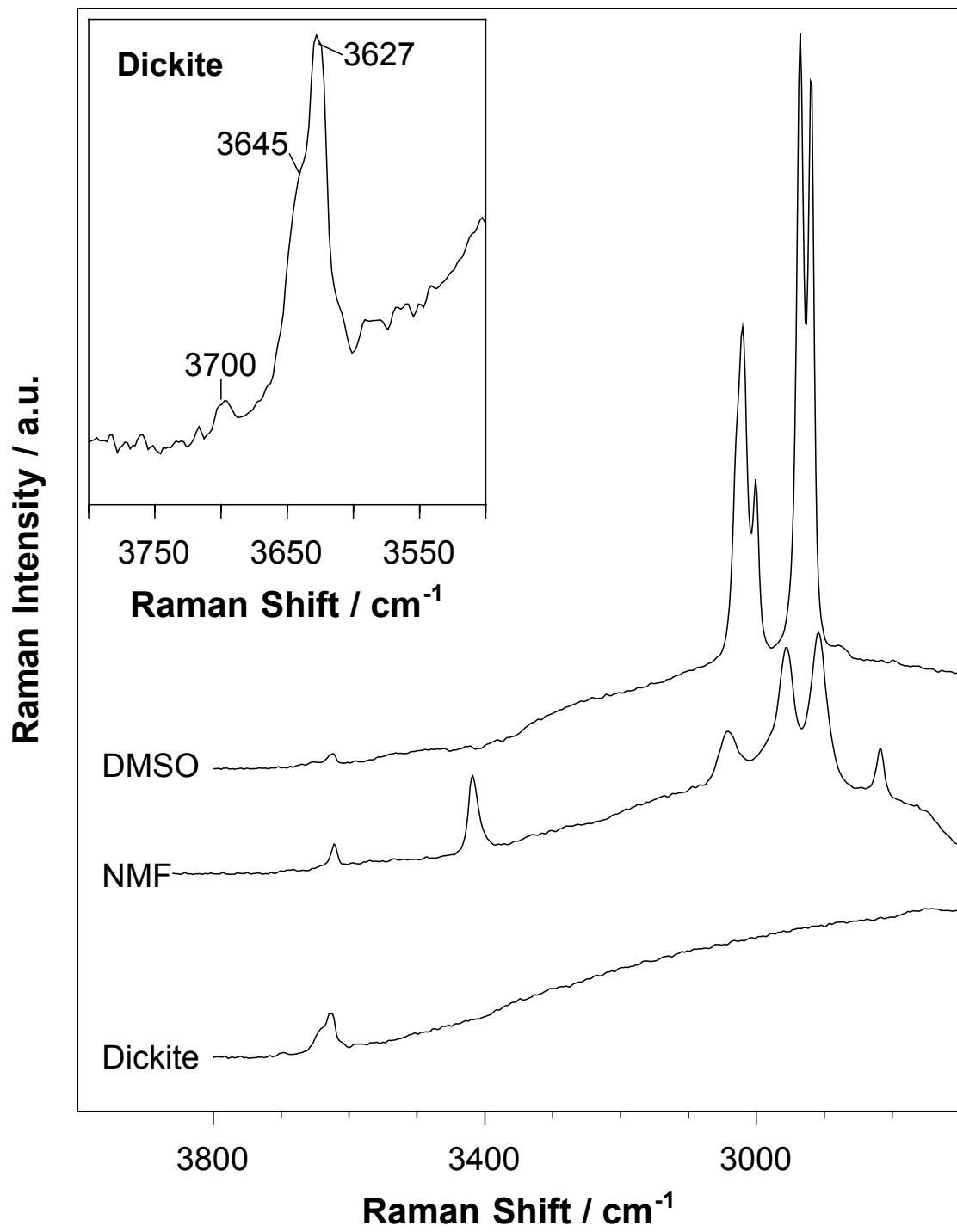


Figure 8.10 FT-Raman spectra of dickite and its intercalates in the hydroxyl stretching region.

Table 8.3 Observed Raman modes of dickite, dickite:DMSO and liquid DMSO, and their assignments.

Dickite		Dickite:DMSO		DMSO (liquid)		Suggested assignments
cm ⁻¹	I ^{a)}	cm ⁻¹	I	cm ⁻¹	I	
3700	vw	-	-	-	-	Stretch inner surface OH
3645	wsh	-	-	-	-	Stretch inner surface OH
3627	w	3627	w	-	-	Stretch inner OH
-	-	3020	m	-	-	C-H antisymmetric stretching
-	-	3001	w	2997	m	C-H antisymmetric stretching
-	-	2935	s	-	-	C-H symmetric stretching
-	-	2920	s	2913	vs	C-H symmetric stretching
-	-	2873	vwsh	2873	wsh	C-H antisymmetric stretching
-	-	-	-	2810	vb	C-H antisymmetric stretching
-	-	1429	s	-	-	CH ₃ bending
-	-	1412	s	1419	s	CH ₃ bending
-	-	1317	w	1307	w	Methyl deformation
-	-	1066	m	-	-	S=O symmetric stretch of monomer
-	-	1053	w	-	-	S=O symmetric stretch of monomer
-	-	-	-	1043	m	S=O symmetric stretch of dimer
-	-	1026	w	-	-	S=O symmetric stretch of dimer
-	-	1012	w	-	-	S=O antisymmetric stretch of polymer
-	-	953	w	953	w	Methyl symmetric rocking
936	vw	941	w	-	-	OH deformation
916	m	906	w	-	-	OH deformation
796	m	793	w	-	-	OH translation
747	m	739	sh	-	-	OH translation
-	-	719	vs	698	vs	CS symmetric stretch
-	-	688	vs	667	vs	CS antisymmetric stretch
508	vw	505	vw	-	-	SiO ₄ symmetric stretch
462	m	463	m	-	-	SiO ₄ symmetric stretch
434	m	436	w	-	-	SiO ₄ symmetric stretch
416	vb wsh	417	vw	-	-	SiO ₄ symmetric stretch
-	-	388	w	382	m	SiO ₄ + CH / C-S=O in-plane rock
-	-	353	s	-	-	SiO ₄ + CH / C-S=O in-plane rock
336	m	-	-	-	-	SiO ₄ symmetric stretch
-	-	-	-	332	s	C-S=O out-of-plane rock
-	-	318	m	307	m	C-S-C symmetric bending
297	m	-	-	-	-	
267	w	267	m	-	-	Al-OH
240	w	252	m	-	-	Al-OH
-	-	216	vw	-	-	
199	vw	202	w	-	-	Al(O/OH) ₆ symmetric stretch
145	s	145	s	-	-	Al(O/OH) ₆ symmetric stretch
135	sh	135	sh	-	-	O-Al-O symmetric bending
120	sh	120	sh	-	-	Si ₂ O ₅ out-of-plane rock

Table 8.4 Observed Raman modes of dickite, dickite:NMF and liquid NMF, and their assignments.

Dickite		Dickite:NMF		NMF (liquid)		Suggested assignments
cm ⁻¹	I ^{a)}	cm ⁻¹	I	cm ⁻¹	I	
3700	Vw	-	-	-	-	Inner surface OH stretch
3645	wsh	-	-	-	-	Inner surface OH stretch
3627	W	3627	vw	-	-	Inner OH stretch
-	-	3417	m	-	-	N-H stretching (ν _{NH8})
-	-	-	-	3278	vb	N-H stretch
-	-	-	-	3060	vb	N-H stretch
-	-	3043	m	-	-	N-H stretching (ν _{NH6})
-	-	-	-	3010	vb	
-	-	2954	vs	2943	vs	C-H symmetric stretching
-	-	2908	vs	2893	s sh	C-H symmetric stretching
-	-	2817	m	2806	wsh	C-H symmetric stretching
-	-	-	-	1686	sh	C=O stretch + C-N stretch
-	-	1674	s	1653	s	N-H deformation
-	-	1529	m	1548	m	C=O stretch
-	-	1460	w	1454	m	C-H deformation
-	-	1419	m	1412	wsh	C-H deformation
-	-	1378	vs	1385	vs	C-H deformation
-	-	1235	s	1248	s	C-H deformation
-	-	1161	s	1149	s	N-H deformation
-	-	963	vs	963	vs	Methyl symmetric rocking
936	Vw	-	-	-	-	Inner surface OH deformation
916	M	908	m	-	-	Inner surface OH deformation
796	M	791	m	-	-	OH translation
-	-	777	w	772	w	
747	M	739	m	-	-	OH translation
-	-	638	m	617	w	
508	Vw	508	w	-	-	SiO ₄ symmetric stretch
462	M	465	s	-	-	SiO ₄ symmetric stretch
434	M	436	m	-	-	SiO ₄ symmetric stretch
416	Vb wsh	-	-	-	-	SiO ₄ symmetric stretch
-	-	359	m	359	m	
336	M	335	m	-	-	SiO ₄ symmetric stretch
297	M	-	-	299	m	
267	W	266	m	-	-	Al-OH stretch
240	W	247	m	-	-	Al-OH stretch
199	Vw	200	w	-	-	Al(O/OH) ₆ symmetric stretch
145	S	-	-	-	-	Al(O/OH) ₆ symmetric stretch
135	Sh	135		-	-	O-Al-O symmetric bending
120	Sh	-	-	123	vs	Si ₂ O ₅ out-of-plane rock

The OH-translational vibration at 747 cm^{-1} shows a similar behaviour. It also slightly shifts to lower wavenumbers (739 cm^{-1}) and strongly decreases its intensity. In contrast to this the 796 cm^{-1} OH-vibration is not affected by the intercalation, which possibly means, that it was not involved in hydrogen bondings to Si-O tetrahedra before intercalation.

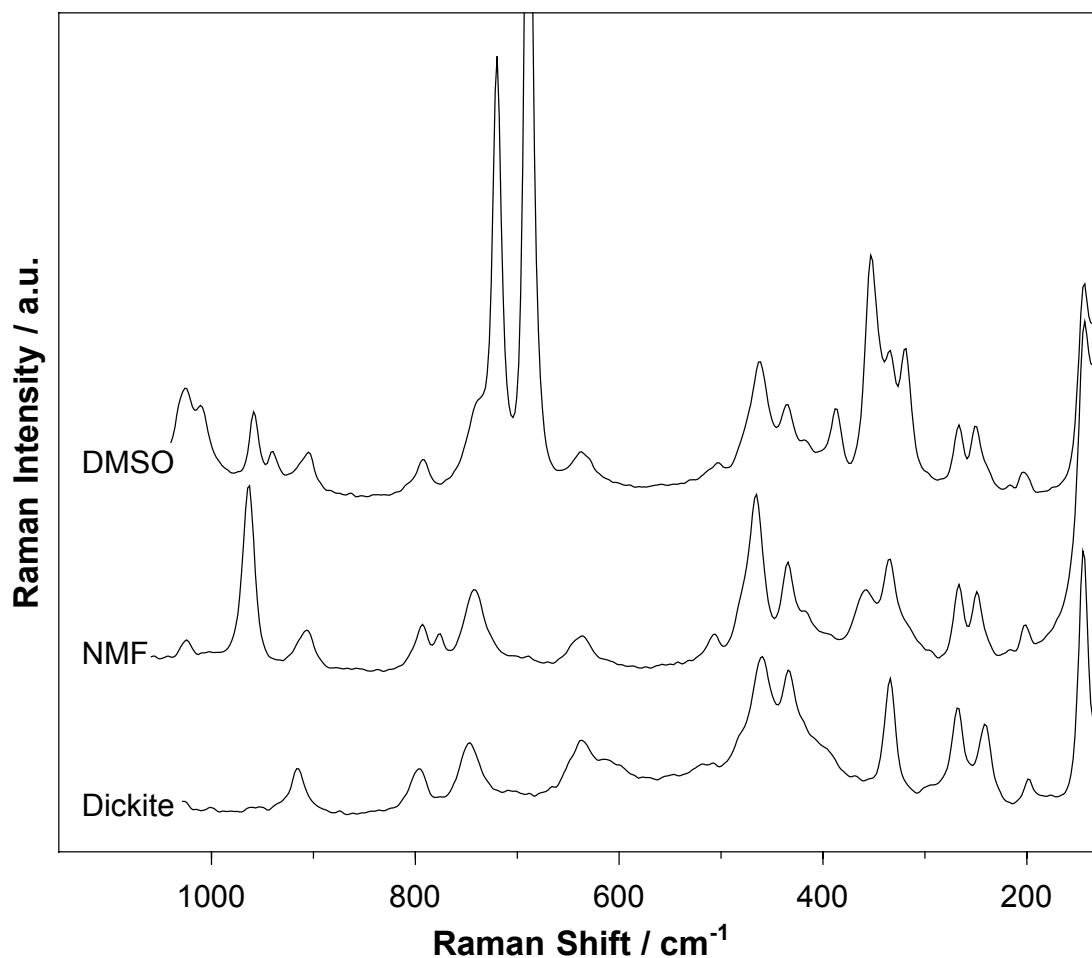


Figure 8.11 FT-Raman spectra of dickite and its intercalates showing the hydroxyl deformation and the low frequency regions between 1100 and 150 cm^{-1} .

The spectral region below 650 cm^{-1} is characterized by several symmetric stretching vibrations of the SiO_4 -tetrahedra at 508 , 462 , 434 , 416 and 336 cm^{-1} , whose intensity changes upon intercalation are attributed to changes in their symmetry (Frost 1995). Additional new bands are observed at 386 , 353 cm^{-1} in the intercalate spectra. These bands are also assigned to SiO_4 vibrations and occur, because the formation of the intercalate has removed the hydrogen bondings between the SiO-groups and the inner surface hydroxyls of the next

adjacent dickite layer. According to Frost *et al.* (1998b) the formation of the intercalate causes single layer dickite, separated by DMSO or NMF layers. Thus the formation of the intercalate has removed the equivalence of the Si-O groups, which results in increased complexity in the 300 to 400 cm^{-1} region.

In the low frequency region below 300 cm^{-1} two more hydrogen bonding vibrations are observed at 267 cm^{-1} and 240 cm^{-1} . Whilst the intensity of the first mode merely decreases slightly upon intercalation, the band at 240 cm^{-1} shows a remarkable shift to 252 cm^{-1} and is diminished in intensity in the spectra of the intercalates. These observations fit well to the conclusion that the hydrogen bonding between the inner surface OH groups and the adjacent next silica layer has been removed on intercalation.

In contrast to Frost *et al.* (1998a) the weak band at 199 cm^{-1} shows no complexity and no shift of its peak position, and also the strong band at 145 cm^{-1} seems not to be affected upon intercalation. Both bands can be assigned to symmetric stretching vibrations of the $\text{Al}(\text{O}/\text{OH})_6$ -octahedra. But the lack of spectral changes is difficult to explain, because of the direct influence of intercalation on the hydroxyls of the octahedral layer. Particularly the intensity of the shoulders at 135 and 120 cm^{-1} strongly increase in the intercalate spectra. While the shoulder at 135 cm^{-1} is assigned to the O-Al-O symmetric bending (Frost 1995), the band at 120 cm^{-1} was predicted as an out-of-plane vibration of the Si_2O_5 -unit (Ishii *et al.* 1967).

DMSO vibrations in the intercalate. In Figure 8.12a the 3200 – 2700 cm^{-1} region of the Raman spectra of DMSO intercalated dickite is compared with liquid DMSO. For DMSO the two strong bands at 2913 and 2997 cm^{-1} are assigned to symmetric and antisymmetric C-H stretching vibrations (Martens *et al.* 2002). Upon intercalation the band at 2913 cm^{-1} splits into two bands at 2920 and 2935 cm^{-1} , while the DMSO band at 2997 splits into bands at 3001 and 3020 cm^{-1} . It is noteworthy, that in contrast to intercalated kaolinite all the new bands occur at higher wavenumbers than the pure DMSO bands (Martens *et al.* 2002). The splittings can be attributed to different molecular structures of the DMSO in the intercalated dickite (Frost *et al.* 1998b). Upon intercalation the C-H

bands of the DMSO are no longer degenerated and so additional bands are observed in the C-H stretching region. While the broad antisymmetric C-H stretching vibration of DMSO at 2810 cm^{-1} is not observed in the intercalate spectrum, the weak shoulder at 2873 cm^{-1} occurs as a small band in the intercalate. The increased complexity of the C-H stretching vibrations suggests, that the methyl groups are locked into a rigid interlayer structure of the dickite as predicted by earlier studies (Raupach *et al.* 1987, Frost *et al.* 1997).

A similar complexity is observed for the methyl bending region around 1400 cm^{-1} (Figure 8.12b). The CH_3 -bending vibration at 1419 cm^{-1} splits into two bands at 1412 and 1429 cm^{-1} and the very weak band at 1307 cm^{-1} shifts to 1317 cm^{-1} upon intercalation. It is also assigned to a methyl deformation mode. One description for these splitted bands might be two different methyl structures. Martens *et al.* (2002) suggested the presence of hydrogen bonded and non-hydrogen bonded methyl groups. Possibly the hydrogens of some of the CH_3 interact with the $\text{S}=\text{O}$ units of an adjacent DMSO molecule, whereas others are not involved in these interactions. In good agreement with these observations are the changes of the $\text{S}=\text{O}$ stretching band at 1043 cm^{-1} . Upon intercalation this band splits into a broad region with several peaks at 1026 , 1053 and 1066 cm^{-1} . They are attributed to the unassociated monomer and the out-of-plane and in-plane vibrational modes of the DMSO dimer (Rintoul and Shorvel, 1990). An additional shoulder at 1012 cm^{-1} is associated with polymeric DMSO (Martens *et al.* 2002). The band at 953 cm^{-1} occurs in both the DMSO and the intercalate spectra, and is not affected by the intercalation procedure. It is assigned to the symmetric methyl rocking vibration.

The antisymmetric and symmetric stretching C-S modes of DMSO are observed at 667 and 698 cm^{-1} . Upon intercalation they shift to 688 and 719 cm^{-1} . This shift of band positions to higher wavenumbers occurs due to the increasing influence of adjacent units (DMSO molecules, oxygens of the tetrahedral layer) during the formation of the intercalation complexes (Frost *et al.* 1998c).

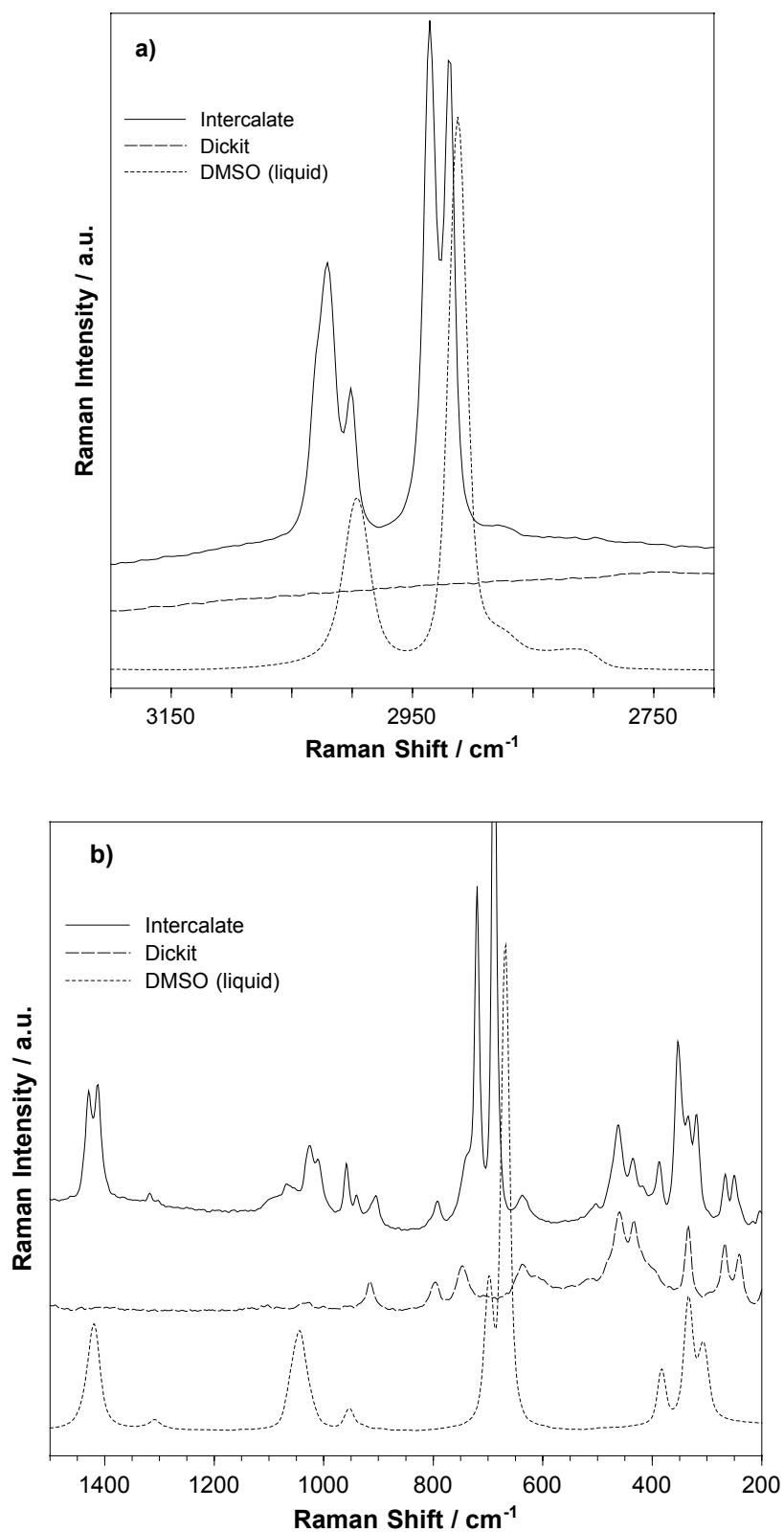


Figure 8.12 a) FT-Raman spectrum of dickite and dickite:DMSO in the CH stretching region ($3200 - 2700 \text{ cm}^{-1}$) compared to the spectrum of liquid DMSO. b) FT-Raman spectra of dickite and dickite:DMSO in the region below 1500 cm^{-1} compared to the spectrum of liquid DMSO.

The Raman spectral region between 400 and 300 cm^{-1} is characterized by the bending vibrations of the C-S=O and the C-S-C units. Three bands are observed at 382, 332 and 307 cm^{-1} . While the band at 307 cm^{-1} can be ascribed to a C-S-C symmetric bend, the others are attributed to the in-plane and out-of-plane bending vibrations of C-S=O. Upon intercalation all bands strongly shift to higher wavenumbers (388, 353, 318 cm^{-1}), and their bandwidths decrease. In accordance with the spectral changes in the methyl stretching region, these observations suggest that the DMSO molecules are fixed relatively rigid in the dickite interlayer. Martens et al. (2002) designated this as 'crystalline-like' structure of the DMSO in the interlayer.

NMF vibrations in the intercalate. In contrast to the relatively extensive literature on vibrational spectroscopy of DMSO and DMSO intercalated kaolinites and dickites, the lack of data about the vibrational spectroscopy of NMF and its intercalation compounds makes it very difficult to interpret the spectral features in this study.

Similar to the DMSO intercalated samples, the spectra in Figure 8.13a and b show a number of new bands upon intercalation. Especially the N-H stretching region between 3500 and 2800 cm^{-1} is strongly affected upon intercalation (Figure 8.13a). The bandwidths of the vibrational modes at 2806, 2893, 2943 are remarkably decreased and the bands shift to higher wavenumbers (2817, 2908, 2954 cm^{-1}). In addition, their intensities strongly increase during intercalation. It is not clear if the broad and weak bands at 3060 and 3278 cm^{-1} are in direct correspondence to the new bands at 3043 and 3417 cm^{-1} . Frost et al. (2001a) assigned them to the ν_{NH6} and ν_{NH8} modes of the N-H stretching vibrations. Thus all these observations can be explained by the incorporation of the NMF molecules into the dickite interlayers, where the N-H units are fixed to the siloxane groups via hydrogen bonds. As the bands at 2806, 2893 and 2943 cm^{-1} are at comparable positions with the methyl stretching vibrations of DMSO (2810, 2875, 2935 cm^{-1}), these bands can be attributed to C-H stretching modes (Martens et al. 2002). Thus it can be concluded, that the CH_3 groups of the NMF molecules are also involved in the formation of hydrogen bonds to adjacent dickite sheets.

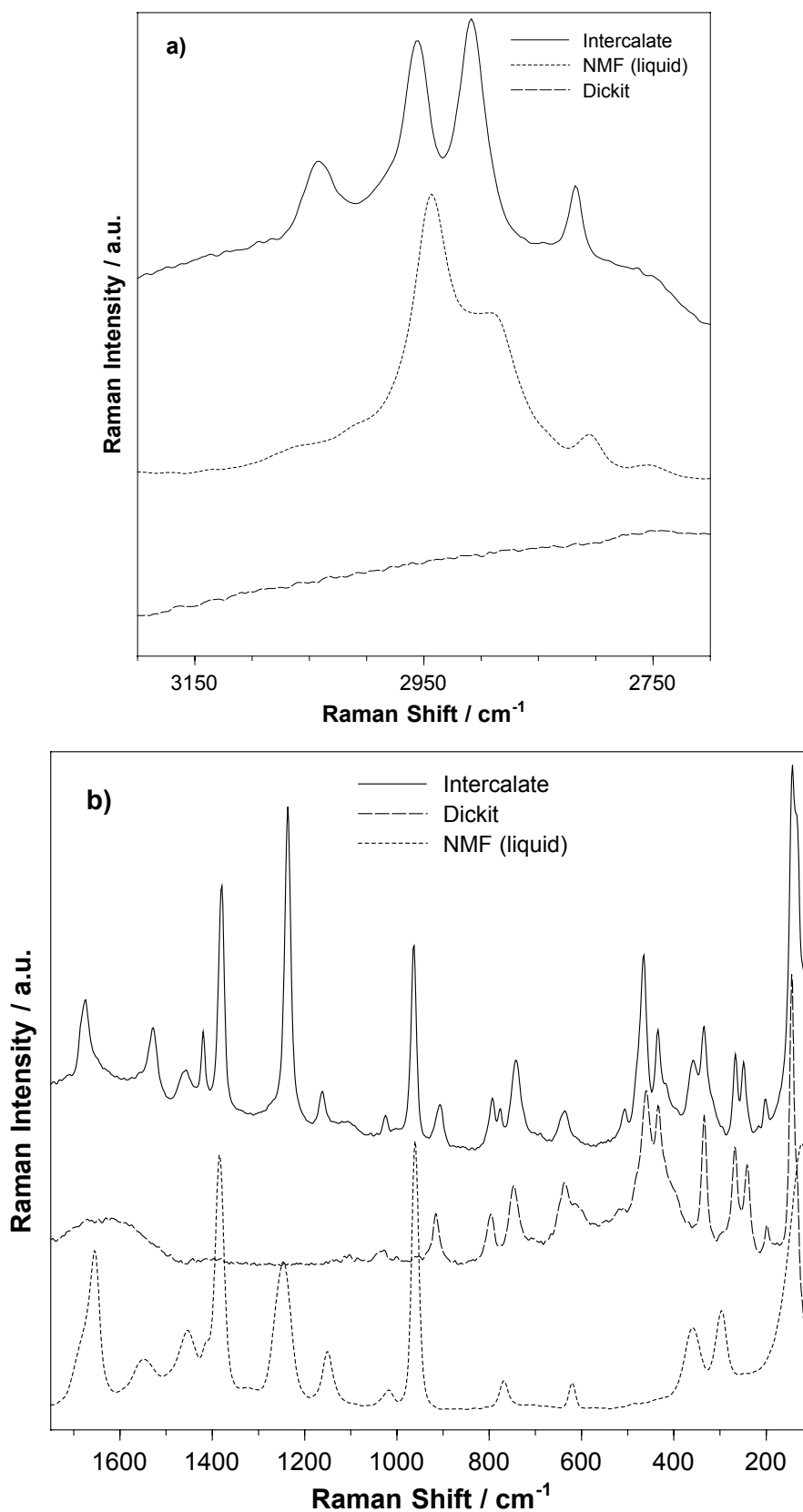


Figure 8.13 a) FT-Raman spectra of dickite and dickite:NMF in the CH stretching region ($3500 - 2700 \text{ cm}^{-1}$) compared to the spectrum of liquid NMF. b) FT-Raman spectra of dickite and dickite:NMF in the region below 1600 cm^{-1} compared to the spectrum of liquid NMF.

Also the 1700 – 1100 cm^{-1} region shows strong changes upon the intercalation of NMF (Figure 8.13b). In this region the C=O stretching, N-H deformation and C-H bending modes are observed (Frost et al. 2001b). Similar to the N-H stretching region the band intensities increase during intercalation and the peak positions are slightly shifted. For example the C=O stretching mode at 1548 cm^{-1} shifts to 1529 cm^{-1} , while the N-H deformation mode even shifts from 1653 cm^{-1} to 1674 cm^{-1} . The band at 1686 cm^{-1} can not be attributed to C=O stretching vibrations alone, because it is normally located between 1640 and 1680 cm^{-1} . Therefore this vibrational mode can be described as a combination of a C=O stretching mode and a minor C-N stretching component (Lee 1997, Martens et al. 2002). For formamide diluted in polar solvents Ojha et al. (2004) assigned similar band shifts of the C=O stretching vibrations to the formation of hydrogen bonded complexes.

Two weaker bands at 1454 and 1412 cm^{-1} slightly shift to a higher wavenumber (1460, 1419 cm^{-1}) and decrease their bandwidths. Their assignment is difficult due to the lack of literature data. But as H-C-H deformation modes in DMSO or methylamine are located at very similar positions (DMSO: 1417, 1426 cm^{-1} , Martens et al. 2002; methylamine: 1428 cm^{-1} , Kohlrausch 1972), one may assign these bands to C-H bending vibrations, which are influenced by the fixation of NMF to the dickite sheets.

Observed C-H deformation bands at 1385 and 1248 cm^{-1} shift to lower wavenumbers (1378 and 1235 cm^{-1}). This can be explained by a lengthening of the C-H bonds and therefore a decrease in bond strength due to interactions with the SiO_4 units of dickite (Frost et al. 2001b).

The strong band at 1149 cm^{-1} remarkably shifts to 1161 cm^{-1} . However, Frost et al. (2001a) assigned this vibration to a quartz impurity in formamide intercalated kaolinite. As the dickite spectrum in Figure 8.13b does not show any band at this position, this band can not be assigned to a mineral vibration. As Kohlrausch (1972) attributed two bands at 1110 and 1174 cm^{-1} to N-H deformation modes in methylamine, this seems to be a more convincing assignment.

8.5 CONCLUSIONS

Spectroscopic investigations on muscovite powders using various Raman sampling techniques, revealed strongly disturbed spectra with extremely high backgrounds and strong fluorescence and background features. Up to now, only single crystal spectra collected with the SERS technique show complete spectra of good quality with a low background. Compared to other sample preparation techniques, preliminary SERS measurements on powdered micas show similar spectra with a strongly decreased background and some assignable bands.

In contrast to these difficulties, it is much easier to obtain FT-Raman spectra of dickite and its intercalates. No background and fluorescence features are observed. And also no disturbing influences due to the kind of sample holder are detected. This gives a strong hint, that the main, possibly the only source for the highly disturbed muscovite spectra is their ten-fold higher Fe^{3+} content.

The structural analysis of the FT-Raman spectra of dickite and its intercalates give a lot of information about the changes especially in the interlayer region. It is shown, that both DMSO and NMF are fixed relatively rigid in the dickite interlayers via hydrogen bonds. Besides the C=O group additional units like methyl and NH-groups are involved in the bonding to the adjacent tetrahedral and octahedral sheets of dickite.

The observations in this chapter show, that in contrast to the minerals of the kaolinite group, common Raman sampling techniques are not successful for the measurement of powdered micas. Preliminary measurements on additional micas, serpentine and illite samples show that the sampling and preparation parameters have to be specially optimised for every kind of clay mineral. Thus two promising methods for a further systematic investigation of clays could be the use of SERS and Raman microscopy, which successfully was used for powdered kaolinite samples and for muscovite single crystals (Frost *et al.* 1998a, 2001b).

REFERENCES

- Aminzadeh, A. (1997) Excitation frequency dependence and fluorescence in the Raman spectra of Al_2O_3 . *Applied Spectroscopy*, **51**, 817 – 819.
- Frost, R.L. (1995) Fourier transform Raman spectroscopy of kaolinite, dickite and halloysite. *Clays and Clay Minerals*, **43**, 191 – 195.
- Frost, R.L., Fredericks, P.M., Bartlett, J.R. (1993) Fourier transform Raman spectroscopy of kandite clays. *Spectrochimica Acta Part A*, **49**, 667 – 674.
- Frost, R.L., Tran, T.H., Kristof, J. (1997) FT-Raman spectroscopy of the lattice region of kaolinite and its intercalates. *Vibrational Spectroscopy*, **13**, 175 – 186.
- Frost, R.L., Forsling, W., Holmgren, Allan, Klopogge, J.T., Kristof, J. (1998a) Raman spectroscopy at temperatures between 298 and 423 K and at 77 K of kaolinites intercalated with formamide. *Journal of Raman Spectroscopy*, **29**, 1065 – 1069.
- Frost, R.L., Tran, T.H., Rintoul, L., Kristof, J. (1998b) Raman microscopy of dickite, kaolinite and their intercalates. *The Analyst*, **123**, 611 – 616.
- Frost, R.L., Kristof, J., Paroz, G.N., Klopogge, J.T. (1998c) Molecular structure of dimethyl sulfoxide intercalated kaolinites. *Journal of Physical Chemistry B*, **102**, 8519 – 8532.
- Frost, R.L., Kristof, J., Horvath, E., Klopogge, J.T. (2000) Vibrational spectroscopy of formamide-intercalated kaolinites. *Spectrochimica Acta Part A*, **56**, 1191 – 1204.
- Frost, R.L., Kristof, J., Horvath, E., Klopogge, J.T. (2001a) Raman microscopy of formamide-intercalated kaolinites treated by controlled-rate thermal analysis technology. *Journal of Raman Spectroscopy*, **32**, 873 – 880.
- Frost, R.L., Kristof, J., Horvath, E., Klopogge, J.T. (2001b) Separation of adsorbed formamide and intercalated formamide using controlled rate thermal analysis methodology. *Langmuir*, **17**, 3216 – 3222.
- Haley, L.V., Wylie, I.W. and Koningstein, J.A. (1982) An investigation of the lattice and interlayer water vibrational spectral regions of muscovite and vermiculite using Raman microscopy. *Journal of Raman Spectroscopy*, **13**, 203 – 205.
- Hendra, P., Jones C., Warnes, G. (1991) *Fourier transform Raman spectroscopy. Instrumentation and chemical applications*. Ellis Horwood LTD, New York, 311 p.
- Ishii, M., Shimanouchi, T., Nakahira, M. (1967) Far-infrared absorption spectra of layer silicates. *Inorganica Chimica Acta*, **1**, 387 – 392.
- Kohlrausch, K.W.F. (1972) *Ramanspektren*. Heyden & son LTD, London, 469 p.

- Lee, Y.T. (1997) Hydrogen bond effect on the Raman shift of the carbonyl stretching mode of various amide solutions. *Journal of Raman Spectroscopy*, **28**, 45 – 51.
- Martens, W.N., Frost, R.L., Kristof, J., Kloprogge, J.T. (2002) Raman spectroscopy of dimethyl sulfoxide and deuterated dimethyl sulphoxide at 298 and 77 K. *Journal of Raman Spectroscopy*, **33**, 84 – 91.
- McKeown, D.A., Bell, M.I. and Etz, E.S. (1999a) Raman spectra and vibrational analysis of the trioctahedral mica phlogopite. *American Mineralogist*, **84**, 970 – 976.
- McKeown, D.A., Bell, M.I. and Etz, E.S. (1999b) Vibrational analysis of the dioctahedral mica: $2M_1$ muscovite. *American Mineralogist*, **84**, 1041 – 1048.
- Mortensen, A., Christensen, D.H., Nielsen, O.F., Pederson, E. (1991) Raman spectra of amorphous Al_2O_3 and Al_2O_3 MoO_3 obtained by visible and infrared excitation. *Journal of Raman Spectroscopy*, **22**, 47 – 49.
- Ojha, A.K., Srivastava, S.K., Koster, J., Shukla, M.K., Leszczynski, J., Asthana, B.P., Kiefer, W. (2004) Investigation of hydrogen bonding and self-association in neat $HCONH_2$ and the binary mixture ($HCONH_2 + CH_3OH$) by concentration dependent Raman study and ab initio calculations. *Journal of Molecular Structure*, **689**, 127 – 135.
- Raupach, M., Barron, P.F., Thompson J.G. (1987) Nuclear magnetic resonance, infrared and X-ray powder diffraction study of dimethylsulfoxide and dimethylselenoxide intercalates with kaolinite. *Clays and Clay Minerals*, **35**, 208 – 219.
- Rintoul, L. and Shurvell, H.F. (1990) Raman-spectroscopic study of complex-formation between dimethyl-sulfoxide and chloroform. *Journal of Raman Spectroscopy*, **21**, 501 – 507.
- Tanner, P.A., Mak, C.S.K. and Siu, G.G. (2002) Additional bands in the FT-Raman spectra of lanthanide compounds. *Applied Spectroscopy*, **56**, 670 – 673.
- Varetti, E.L. and Baran, E.J. (1994) Raman or fluorescence spectra? About the use of FT-Raman techniques on inorganic compounds. *Applied Spectroscopy*, **48**, 1028 – 1029.

CHAPTER 9

NEAR INFRARED AND MID INFRARED SPECTROSCOPIC STUDY OF DICKITE AND ITS INTERCALATES

9.1 INTRODUCTION

The use of infrared spectroscopy in the study of minerals of the kaolinite group and their intercalates is widely established. Especially the mid infrared region between 4000 and 400 cm^{-1} reveals a lot of information on the lattice structure and the vibrations of the hydroxyl groups, thus statements about bonds to incorporated molecules or cations can be made. Furthermore, spectroscopic investigations over the extended spectral range between 8000 – 400 cm^{-1} are not very common, even though the near infrared region reveals additional information about the composition of the octahedral sheets and of the state of the hydroxyl groups and of incorporated water molecules. Hence, in this chapter the results of an infrared spectroscopic study of dickite, dickite:DMSO and dickite:NMF over this spectral range are presented. The results are compared to the FT-Raman data discussed in the preceding chapter and they provide a comprehensive view on the structure of intercalated dickite.

9.2 MATERIALS AND METHODS

The infrared investigations between 8000 and 400 cm^{-1} were done on the same samples which were used for the FT-Raman measurements discussed in the previous chapter. The preparation of the intercalates is described in chapter 2.

The FTIR and NIR spectra were collected on a Bruker IFS66/S spectrometer, using a DRIFT accessory. For the measurements 10 mg sample powder was

mixed with 500 mg KBr. All spectrometer details are extensively described in chapter 3.

Additionally the dickite sample and its intercalates were characterized by X-ray diffractometry. The XRD patterns were recorded over a range between 3° and $63^\circ 2\theta$ according to the parameters described in chapter 4.

9.3 RESULTS

9.3.1 X-RAY DIFFRACTION

The XRD patterns of the dickite and its intercalates with DMSO and NMF are shown in Figure 9.1. Upon intercalation of the dickite, new strong (001) Bragg peaks were obtained with d -values of 1.08 nm for the dickite:NMF intercalation complex and a value of 1.12 nm for the DMSO intercalated dickite.

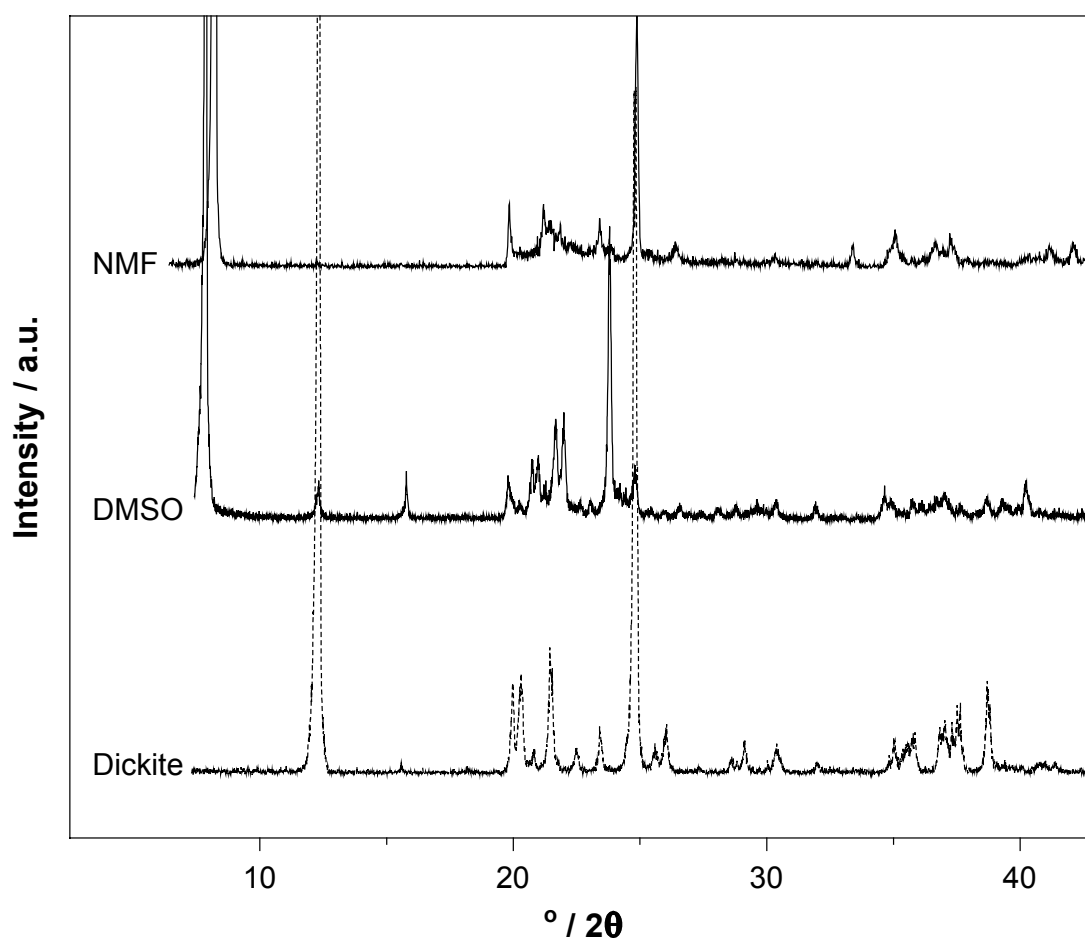


Figure 9.1 X-ray diffraction patterns of dickite, dickite:DMSO and dickite:NMF in the range between 3 and $43^\circ 2\theta$.

Additionally the XRD peak heights of these (001) peaks were determined and were used as a guide for the degree of intercalation using the formula of Theng (1974):

$$\text{Intercalation ratio} = \frac{\text{Intensity}(001)_{\text{Intercalate}}}{(\text{Intensity}(001)_{\text{Dickite}} + \text{Intensity}(001)_{\text{Intercalate}})}$$

According to this equation intercalation rates of more than 97 % for the DMSO intercalated sample and of 99 % for the NMF treated dickite are calculated.

9.3.2 MID INFRARED SPECTROSCOPY (4000 – 400 CM⁻¹)

OH stretching region (3800 – 2800 cm⁻¹). In the OH-stretching region the dickite spectra show a set of three sharp bands at 3700, 3650 and 3629 cm⁻¹ (Figure 9.2 a, Table 9.1). The position of the band at 3700 is not affected by the intercalation of DMSO, only its intensity is strongly decreased due to the intercalation process. In contrast to this the 3650 cm⁻¹ band shifts to 3664 cm⁻¹ and increases its intensity, while the mode at 3629 cm⁻¹ shifts to a lower wavenumber (3621 cm⁻¹). In the original dickite sample two further weak and broad water bands occur at 3431 and 3031 cm⁻¹. Due to the intercalation they are superimposed by two sharp bands at 3538 and 3504 cm⁻¹ and a small triplet at 3023, 2937 and 2917 cm⁻¹.

Similar changes occur due to the intercalation of NMF (Figure 9.2 b, Table 9.2). Here the dickite band at 3700 cm⁻¹ disappears within the shoulder of a new strong band at 3675 cm⁻¹.

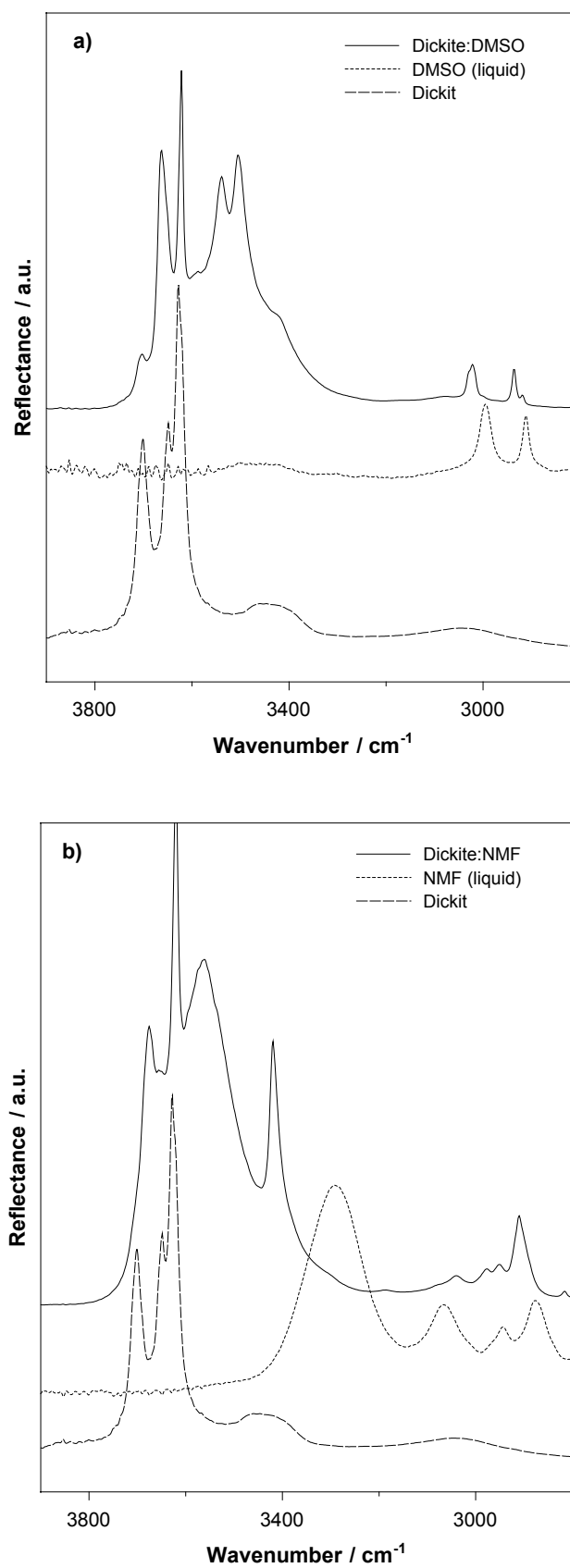


Figure 9.2 DRIFT spectra of the OH stretching region of dickite and its intercalates compared to the liquid intercalate phases. a) DMSO, b) NMF.

Table 9.1 Observed infrared modes of dickite, dickite:DMSO and liquid DMSO and their assignments.

Dickite		Dickite:DMSO		DMSO		Suggested assignments
cm ⁻¹	I ^{a)}	cm ⁻¹	I	cm ⁻¹	I	
3700	S	3700	msh	-	-	Inner surface O-H stretch
3650	Ssh	3664	s	-	-	Inner surface O-H stretch
3629	Vs	3621	vs	-	-	Inner O-H stretch
-	-	3538	s	-	-	Inner surface O-H, H-bonded to S=O
-	-	3504	s	-	-	Inner surface O-H, H-bonded to S=O
3431	B	3426	sh	-	-	Water molecules
3031	Vb	-	-	-	-	Water molecules
-	-	3023	m	2995	m	C-H asymmetric stretch
-	-	2937	m	-	-	Splitted C-H symmetric stretch
-	-	2917	-	-	-	Splitted C-H symmetric stretch
-	-	-	-	2911	m	C-H symmetric stretch
-	-	-	-	1473	w	
-	-	1457	vw	1455	wsh	CH ₃ asymmetric deformation
-	-	1428	s	1437	vs	CH ₃ asymmetric deformation
-	-	-	-	1418	s sh	CH ₃ asymmetric deformation
-	-	1407	s	1406	vs	
-	-	1396	s	-	-	
-	-	1376	w	1361	vw	
-	-	-	-	1331	sh	CH ₃ symmetric deformation
-	-	1317	s	1310	s	CH ₃ symmetric deformation
-	-	1300	w	1293	w sh	CH ₃ symmetric deformation
1225	b m	1225	b m	-	-	
-	-	-	-	1042	vs	S=O symmetric stretch
1116	S	1122	s	-	-	Si-O in-plane vibration, affected by S=O stretch
-	-	1099	b m	-	-	
1029	S	1029	vs	-	-	Si-O stretch
-	-	-	-	1020	s sh	S=O stretch
1008	Sh	1004	s	-	-	Si-O stretch
998	S	-	-	-	-	
956	W	958	s	-	-	Al-OH bending (affected by CH ₃ rocking)
-	-	-	-	951	m	CH ₃ rocking
931	M	941	vw	-	-	Al-OH bending, H-bonded to S=O
-	-	-	-	929	sh	CH ₃ rocking
914	S	904	s	-	-	Al-OH bending, H-bonded to S=O
-	-	-	-	894	w	CH ₃ rocking

a) Abbreviations for absorption intensities: s = strong, m = moderate, w = weak, sh = shoulder, v = very, b = broad

Table 9.2 Observed infrared modes of dickite, dickite:NMF and liquid NMF and their suggested assignments.

Dickite		Dickite:NMF		NMF		Suggested assignments
cm ⁻¹	I ^{a)}	cm ⁻¹	I	cm ⁻¹	I	
3700	S	-	-	-	-	Inner surface O-H stretch
-	-	3675	s	-	-	Inner surface O-H stretch, perturbed
3650	Ssh	3650	vw	-	-	Inner surface O-H stretch
3629	Vs	3619	vs	-	-	Inner O-H stretch
-	-	3561	b vs	-	-	C=O stretch, hydrogen bonded to OH
3431	B	3421	s	-	-	Water molecules / N-H H-bonded to Si-O
-	-	-	-	3292	b s	N-H stretch
-	-	-	-	3066	m	N-H stretch
3031	Vb	3039	w	-	-	Water molecules
-	-	2979	w	-	-	C-H stretch H-bonded to Si-O
-	-	2950	w	-	-	C-H stretch H-bonded to Si-O
-	-	-	-	2943	m	C-H stretch
-	-	2910	m	-	-	C-H stretch H-bonded to Si-O
-	-	-	-	2874	m	C-H stretch
-	-	2817	vw	-	-	
-	-	1733	w	-	-	C=O stretch H-bonded to inner surface OH
-	-	1681	vs	1652	vs	N-H deformation / C=O stretch (amide II)
-	-	1525	s	1535	m	
-	-	1455	w	1452	w b	Complex amide vibrations
-	-	1419	s	1412	w	mix of C=O, C-N and C-H vibrations
-	-	1378	s	1379	s	(amide I, amide II, amide II vibrations)
-	-	-	-	1319	w b	
-	-	-	-	1240	m	C-H deformation ?
1225	b m	1236	m	-	-	
-	-	1162	m	-	-	
-	-	-	-	1149	s	C-H out of plane?
1116	S	1110	w	-	-	Si-O in-plane vibration
-	-	-	-	1040	vw	
1029	S	1024	s	-	-	Si-O in-plane vibration
-	-	-	-	1014	w	
1008	Sh	-	-	-	-	Si-O stretch
998	S	997	s	-	-	Si-O stretch ?
-	-	985	s sh	-	-	
-	-	-	-	959	m	
956	W	964	s sh	-	-	Al-OH
931	s sh	940	vw	-	-	Al-OH bending, H-bonded to C=O
914	S	906	s	-	-	Al-OH bending, H-bonded to C=O

b) Abbreviations for absorption intensities: s = strong, m = moderate, w = weak, sh = shoulder, v = very, b = broad

While the band at 3629 cm^{-1} shifts to 3619 cm^{-1} due to the intercalation of NMF, the vibrational mode at 3650 cm^{-1} still exists, but only as a very small shoulder between the other two strong bands. Additionally at 3561 cm^{-1} a new strong and broad band occurs. The broad water band at 3431 cm^{-1} is also superimposed by a sharp and strong band at 3421 cm^{-1} . In the range of the second water band the intercalation of NMF leads to a number of small bands at $3039, 2979, 2950, 2910$ and 2817 cm^{-1} .

Spectral range $1800 - 1200\text{ cm}^{-1}$. This spectral region is clearly affected by the intercalation of organic molecules (Figures 9.3 a, b). While the dickite spectrum only shows one broad band at 1225 cm^{-1} , especially the intercalation of NMF leads to the development of several new and partly strong bands at $1681, 1527, 1455, 1419$ and 1378 cm^{-1} (Table 9.2). In contrast to this, the incorporation of DMSO yields much weaker bands at $1457, 1428, 1407, 1396, 1373, 1317$ and at 1300 cm^{-1} . The band at 1225 cm^{-1} is not affected by the intercalation of DMSO, but due to the treatment with NMF it shifts to higher wavenumbers (1236 cm^{-1}).

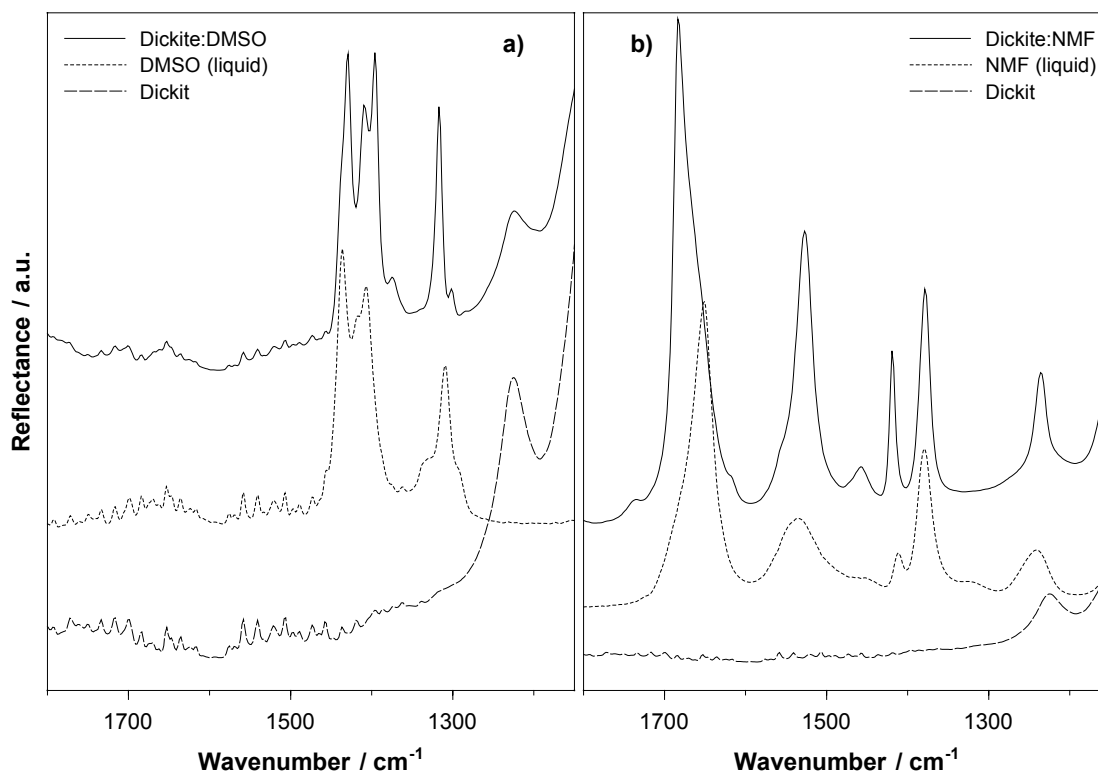


Figure 9.3 DRIFT spectra of the $1800 - 1150\text{ cm}^{-1}$ region of dickite and its intercalates compared to the liquid intercalate phases. a) DMSO, b) NMF.

Spectral range 1200 – 800 cm⁻¹. The observed changes in the intercalate spectra show that the vibrations of the tetrahedral SiO₄ sheets and the AlO/OH₆ octahedra are strongly affected by intercalation (Figures 9.4 a, b).

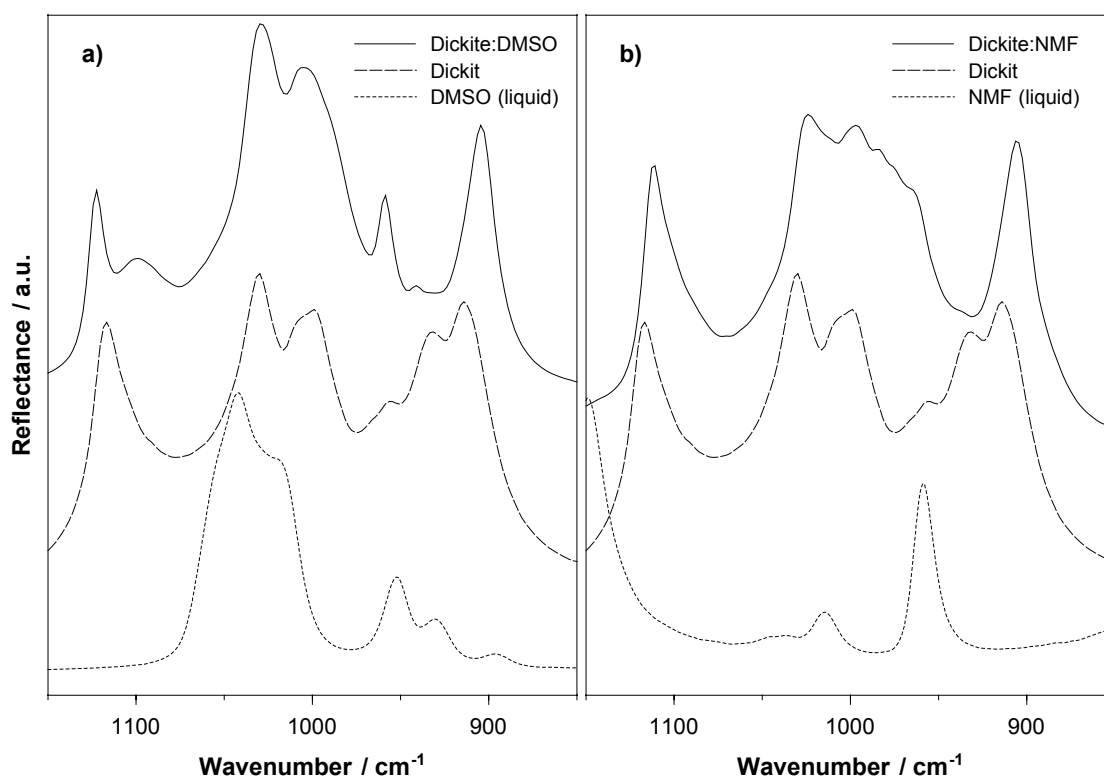


Figure 9.4 DRIFT spectra of the OH-bending region (1200 – 850 cm⁻¹) of dickite and its intercalates compared to the liquid intercalate phases. a) DMSO, b) NMF.

For example the sharp band at 1116 cm⁻¹ shifts to a lower wavenumber (1110 cm⁻¹) due to the NMF treatment, while its wavenumber slightly increases in the DMSO spectrum (1122 cm⁻¹), where an additional broad band appears at 1099 cm⁻¹. While the mode at 1029 cm⁻¹ is not affected, the intensity of the shoulder at 1008 cm⁻¹ strongly increases. In contrast to that, in the NMF spectrum this vibrational mode is no longer visible, perhaps due to its disappearance within the very broad and strong bands of this spectral region. This possibly applies also to the band at 998 cm⁻¹. It seems, that its position is not affected, but the band is no more visible (as a shoulder?) in the intercalate spectra. In the following the dickite spectrum shows some more bands which are remarkably affected by the intercalation of NMF and DMSO. While the small shoulder at 956 cm⁻¹ strongly increases its intensity, the intensity of the shoulder at 931 cm⁻¹ decreases dramatically during the intercalation processes

and slightly shifts to higher wavenumbers (DMSO: 941 cm^{-1} , NMF: 940 cm^{-1}). The sharp band at 914 cm^{-1} shifts to 904 cm^{-1} during the DMSO treatment and to 906 cm^{-1} due to the NMF incorporation.

9.3.3 NEAR INFRARED SPECTROSCOPY ($8000 - 4000\text{ cm}^{-1}$)

Figure 9.5 shows the spectra of dickite and its intercalates. The spectral features in this range are concentrated in two regions: one with a few sharp bands around 7000 cm^{-1} and a second one with several small and broader peaks between 5000 and 4000 cm^{-1} . The observed bands are listed in Table 9.3.

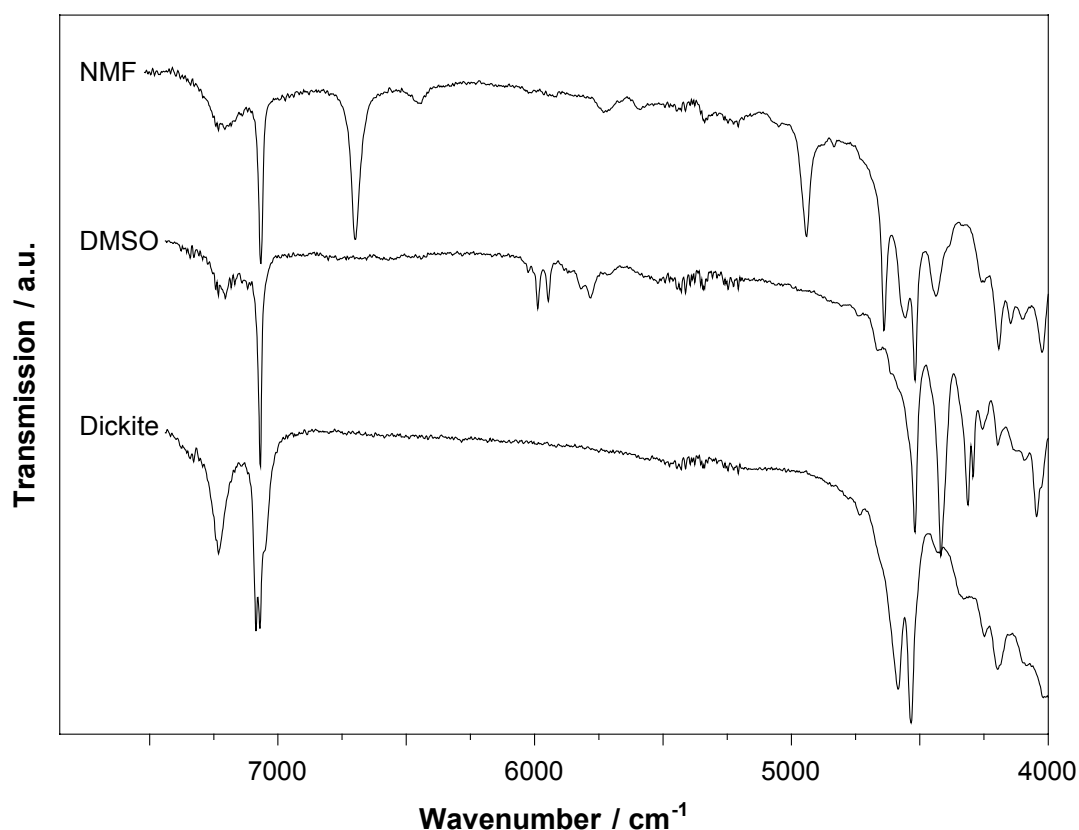


Figure 9.5 Near infrared spectra of dickite and its intercalates over the range between 8000 and 4000 cm^{-1} .

In the region around 7000 cm^{-1} the dickite spectrum shows only one strong band at 7233 cm^{-1} and a very sharp doublet at 7087 and 7071 cm^{-1} with a shoulder at 7048 cm^{-1} (Figure 9.6). Above 5000 cm^{-1} no further bands appear.

In NMF intercalated samples a shift of the first band to lower wavenumbers is observed (7212 cm^{-1}), while in DMSO intercalates only its intensity decreases.

Table 9.3 Observed near infrared bands of dickite and the intercalates dickite:DMSO and dickite:NMF.

Dickite		Dickite:DMSO		Dickite:NMF	
cm^{-1}	I ^{a)}	cm^{-1}	I	cm^{-1}	I
7340	vb	7340	w	-	-
7233	s	7230	m / b	7212	m / b
7087	vs	-	-	-	-
7071	vs	7070	vs	7064	vs
7048	sh	-	-	-	-
-	-	-	-	6696	Vs
-	-	-	-	6439	M
-	-	6030	w	6030	Vw
-	-	5986	m	-	-
-	-	5949	m	-	-
-	-	-	-	5930	Vw
-	-	5868	wsh	-	-
-	-	5820	m	-	-
-	-	5783	m	-	-
-	-	-	-	5730	m / b
-	-	5710	wsh	-	-
-	-	-	-	5592	w / b
-	-	5515	vw b	-	-
5428	vw b	5428	vw b	5430	vw b
5345	vw b	-	-	-	-
-	-	5336	vw b	5336	vw b
5243	vw b	5231	vw b	5231	vw b
-	-	-	-	4942	S
4736	w	4740	w	-	-
4655	sh	4663	w	-	-
-	-	-	-	4637	S
-	-	4615	b	-	-
4586	vs	4581	bsh	-	-
-	-	-	-	4556	s / b
-	-	4547	bsh	-	-
4533	vs	4520	vs	4518	Vs
-	-	-	-	4439	m / b
4430	w / b	-	-	-	-
-	-	4416	vs	-	-
4340	vb	-	-	-	-
-	-	4314	s	-	-
-	-	4290	m	-	-
-	-	4256	m	4256	Sh
-	-	4232	sh	-	-
4248	m	-	-	-	-
4196	m	4196	m	4194	S
-	-	-	-	4146	W
-	-	4132	vb	-	-
4090	vb	4092	vw	4097	w / b
-	-	4046	s	-	-
-	-	4027	sh	4023	S
4013	vb	-	-	-	-

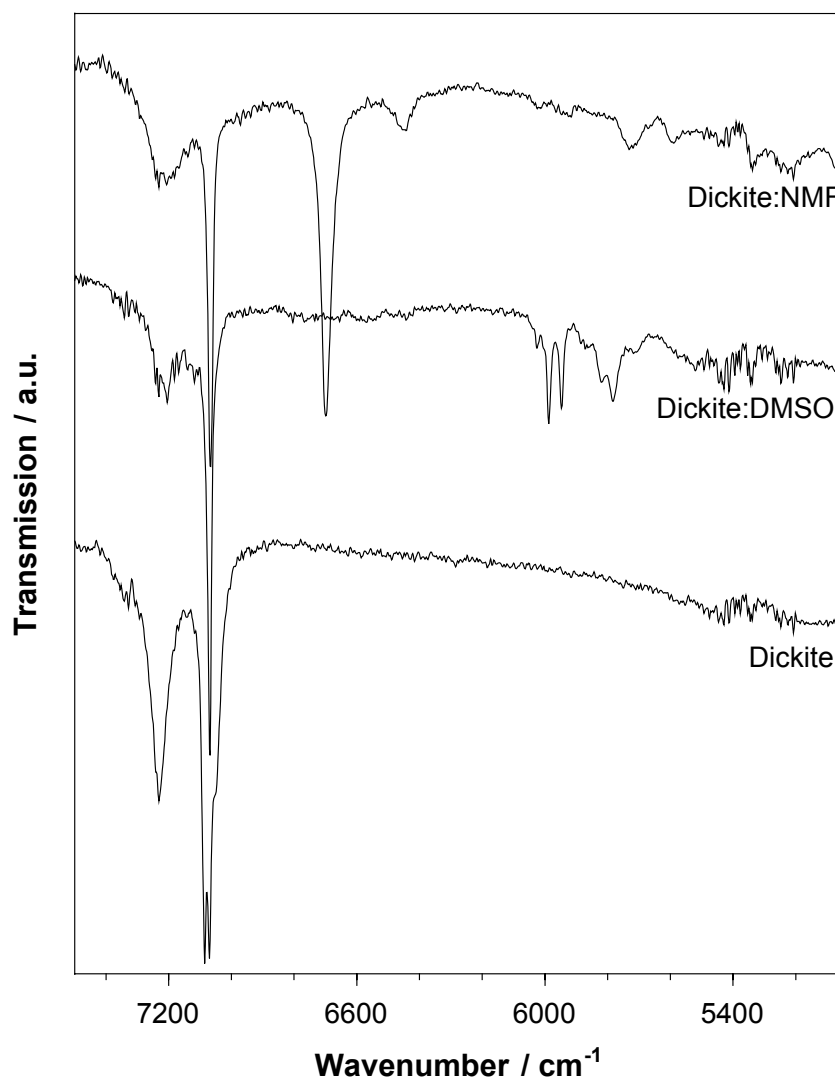


Figure 9.6 Detailed view on the near infrared spectra of dickite and its intercalates in the OH-overtone region ($7300 - 5200 \text{ cm}^{-1}$).

Furthermore both samples do not show the strong doublet any longer, here only one band occurs at 7070 cm^{-1} (DMSO) and 7064 cm^{-1} (NMF). Additionally in the NMF sample a very strong mode appears at 6696 cm^{-1} together with a broad band at 6439 cm^{-1} . While in the DMSO intercalate five small and relatively sharp bands at 6022 , 5986 , 5949 , 5820 and 5783 cm^{-1} appear together with two broad shoulders at 5868 and 5710 cm^{-1} , the NMF spectrum only shows three very weak and broad bands in this region (6030 , 5930 , 5592 cm^{-1}), besides a somewhat sharper mode at 5730 cm^{-1} . Additionally in all spectra a noisy region with a few very weak and broad bands is observed. These bands appear at 5428 , 5345 and 5243 cm^{-1} in the dickite spectrum, at

5515, 5428, 5336 and 5231 cm^{-1} upon the intercalation of DMSO. And in the NMF intercalate they appear at 5430, 5336 and also at 5231 cm^{-1} .

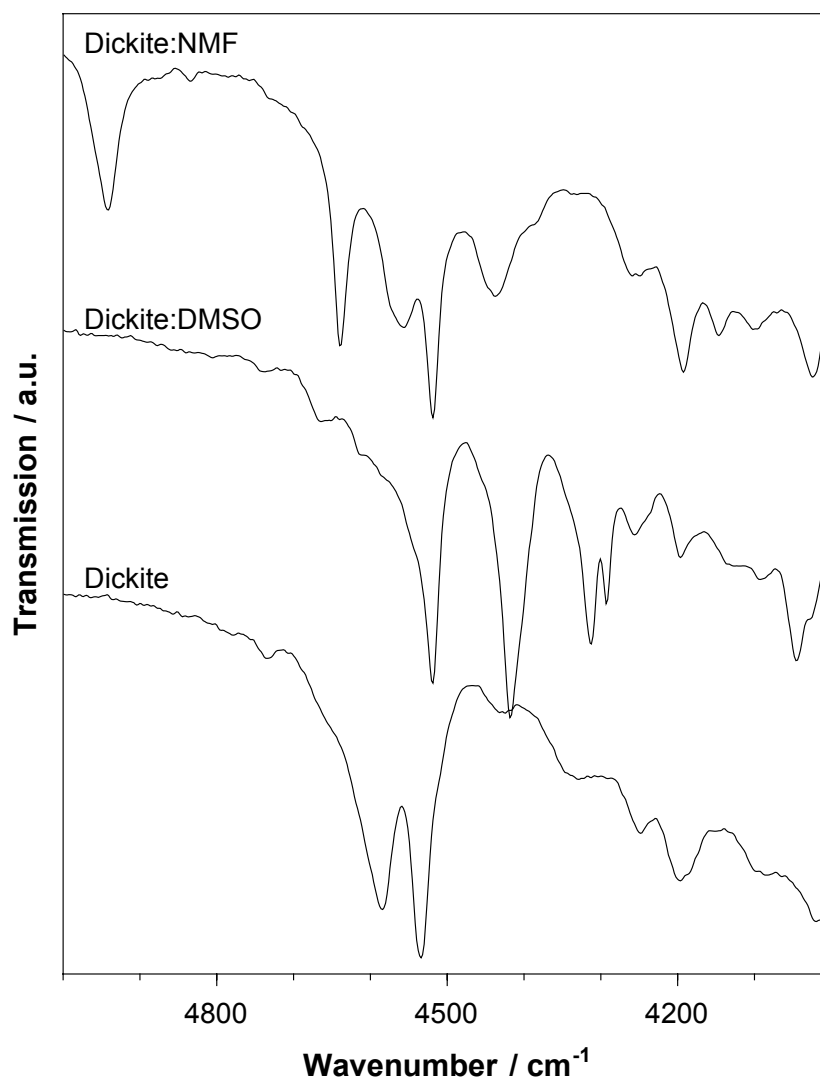


Figure 9.7 Detailed view on the near infrared spectra of dickite and its intercalates in the combination band region ($5000 - 4000 \text{ cm}^{-1}$).

The spectral region below 5000 cm^{-1} is characterized by a number of strong and sharp bands, whose positions shift remarkably due to the intercalation procedures (Figure 9.7). The dickite spectrum is dominated by two strong bands at 4586 and 4533 cm^{-1} , together with a broad shoulder at higher wavenumbers (4655 cm^{-1}) and a weak band at 4736 cm^{-1} . The band at 4533 cm^{-1} is strongly affected by the intercalation reactions, it shifts to 4520 cm^{-1} due to the DMSO treatment and even to 4519 cm^{-1} in the NMF sample. Here two additional modes appear at higher wavenumbers ($4942, 4637 \text{ cm}^{-1}$) together with a broad

but strong band at 4556 cm^{-1} . The dickite:DMSO spectrum shows a broad band at 4740 cm^{-1} , the band at 4655 cm^{-1} splits into 4663 and 4615 cm^{-1} , and two broad shoulders are visible at 4581 and 4547 cm^{-1} . While in the dickite spectrum only weak and broad bands at 4430 , 4340 , 4248 , 4196 , 4090 and 4013 cm^{-1} are visible, especially the DMSO intercalated sample shows three strong modes at 4416 , 4314 and 4290 cm^{-1} . In the NMF spectrum one strong but broad band appears at 4439 cm^{-1} with a broad shoulder at 4385 cm^{-1} . In both intercalate spectra a band appears at 4256 cm^{-1} with a shoulder at 4232 cm^{-1} in the DMSO spectrum. The band at 4196 cm^{-1} appears in all the spectra, but has the highest intensity due to the NMF intercalation. In this spectrum another small band develops at a wavenumber of 4146 cm^{-1} . A broad mode at 4132 cm^{-1} appears in the DMSO sample together with a sharp band at 4046 cm^{-1} which shows a shoulder at 4027 cm^{-1} . This shoulder appears too, as a strong band in the spectrum of the NMF treated sample (at 4023 cm^{-1}).

9.4 DISCUSSION AND CONCLUSIONS

X-ray diffractometry

The observed shifts of the basal spacings upon intercalation clearly indicate the incorporation of the foreign molecules into the interlayer space of the dickite. But not only the (00l)-peaks are affected due to intercalation, additionally the patterns show strong changes in the range between 19 and $27^\circ 2\theta$. This indicates, that the incorporation of small polar molecules like DMSO and NMF within the clay interlayers not only removes pre-existing hydrogen bonds between the tetrahedral and octahedral sheets of the dickite, expanding the interlamellar spaces, but it also obviously affects the $\text{Al}(\text{O}/\text{OH})_6$ and SiO_4 -units.

Mid infrared spectroscopy

Table 9.4 shows a comparison of the dickite and dickite:DMSO bands in the mid infrared from literature data. It is obvious, that the two spectra are in good agreement with previously published work (Frost et al. 1993, 1998b, Vempati et al. 1996), while to our knowledge, no complete infrared spectroscopic

investigation of dickite:NMF is published yet. Only the bands in the OH region are discussed by Lipsicas *et al.* (1986) and Komori *et al.* (1998).

Table 9.4 Comparison of the observed infrared bands of dickite and dickite:DMSO to literature data.

Dickite		Dickite:DMSO		
This study	Frost <i>et al.</i> (1993)	This study	Vempati <i>et al.</i> (1996)	Frost <i>et al.</i> (1998)
3700	3704	3700	3695	3697
-	3681	-	-	-
3650	3654	3664	3664	3660
3629	3622	3621	3621	3620
-	-	3538	3540	3538
-	-	3504	3505	3502
3431	-	3426	-	3413
3031	-	3023	3022	3021
-	-	2937	2937	2935
-	-	2917	2919	2917
-	-	1428	1428	1429
-	-	1407	1408	1408
-	-	1396	1393	1392
-	-	1373	-	1373
-	-	1317	1318	-
-	-	1300	-	-
1225	-	1225	-	-
1118	1118	1122	-	-
-	-	1099	1099	1083
1029	1033	1028	1032	1028
1004	1000	1004	-	1004
998	-	998	-	987
956	-	958	959	958
933	935	941	-	940
914	912	904	912	906
800	-	-	-	-
-	794	790	789	-
754	755	742	744	-
-	-	719	-	721
693	696	685	687	690
-	-	630	-	n.a. ¹⁾
599	-	603	-	n.a.
538	534	-	553	n.a.
526	-	526 (?)	-	n.a.
-	-	511	-	n.a.
495	-	-	-	n.a.
474	-	470	-	n.a.
468	468	460	469	n.a.
453	-	-	-	n.a.
435	-	435	435	n.a.
426	423	-	-	n.a.
416	-	-	-	n.a.
406	-	408	-	n.a.

Hydroxyl stretching region. The DRIFT spectra of the OH stretching region are considerably different from the previously discussed Raman spectra (Figure 9.3, 9.4; see also Figure 8.10). These differences may be attributed to the polar character of the Al-O-H bonds, leading to strong IR-vibrations, and to the crystal orientation dependence of the Raman vibrations in this spectral region (Frost et al. 1998a). The assignment of the OH modes has been extensively discussed in recent years. Correspondingly, the two higher frequency bands are assigned to the inner surface OH groups, whereas the band at 3629 cm^{-1} is due to the inner hydroxyl (e.g., Anton and Rouxhet 1977, Kristof et al. 1997, Frost et al. 2000). In contrast to the observations of Vempati et al. (1996), it shifts to 3621 cm^{-1} upon intercalation with DMSO, and to 3619 cm^{-1} for NMF. As this inner hydroxyl group is located deep in the pseudo-hexagonal hole of the tetrahedral layer, it should not be affected by the incorporation of foreign molecules. But according to theoretical calculations of Bridgeman and Skipper (1997) one can assume hydrogen bonded water molecules in the pseudo hexagonal holes of the siloxane sheet of dickite. This assumption is confirmed by the two water bands at 3431 and 3061 cm^{-1} . These H_2O molecules possibly cause the higher wavenumber of the inner hydroxyl band. The intercalation procedure then should remove them and thus the H-O bond strength in the Al-OH unit increases and therefore the vibrational mode shifts back from 3629 cm^{-1} to the predicted position at the lower wavenumber (3621 cm^{-1}). Additionally, the water band at 3431 cm^{-1} shifts to lower wavenumbers upon intercalation. This can be attributed to interactions of the H_2O molecules with the C=O units of NMF and the S=O group of DMSO respectively, as proposed by Frost et al. (1998b).

The formation of new bands at 3538 and 3504 cm^{-1} upon DMSO intercalation can be linked to the formation of hydrogen bonds between the inner surface hydroxyls and the S=O unit of DMSO. In the NMF intercalate only one strong and very broad band is observed at 3561 cm^{-1} . This band is also observed at 3550 cm^{-1} in a spectrum presented by Cruz et al. (1969) and is assigned to the strongly shifted stretching mode of the inner surface OH (3612 cm^{-1}), forming a strong hydrogen bond to the C=O unit of NMF. A similarly large shift was determined by Zamama and Knidiri (2000) for formamide (FAM)

intercalated dickite. They even proposed that one of the three inner surface hydroxyl groups of the dickite contracts a bifurcated hydrogen bond with the oxygen and the nitrogen atoms of the FAM molecule.

The weak bands between 3000 and 2900 cm^{-1} are attributed to methyl stretching vibrations for both intercalates. In liquid DMSO the higher mode is assigned to an asymmetric stretching vibration of C-H, and the 2911 cm^{-1} vibration can be attributed to the symmetric stretch of C-H. In liquid NMF they occur at 2874 and 2943 cm^{-1} . Upon intercalation the DMSO bands slightly shift to higher wavenumbers and the band at 2911 cm^{-1} splits into two bands at 2917 and 2937 cm^{-1} . In the NMF intercalate the higher band splits into modes at 2950 and 2979 cm^{-1} , while the lower band shifts to a higher wavenumber (2910 cm^{-1}). Frost *et al.* (1998b) attributed this splitting to a loss of degeneracy. According to Martens *et al.* (2002) the splitted bands show that the two methyl groups in the intercalated DMSO are bonded differently to the adjacent siloxane sheet. As NMF contains only one methyl group, an explanation for the splitting of its C-H stretching vibration is more difficult. Possibly the two new bands can be attributed to a combination of vibrational modes of hydrogen bonded methyl groups and H-bonded N-H units, which would be a strong hint to a more rigid bonding of the NMF molecules within the interlayer space (Lipsicas *et al.* 1996, Frost *et al.* 1998b). This explanation is in good correspondence with the results of the Raman investigations (chapter 8).

The methyl deformation region in DMSO consists of a complex arrangement of vibrational modes at 1455, 1437, 1418, 1406, 1361, 1331, 1310 and 1293 cm^{-1} . Most of them shift to higher wavenumbers (1428, 1317, 1300 cm^{-1}), and the band at 1361 cm^{-1} splits into bands at 1376 and 1396 cm^{-1} . These observations also suggest various orientations and bonds of the methyl groups and thus of the DMSO molecules in the dickite interlayers (Frost *et al.* 1998b).

Besides hydrogen bonds of the methyl groups to the adjacent siloxane sheets Frost *et al.* (1998b) postulated a partial “dimerization” and “polymerization” of DMSO molecules via hydrogen bonds between incorporated water molecules and the S atoms of DMSO. They attributed a band at 1029

cm^{-1} to polymeric S=O stretching modes in DMSO, as well as two further bands at 1023 and 1010 cm^{-1} . Furthermore a vibration at 1040 cm^{-1} was assigned to monomeric DMSO S=O vibrations. In this study two S=O stretching vibrations are observed at 1020 and 1042 cm^{-1} in pure DMSO. Furthermore, both the dickite and the intercalate spectra show bands at 1029 cm^{-1} and 1008 cm^{-1} , which are merely affected by the intercalation. Additionally no corresponding band could be observed at about 1040 cm^{-1} in the dickite:DMSO spectrum, which could prove the thesis of polymeric DMSO in the interlayers. Also no vibrations of coordinated water at 1680 cm^{-1} are observed in the spectra, which would be the case, if water molecules are the connection between DMSO molecules (Frost et al. 1998b). Thus, it is proposed that the intercalated DMSO is bonded to dickite via various hydrogen bonds between the S=O units and the inner surface OH groups. But, in contrast to the Raman results in chapter 8 no hints for interactions between the methyl groups and the S=O units of adjacent DMSO molecules could be found in the infrared spectra. Furthermore a connection of DMSO molecules via H-bonds with water molecules can be excluded, due to the lack of strong water bands in that region.

The OH bending region around 900 cm^{-1} is dominated by remarkably shifting Al-OH vibrations (931 cm^{-1} \rightarrow 941 cm^{-1} , 914 cm^{-1} \rightarrow 904 cm^{-1}) and an intensity increasing vibration at 958 cm^{-1} . It is assigned to the stretching of the siloxane group (Bougeard et al. 2000) affected by the CH_3 rocking vibration at 951 cm^{-1} . The other bands are assigned to the inner surface hydroxyls, their shifts occur due to the formation of H-bonds to the S=O group, and thus are a good proof for the above proposed model.

One of the difficulties in studying the 1700 – 1200 cm^{-1} region in infrared spectra of NMF intercalated dickite is the overlapping of some of the amide bands. The most prominent band appears at 1652 cm^{-1} in liquid NMF, which is attributed to a combination of a C=O stretching vibration and a N-H deformation (Frost et al. 2000). All the other bands in this region (1535, 1452, 1412, 1379, 1319 cm^{-1}) are assigned to complex amide vibrations (Frost et al. 2000). These authors proposed a mix of C=O, C-N and C-H vibrations for these bands and designated them as amide I, amide II and amide III vibrations (Table 9.2). Their

shifts and intensity changes upon intercalation (1525, 1455, 1419, 1378 cm^{-1}) are attributed to the formation of H-bonds to the adjacent siloxane sheets and inner surface hydroxyls. As the band positions in this region are very different for various amides, a comparison between the vibrational modes and thus a more accurate assignment is impossible.

The Si-O stretching region around 1000 cm^{-1} is affected not as strong as the other spectral regions by the incorporation of NMF. The Si-O in-plane vibrations at 1116 and 1029 cm^{-1} slightly shift to lower wavenumbers (1110 and 1024 cm^{-1}). This is possibly due to the formation of H-bonds to the NMF molecule.

Similar to the observed changes in the DRIFT spectra of DMSO intercalated dickite the OH bending vibrations at 956, 931 and 914 cm^{-1} strongly shift their positions upon NMF intercalation to 964, 940 and 906 cm^{-1} , respectively. The first band is assigned to a Si-O stretching vibration, which is perturbed due to hydrogen bonds to the methyl group of the NMF molecule. This CH_3 rocking vibration is observed in the pure NMF spectrum at 959 cm^{-1} , very near to the position of the methyl deformation mode in DMSO. The two bands at lower wavenumbers are attributed to hydroxyl deformation vibrations of inner surface hydroxyls hydrogen bonded to the C=O of NMF (Frost et al. 2000).

Near infrared spectroscopy

Near-IR spectroscopy has often been described as spectroscopy of the hydroxyl vibrations (e.g. Frost et al. 2002, Petit et al. 2004), so that any part of the dickite structure involving hydroxyl groups or water molecules is readily observed in the NIR spectra. Thus, the major spectral features of silicate minerals are located in the high frequency region between 7300 and 6400 cm^{-1} , in the 6000 – 5000 cm^{-1} and in the 4800 – 4000 cm^{-1} region. The observed signals correspond either to the first overtone ($2\nu_{\text{OH}}$) of OH stretching fundamental vibrations, to combinations ($2\nu_{\text{OH}} + \delta_{\text{Al-OH}}$) of stretching and bending fundamental modes of X-OH groups (X = Al, Mg, Fe mainly), or to combinations of OH stretching modes with lattice vibrations (Petit et al. 1999). Additionally the overtones of polar molecular units like S=O in DMSO or C=O in NMF and their combination bands with the dickite fundamental modes should

be observable, while the Si-O fundamentals occur at frequencies being too low ($600 - 400 \text{ cm}^{-1}$) to expect their overtone vibrations in the NIR range (Hunt and Salisbury 1970).

Again the lack of published data about the assignment of most of the near infrared modes of phyllosilicates, especially of the kaolinite group and their intercalates makes the interpretation of the spectra very difficult. According to this a set of possible overtone and combination bands are calculated from the MIR bands presented in chapter 9.1. The resulting wavenumbers are used for the interpretation of the spectral features. Besides, obviously senseless or forbidden band combinations like 3ν or 4ν of Si-O lattice vibrations have been excluded (Hunt and Salisbury 1970). A similar technique was chosen by Delineau *et al.* (1994) or Petit *et al.* (1999). Tables A.1 – A.4 in appendix I show the calculations of the NIR bands of dickite and the NMF- and DMSO-intercalates. Tables 9.5 and 9.6 show the resulting assignments of the vibrational modes of the intercalates. Deviations in the wavenumbers of observed and calculated overtone and combination modes are explained by Alpert *et al.* (1964) with the inharmonic character of vibrations. Moreover the possible substitution of Fe^{3+} or other trivalent cations for Al^{3+} in the octahedral position remarkably affects the wavenumbers of all OH modes in NIR spectra (Delineau, *et al.* 1994, Petit *et al.* 1999). As it was not possible to consider these effects in my calculations, this can be a further explanation for some observed differences, as well as the influences of intercalation and hydrogen bonds on the vibrational modes.

The three spectral regions are shown in detail in Figures 9.6 and 9.7. Five bands are identified in the first hydroxyl stretching overtone region of the dickite spectrum centered around 7340, 7233, 7087, 7071 and 7048 cm^{-1} . By comparison with the MIR spectra most of them can be assigned to the $2\nu_{\text{OH}}$ of the inner surface hydroxyl vibrations at 3700, 3650, or 3629 cm^{-1} (Frost *et al.* 2002). Upon intercalation only two strong bands remain at 7230 and 7070 cm^{-1} in the DMSO spectrum and at 7212 and 7064 cm^{-1} in the NMF intercalate. This is due to the strong changes in the hydroxyl stretching region due to the formation of H-bonds to the intercalated molecules. As the $2\nu_{\text{OH}}$ of the inner

Table 9.5 Calculated modes and suggested assignments of the near infrared bands of dickite:DMSO.

Band / cm ⁻¹	Intensity	Suggested assignments	Calculated wavenumbers	
7340	w	Intercalate-overtone	2 x 3664	= 7328
7230	m / b	Intercalate-overtone	2 x 3621	= 7242
		Intercalate-combination	3700 + 3538	= 7238
7070	vs	Intercalate-overtone	2 x 3538	= 7076
6030	w	Intercalate-overtone	2 x 3023	= 6046
5986	m	DMSO-overtone	2 x 2995	= 5990
5949	m	Intercalate-combination	3023 + 2917	= 5940
5868	wsh	Intercalate-overtone	2 x 2937	= 5874
5820	m	DMSO-overtone	2 x 2911	= 5822
5783	m			
5710	wsh	Intercalate-overtone	4 x 1428	= 5712
5515	vw b	Water-overtone & combination		
5428	vw b	Water-overtone & combination		
5336	vw b	Water-overtone & combination		
5231	vw b	Water-overtone & combination		
4740	w	Intercalate-combination	3426 + 1317	= 4743
		Intercalate-combination	3621 + 1122	= 4743
4663	w	Intercalate-combination	3538 + 1122	= 4660
		Intercalate-combination	3700 + 958	= 4658
4615	b	Intercalate-combination	3664 + 958	= 4622
4581	bsh	Intercalate-combination	3621 + 958	= 4579
		Dickite-combination	3650 + 931	= 4581
4547	bsh	Intercalate-combination	3538 + 1004	= 4542
		Intercalate-combination	3426 + 1122	= 4548
4520	vs	Intercalate-combination	3621 + 904	= 4525
		Intercalate-combination	1099 + 3426	= 4515
4416	vs	DMSO-combination	2995 + 1418	= 4413
4314	s	DMSO-combination	2911 + 1406	= 4317
4290	m	Intercalate-overtone	3 x 1430	= 4290
		DMSO-combination	2995 + 1293	= 4288
4256	m	DMSO-overtone	3 x 1419	= 4257
		Intercalate-combination	2937 + 1317	= 4254
4232	sh	Intercalate-overtone	3 x 1407	= 4221
4196	m	Intercalate-overtone	3 x 1396	= 4188
		DMSO-combination	1293 + 2911	= 4204
4132	vb	Intercalate-overtone	3 x 1376	= 4128
		Intercalate-combination	2917 + 1225	= 4142
4092	vw	DMSO-overtone	4 x 1020	= 4080
4046	s			
4027	sh	Intercalate-combination	3023 + 1004	= 4027

Table 9.6 Calculated modes and suggested assignments of the near infrared bands of dickite:NMF.

Band / cm ⁻¹	Intensity	Assigned overtone modes	Calculated bands
7212	m / b	Intercalate-Combination NMF-Overtone	3650 + 3561 = 7211 2 x 3606 = 7212
7064	vs	Dickite-Combination	3629 + 3431 = 7060
6696	vs	Intercalate-Combination NMF-Oberton	3650 + 3039 = 6689
6439	m	Intercalate-combination	3619 + 2817 = 6436
6030	vw	Intercalate-combination	3039 + 2979 = 6018
5930	vw	Intercalate-combination	2979 + 2950 = 5929
5730	m / b	Intercalate-combination	2910 + 2817 = 5727
5592	w / b		
5430	vw b		
5336	vw b	Intercalate-combination	3650 + 1681 = 5331
5231	vw b	Intercalate-combination	3561 + 1681 = 5242
4942	s	Intercalate-overtone Intercalate-combination	4 x 1236 = 4942 3561 + 1378 = 4939
4637	s	Intercalate-combination Dickite-combination	3675 + 964 = 4639 1008 + 3629 = 4637
4556	s / b	Intercalate-combination Intercalate-combination	3650 + 906 = 4556 3561 + 997 = 4558
4518	vs	Intercalate-combination	3561 + 964 = 4525
4439	m / b	Intercalate-overtone Intercalate-combination	4 x 1110 = 4440 2979 + 1455 = 4434
4385	bsh	Intercalate-combination	3421 + 964 = 4385
4256	sh	Intercalate-overtone	3 x 1419 = 4257
4194	s	Intercalate-combination Intercalate-combination	1236 + 2950 = 4186 1378 + 2817 = 4195
4146	w	Intercalate-combination NMF-overtone	1236 + 2910 = 4146 4 x 1040 = 4148
4097	w / b	Intercalate-overtone Intercalate-combination	4 x 1024 = 4096 1110 + 2979 = 4089
4023	s	Intercalate-combination Intercalate-combination	2910 + 1110 = 4020 985 + 3039 = 4024

hydroxyl stretching vibration at (3629 cm^{-1}) still exists after intercalation, it is a strong proof for the suggestion that this OH group is not involved in hydrogen bonds to the incorporated molecules.

The broad region around 5300 cm^{-1} is characterized by three or four very broad bands, which are attributed to water combination bands (Frost et al. 2002). Especially the band at 5243 cm^{-1} is a diagnostic band of adsorbed water which can be observed in spectra recorded at ambient atmosphere (Hunt and Salisbury 1970). Delineau et al. (1994) showed that this water band disappears in vacuum. Furthermore, the low intensities and the broad character of all three bands indicate, that only low amounts of water are present in the samples and that they are relatively disordered. Thus the water molecules can not act as links between the incorporated DMSO molecules.

The complex domain below 5000 cm^{-1} is characterized by a great number of combination bands. The major bands at 4586 and 4533 cm^{-1} are attributed to the combination of OH stretching and deformation modes of Al-OH-Al groups ($3650 + 931\text{ cm}^{-1}$, $3629 + 914\text{ cm}^{-1}$) (Delineau et al. 1994). Their shifts to lower wavenumbers and the strong decrease of the 4586 cm^{-1} mode are assigned to the changes of the OH bonds upon intercalation. The weak bands at 4736 and 4655 cm^{-1} are likely due to a combination of an OH stretching mode (3700 cm^{-1}) and a water stretching mode (3431 cm^{-1}), respectively, with lattice vibrations (1225 , 1029 cm^{-1}). As discussed previously, the water combination band decreases upon intercalation. In the NMF intercalate it disappears within a sharp combination band of a perturbed OH stretching mode at 3650 cm^{-1} with a lattice vibration at 964 cm^{-1} (4637 cm^{-1}). Also the further weak combination bands which correspond to adsorbed water modes at 4430 , 4340 and 4248 cm^{-1} disappear upon intercalation. The broad bands below 4200 cm^{-1} in the intercalate-spectra never have been reported in the literature, therefore their assignment is difficult. Probably in the dickite:DMSO spectrum they are combinations of the S=O stretching bands with methyl vibrations, overlaying weak combination bands of OH stretching bands with low frequency vibrations of the Si-O lattice. For example, the 4027 cm^{-1} mode can be assigned to a combination of a methyl stretch 2995 and a S=O stretch 1024 cm^{-1} , and the

combination of 2995 cm^{-1} with the second S=O stretch at 1042 cm^{-1} reveals a vibration near 4046 cm^{-1} . At least the band at 4096 cm^{-1} can be assigned to an overtone vibration of 1024 cm^{-1} .

A remarkable difference between the intercalate spectra and the pure dickite spectrum can be observed in the spectral region between $6000 - 5000\text{ cm}^{-1}$, where several new bands appear upon intercalation. As the dickite spectrum does not show any bands in this region, all the features are attributed to overtones of the incorporated molecules. For example the DMSO spectrum shows two sharp bands at 5986 and 5820 cm^{-1} , which can be assigned to the first overtones of the CH-stretching modes at 2995 and 2911 cm^{-1} . The strong band at 5949 cm^{-1} can be assigned to a combination band of perturbed OH stretching vibrations with a CH stretching mode. Additionally, the weak shoulder at 5868 cm^{-1} can be assigned to the $2\nu_{\text{CH}}$ of the perturbed symmetric CH stretching mode at 2937 cm^{-1} . The sharp band at 5949 cm^{-1} is difficult to explain. If the MIR mode at 3023 cm^{-1} is correctly attributed to a H-bonded CH stretching vibration, the NIR band probably is a combination of this methyl vibration with the perturbed CH mode at 2917 cm^{-1} . A similar explanation is proposed for the vibration at 5710 cm^{-1} . It possibly can be attributed to a combination mode of the CH bands at 2995 and 2917 cm^{-1} .

The NMF spectrum additionally shows some bands close to the $2\nu_{\text{OH}}$ region which are suggested to be combination vibrations of NMF stretching modes. For example the mode at 6696 cm^{-1} can be assigned to a combination of a perturbed OH stretching band at 3619 cm^{-1} with the NH stretching mode at 3066 cm^{-1} . The 6439 cm^{-1} band is due to a CH stretching (2874 cm^{-1}) and the perturbed C=O stretching mode at 3561 cm^{-1} . The weak mode at 6030 cm^{-1} is a combination band of the broad water band at 3039 plus the vibration of a H-bonded methyl group at 2979 cm^{-1} . The two modes at 5930 and 5730 cm^{-1} can be attributed to combinations of H-bonded methyl vibrations. For the two bands at 5730 and 5592 cm^{-1} , the calculations of the combination bands revealed no satisfactory results. Therefore an explicit assignment is not possible, but it seems to be obvious, that they are also combinations of methyl stretching bands.

REFERENCES

- Alpert, N.L., Keiser, W.E., Szymanski, H.A. (1964) *IR – Theory and practice of infrared spectroscopy*. New York, Plenum Press, 380 p.
- Anton, O. and Rouxhet, P.G. (1977) Note on the intercalation of kaolinite, dickite and halloysite by dimethyl-sulfoxide. *Clays and Clay Minerals*, **25**, 259 – 263.
- Bougeard, D., Smirnov, K.S., Geidel, E. (2000) Vibrational spectra and structure of kaolinite: a computer simulation study. *Journal of Physical Chemistry, Part B*, **104**, 9210 – 9217.
- Bridgeman, C.H. and Skipper, N.T. (1997) A Monte Carlo study of water at an uncharged clay surface. *Journal of Physics: Condensed Matter*, **9**, 4081 – 4087.
- Cruz, M., Laycock, Z., White, J.L. (1969) Perturbation of OH groups in intercalated kaolinite donor-acceptor complexes. I. Formamide-, methyl formamide-, and dimethyl formamide-kaolinite complexes. In: Heller, L. (ed.) *Proc. Int. Clay Conf. Tokyo, 1969*, Israel University Press, Jerusalem, 775 – 789.
- Delineau, T., Allard, T., Muller, J.-P., Barres, O., Yvon, J., Cases, J.-M. (1994) FTIR reflectance vs. EPR studies of structural iron kaolinites. *Clays and Clay Minerals*, **42**, 308 – 320.
- Frost, R.L., Fredericks, P.M., Bartlett, J.R. (1993) Fourier transform Raman spectroscopy of kandite clays. *Spectrochimica Acta Part A*, **49**, 667 – 674.
- Frost, R.L., Forsling, W., Holmgren, Allan, Klopogge, J.T., Kristof, J. (1998a) Raman spectroscopy at temperatures between 298 and 423 K and at 77 K of kaolinites intercalated with formamide. *Journal of Raman Spectroscopy*, **29**, 1065 – 1069.
- Frost, R.L., Kristof, J., Paroz, G.N., Klopogge, J.T. (1998b) Molecular structure of Dimethyl sulfoxide intercalated kaolinites. *Journal of Physical Chemistry, Part B*, **102**, 8519 – 8532.
- Frost, R.L., Kristof, J., Horvath, E., Klopogge, J.T. (2000) Vibrational spectroscopy of formamide-intercalated kaolinites. *Spectrochimica Acta, Part A*, **56**, 1191 – 1204.
- Frost, R.L., Mako, E., Kristof, J., Klopogge, J.T. (2002) Modification of kaolinite surfaces through mechanochemical treatment – a mid-IR and near-IR spectroscopic study. *Spectrochimica Acta, Part A*, **58**, 2849 – 2859.
- Hunt, G.R. and Salisbury, J.W. (1970) Visible and near-infrared spectra of minerals and rocks: I silicate minerals. *Modern Geology*, **1**, 283 – 300.
- Komori, Y., Sugahara, Y., Kuroda, K. (1998) A kaolinite-NMF-methanol intercalation compound as a versatile intermediate for further intercalation reaction of kaolinite. *Journal of Materials Research*, **13**, 930 – 934.

-
- Kristof, J., Frost, R.L., Felinger, A., Mink, J. (1997) FTIR spectroscopic study of intercalated kaolinite. *Journal of Molecular Structure*, **410-411**, 119 – 122.
- Lipsicas, M., Raythatha, R., Giese, R.F., Costanzo, P.M. (1986) Molecular motions, surface interactions, and stacking disorder in kaolinite intercalates. *Clays and Clay Minerals*, **34**, 635 – 644.
- Martens, W.N., Frost, R.L., Kristof, J., Horvath, E. (2002) Modification of kaolinite surfaces through intercalation with deuterated dimethylsulfoxide. *Journal of Physical Chemistry, Part B*, **106**, 4162 - 4171.
- Petit, S., Madejova, J., Decarreau, A., Martin, F. (1999) Characterization of octahedral substitutions in kaolinites using near infrared spectroscopy. *Clays and Clay Minerals*, **47**, 103 – 108.
- Petit, S., Martin, F., Wiewiora, A., de Parseval, P., Decarreau, A. (2004) Crystal-chemistry of talc: a near infrared (NIR) spectroscopy study. *American Mineralogist*, **89**, 319 – 326.
- Theng, B.K.G. (1974) The chemistry of clay-organic reactions. Hilger, London.
- Vempati, R.K., Mollah, M.Y.A., Reddy, G.R., Cocke, D.L., Lauer Jr., H.V. (1996) Intercalation of kaolinite under hydrothermal conditions. *Journal of Materials Science*, **31**, 1255 – 2159.
- Zamama, M. and Knidiri, M. (2000) IR study of dickite-formamide intercalate, $\text{Al}_2\text{Si}_2\text{O}_5(\text{OH})_4\text{-H}_2\text{NCOH}$. *Spectrochimica Acta, Part A*, **56**, 1139 – 1147.

CHAPTER 10

OUTLOOK

The presented results offer a comprehensive view of the effects of intercalation and delamination processes on sheet silicates. It has been shown that the high resolution microscopic techniques (HRTEM, ESEM, AFM) revealed a detailed insight into the morphology of the treated phyllosilicates and that vibrational spectroscopy techniques are strong tools to investigate the structure of the modified interlayers due to the incorporation of cations and molecules.

Thus the investigation of the near environment of the migrating cations would offer further information on their positions within the structure. For example, with electron paramagnetic resonance spectroscopy (EPR) the coordinative structure of paramagnetic elements like copper or iron can be investigated. Similar information can be obtained by EXAFS studies for the intercalated cations. Additional MAS NMR investigations especially of Al will give additional information on the changes in the structure of the octahedral layers.

All these methods reveal additional data concerning the migration paths and the bonds of the intercalated cations and hence render possible a discussion of the Hofmann-Klemen effect in micas.

Another urgent question is the direct measurement of the particle thickness of mid-sized materials. While atomic force microscopy is a widespread technique for the imaging and measurement of nanosized clay minerals, the measurement of larger particles is very difficult. Therefore a direct measurement technique would be a very important tool for the investigation of

partly delaminated products. Promising would be the use of profilometers with large scanning areas and scanning heights up to 10 μm .

APPENDIX I

CALCULATED NIR BANDS

Table A-I-2. Calculated NIR modes for dickite:NMF compared to the observed bands. The bold wavenumbers are close to the observed bands. Grey numbers are below 4000 cm⁻¹ and thus are not considered.

Observed NIR-modes	Observed MIR-modes	Calculated 1 st overtone	Calculated combination bands					
			+ 3675	+ 3650	+ 3619	+ 3561	+ 3421	+ 3039
7212	3675	7350	7350	7325	7294	7236	7096	6714
7064	3650	7300	7325	7300	7269	7211	7071	6689
6696	3619	7238	7294	7269	7238	7180	7040	6658
6439	3561	7122	7236	7211	7180	7122	6982	6600
6030	3421	6842	7096	7071	7040	6982	6842	6460
5930	3039	6078	6714	6689	6658	6600	6460	6078
5730	2979	5958	6654	6629	6598	6540	6400	6018
5592	2950	5900	6625	6600	6569	6511	6371	5989
5430	2910	5820	6585	6560	6529	6471	6331	5949
5336	2817	5634	6492	6467	6436	6378	6238	5856
5231	1733	3466	5408	5383	5352	5294	5154	4772
4942	1681	3362	5356	5331	5300	5242	5102	4720
4637	1525	3050	5200	5175	5144	5086	4946	4564
4556	1455	2910	5130	5105	5074	5016	4876	4494
4518	1419	2838	5094	5069	5038	4980	4840	4458
4439	1378	2756	5053	5028	4997	4939	4799	4417
4385	1236	2472	4911	4886	4855	4797	4657	4275
4256	1162	2324	4837	4812	4781	4723	4583	4201
4194	1110	2220	4785	4760	4729	4671	4531	4149
4146	1024	2048	4699	4674	4643	4585	4445	4063
4097	997	1994	4672	4647	4616	4558	4418	4036
4023	985	1970	4660	4635	4604	4546	4406	4024
-	964	1928	4639	4614	4583	4525	4385	4003
-	940	1880	4615	4590	4559	4501	4361	3979
-	906	1812	4581	4556	4525	4467	4327	3945

Table A-I-2. Continued

Observed NIR-modes	Observed MIR-modes	Calculated combination bands						
		+ 2979	+ 2950	+ 2910	+ 1733	+ 1681	+ 1525	+ 1455
7212	3675	6654	6625	6585	5408	5356	5200	5130
7064	3650	6629	6600	6560	5383	5331	5175	5105
6696	3619	6598	6569	6529	5352	5300	5144	5074
6439	3561	6540	6511	6471	5294	5242	5086	5016
6030	3421	6400	6371	6331	5154	5102	4946	4876
5930	3039	6018	5989	5949	4772	4720	4564	4494
5730	2979	5958	5929	5889	4712	4660	4504	4434
5592	2950	5929	5900	5860	4683	4631	4475	4405
5430	2910	5889	5860	5820	4643	4591	4435	4365
5336	2817	5796	5767	5727	4550	4498	4342	4272
5231	1733	4712	4683	4643	3466	3414	3258	3188
4942	1681	4660	4631	4591	3414	3362	3206	3136
4637	1525	4504	4475	4435	3258	3206	3050	2980
4556	1455	4434	4405	4365	3188	3136	2980	2910
4518	1419	4398	4369	4329	3152	3100	2944	2874
4439	1378	4357	4328	4288	3111	3059	2903	2833
4385	1236	4215	4186	4146	2969	2917	2761	2691
4256	1162	4141	4112	4072	2895	2843	2687	2617
4194	1110	4089	4060	4020	2843	2791	2635	2565
4146	1024	4003	3974	3934	2757	2705	2549	2479
4097	997	3976	3947	3907	2730	2678	2522	2452
4023	985	3964	3935	3895	2718	2666	2510	2440
-	964	3943	3914	3874	2697	2645	2489	2419
-	940	3919	3890	3850	2673	2621	2465	2395
-	906	3885	3856	3816	2639	2587	2431	2361

Table A-I-2. Continued

Observed NIR-modes	Observed MIR-modes	Calculated combination bands							
		+ 1455	+ 1419	+ 1378	+ 1236	+ 1162	+ 1110	+ 1024	+ 997
7212	3675	5130	5094	5053	4911	4837	4785	4699	4672
7064	3650	5105	5069	5028	4886	4812	4760	4674	4647
6696	3619	5074	5038	4997	4855	4781	4729	4643	4616
6439	3561	5016	4980	4939	4797	4723	4671	4585	4558
6030	3421	4876	4840	4799	4657	4583	4531	4445	4418
5930	3039	4494	4458	4417	4275	4201	4149	4063	4036
5730	2979	4434	4398	4357	4215	4141	4089	4003	3976
5592	2950	4405	4369	4328	4186	4112	4060	3974	3947
5430	2910	4365	4329	4288	4146	4072	4020	3934	3907
5336	2817	4272	4236	4195	4053	3979	3927	3841	3814
5231	1733	3188	3152	3111	2969	2895	2843	2757	2730
4942	1681	3136	3100	3059	2917	2843	2791	2705	2678
4637	1525	2980	2944	2903	2761	2687	2635	2549	2522
4556	1455	2910	2874	2833	2691	2617	2565	2479	2452
4518	1419	2874	2838	2797	2655	2581	2529	2443	2416
4439	1378	2833	2797	2756	2614	2540	2488	2402	2375
4385	1236	2691	2655	2614	2472	2398	2346	2260	2233
4256	1162	2617	2581	2540	2398	2324	2272	2186	2159
4194	1110	2565	2529	2488	2346	2272	2220	2134	2107
4146	1024	2479	2443	2402	2260	2186	2134	2048	2021
4097	997	2452	2416	2375	2233	2159	2107	2021	1994
4023	985	2440	2404	2363	2221	2147	2095	2009	1982
-	964	2419	2383	2342	2200	2126	2074	1988	1961
-	940	2395	2359	2318	2176	2102	2050	1964	1937
-	906	2361	2325	2284	2142	2068	2016	1930	1903

Table A-I-2. Continued

Observed NIR-modes	Observed MIR-modes	Calculated combination bands			
		+ 985	+ 964	+ 940	+ 906
7212	3675	4660	4639	4615	4581
7064	3650	4635	4614	4590	4556
6696	3619	4604	4583	4559	4525
6439	3561	4546	4525	4501	4467
6030	3421	4406	4385	4361	4327
5930	3039	4024	4003	3979	3945
5730	2979	3964	3943	3919	3885
5592	2950	3935	3914	3890	3856
5430	2910	3895	3874	3850	3816
5336	2817	3802	3781	3757	3723
5231	1733	2718	2697	2673	2639
4942	1681	2666	2645	2621	2587
4637	1525	2510	2489	2465	2431
4556	1455	2440	2419	2395	2361
4518	1419	2404	2383	2359	2325
4439	1378	2363	2342	2318	2284
4385	1236	2221	2200	2176	2142
4256	1162	2147	2126	2102	2068
4194	1110	2095	2074	2050	2016
4146	1024	2009	1988	1964	1930
4097	997	1982	1961	1937	1903
4023	985	1970	1949	1925	1891
-	964	1949	1928	1904	1870
-	940	1925	1904	1880	1846
-	906	1891	1870	1846	1812

Table A-I-4. Calculated NIR modes for liquid DMSO. The bold wavenumbers are close to the observed intercalate-bands. Grey numbers are below 4000 cm^{-1} and thus are not considered.

Observed MIR-modes	Calculated overtones			Calculated combination bands					
	3 rd	2 nd	1 st	+ 2995	+ 2911	+ 1473	+ 1418	+ 1406	+ 1361
2995	8985	11980	5990	5990	5906	4468	4413	4401	4356
2911	8733	11644	5822	5906	5822	4384	4329	4317	4272
1473	4419	5892	2946	4468	4384	2946	2891	2879	2834
1455	4365	5820	2910	4450	4366	2928	2873	2861	2816
1437	4311	5748	2874	4432	4348	2910	2855	2843	2798
1418	4254	5672	2836	4413	4329	2891	2836	2824	2779
1406	4218	5624	2812	4401	4317	2879	2824	2812	2767
1361	4083	5444	2722	4356	4272	2834	2779	2767	2722
1331	3993	5324	2662	4326	4242	2804	2749	2737	2692
1310	3930	5240	2620	4305	4221	2783	2728	2716	2671
1293	3879	5172	2586	4288	4204	2766	2711	2699	2654
1042	3126	4168	2084	4037	3953	2515	2460	2448	2403
1020	3072	4096	2040	4015	3931	2493	2438	2426	2381
951	2853	3804	1902	3946	3862	2424	2369	2357	2312
929	2787	3716	1858	3924	3840	2402	2347	2335	2290
894	2682	3576	1788	3889	3805	2367	2312	2300	2255

Observed MIR-modes	Calculated combination bands							
	+ 1331	+ 1310	+ 1293	+ 1042	+ 1020	+ 951	+ 929	+ 894
2995	4326	4305	4288	4037	4015	3946	3924	3889
2911	4242	4221	4204	3953	3931	3862	3840	3805
1473	2804	2783	2766	2515	2493	2424	2402	2367
1455	2786	2765	2748	2497	2475	2406	2384	2349
1437	2768	2747	2730	2479	2457	2388	2366	2331
1418	2749	2728	2711	2460	2438	2369	2347	2312
1406	2737	2716	2699	2448	2426	2357	2335	2300
1361	2692	2671	2654	2403	2381	2312	2290	2255
1331	2662	2641	2624	2373	2351	2282	2260	2225
1310	2641	2620	2603	2352	2330	2261	2239	2204
1293	2624	2603	2586	2335	2313	2244	2222	2187
1042	2373	2352	2335	2084	2062	1993	1971	1936
1020	2351	2330	2313	2062	2040	1971	1949	1914
951	2282	2261	2244	1993	1971	1902	1880	1845
929	2260	2239	2222	1971	1949	1880	1858	1823
894	2225	2204	2187	1936	1914	1845	1823	1788

Table A-I-5. Calculated NIR modes for liquid NMF. The bold wavenumbers are close to the observed intercalate-bands. Grey numbers are below 4000 cm⁻¹ and thus are not considered.

Observed MIR-bands	Calculated 1 st overtone	Calculated combination bands						
		+ 3292	+ 3066	+ 2943	+ 2874	+ 1652	+ 1535	+ 1452
3292	6584	6584	6358	6235	6166	4944	4827	4744
3066	6132	6358	6132	6009	5940	4718	4601	4518
2943	5886	6235	6009	5886	5817	4595	4478	4395
2874	5748	6166	5940	5817	5748	4526	4409	4326
1652	3304	4944	4718	4595	4526	3304	3187	3104
1535	3070	4827	4601	4478	4409	3187	3070	2987
1452	2904	4744	4518	4395	4326	3104	2987	2904
1412	2824	4704	4478	4355	4286	3064	2947	2864
1379	2758	4671	4445	4322	4253	3031	2914	2831
1319	2638	4611	4385	4262	4193	2971	2854	2771
1240	2480	4532	4306	4183	4114	2892	2775	2692
1149	2298	4441	4215	4092	4023	2801	2684	2601
1040	2080	4332	4106	3983	3914	2692	2575	2492
1014	2028	4306	4080	3957	3888	2666	2549	2466
959	1918	4251	4025	3902	3833	2611	2494	2411

Observed MIR Bands	Calculated combination bands							
	+ 1412	+ 1379	+ 1319	+ 1240	+ 1149	+ 1040	+ 1014	+ 959
3292	4704	4671	4611	4532	4441	4332	4306	4251
3066	4478	4445	4385	4306	4215	4106	4080	4025
2943	4355	4322	4262	4183	4092	3983	3957	3902
2874	4286	4253	4193	4114	4023	3914	3888	3833
1652	3064	3031	2971	2892	2801	2692	2666	2611
1535	2947	2914	2854	2775	2684	2575	2549	2494
1452	2864	2831	2771	2692	2601	2492	2466	2411
1412	2824	2791	2731	2652	2561	2452	2426	2371
1379	2791	2758	2698	2619	2528	2419	2393	2338
1319	2731	2698	2638	2559	2468	2359	2333	2278
1240	2652	2619	2559	2480	2389	2280	2254	2199
1149	2561	2528	2468	2389	2298	2189	2163	2108
1040	2452	2419	2359	2280	2189	2080	2054	1999
1014	2426	2393	2333	2254	2163	2054	2028	1973
959	2371	2338	2278	2199	2108	1999	1973	1918

LEBENS LAUF

- 07/2001 – 07/2004 Promotion am Institut für Technische Chemie, Bereich Wasser- und Geotechnologie (ITC-WGT), Abteilung Nanomineralogie, am Forschungszentrum Karlsruhe.
Thema: *Spectroscopic investigations of delaminated and intercalated phyllosilicates.*
- 07/2000 – 06/2001 Wissenschaftlicher Mitarbeiter am Institut für Mineralogie und Geochemie (IMG) der Universität Karlsruhe (TH)
- 01/1999 – 06/2000 Wissenschaftlicher Mitarbeiter am Mineralogischen Institut der Universität Würzburg
- 09/1992 – 09/1998 Studium und Diplom in Mineralogie, Universität Karlsruhe (TH)
Thema der Diplomarbeit: *Mineralogische und geochemische Untersuchungen an den Evaporitmineralen des Salar de Cauchari in den Anden Nordwest-Argentiniens.*
Referent: Prof. Dr. W. Smykatz-Kloss
- 10/1989 – 06/1992 Studium der Chemie, Universität Karlsruhe (TH)
- 12/1987 – 07/1989 Zivildienst, Ökumenische Sozialstation Limburgerhof/Pfalz
- 09/1977 – 06/1987 Geschwister-Scholl Gymnasium, Ludwigshafen am Rhein

PERSÖNLICHE DATEN

- Geburtsdatum: 18. April 1968
- Geburtsort: Mannheim
- Nationalität: deutsch
- Familienstand: ledig